Geophysical Reconnaissance in the Mount Independence Area: Larrabee's Point to Chipman Point, Lake Champlain.

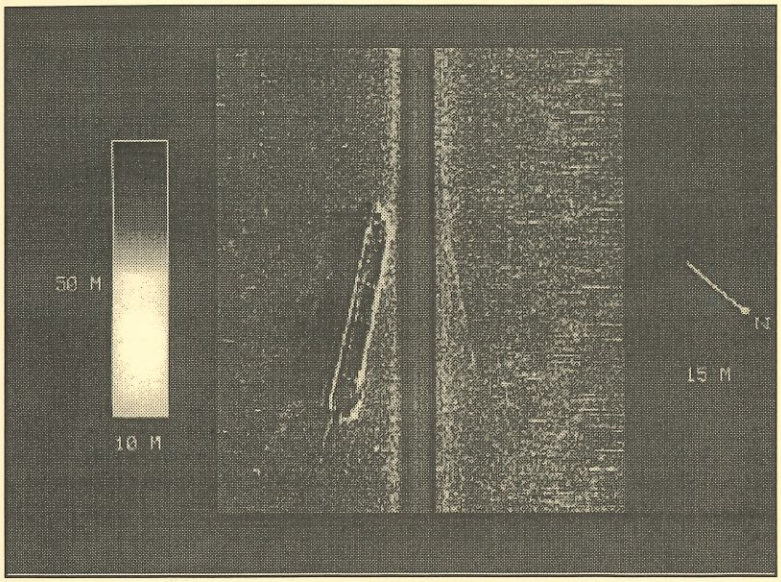

Lake Champlain Basin Program

May 1995

Prepared by Patricia L. Manley, Roger D. Flood, Todd Hannahs

for
Lake Champlain Management Conference

PUBLICATION SERIES

THIS PROGRAM IS SPONSORED BY U.S.E.P.A. AND THE STATES OF NEW YORK AND VERMONT.

This demonstration report is the fourth in a series of reports prepared under the Lake Champlain Basin Program. Those in print are listed below.

Lake Champlain Basin Program Demonstration Reports

1. Case Study of the Town of Champlain, Yellow Wood Associates, October 1993.

2. (A)Demonstration of Local Economic/Other Community Impacts, Community Case Studies for Economic Plan Elements. The City of Vergennes, Vermont. Economic and Financial Consulting Associates, Inc. October 1993.
   (B)Demonstration of Local Economic/Other Community Impacts. Community Case Studies for Economic Plan Elements. Appendix. The City of Vergennes, Vermont. Economic and Financial Consulting Associates, Inc. October 1993.

3. The Archeology of the Farm Project. Improving Cultural Resource Protection on Agricultural Lands: A Vermont Example. Jack Rossen. May 1994.

4. (A)The 1992 Fort Ticonderoga-Mount Independence Submerged Cultural Resource Survey. Executive Summary. Arthur Cohn. May 1995.
   (B)The 1992 Mount Independence Phase One Underwater Archaeological Survey. Kevin Crisman. May 1995.
   (C)The Great Bridge "From Ticonderoga to Independant Point". Arthur Cohn. May 1995
   (D)Geophysical Reconnaissance in the Mount Independence Area: Larrabee's Point to Chipman Point. Patricia Manley, Roger Flood, Todd Hannahs. May 1995.
   (E)Ticonderoga's Floating Drawbridge; 1871-1920. Peter Barranco, Jr. May, 1995.
   (F)Bottom Morphology and Boundary Currents of Southern Lake Champlain. May 1995. Hollistir Hodson.

This report was funded and prepared under the authority of the Lake Champlain Special Designation Act of 1990, P.L.101-596, through the U.S.Environmental Protection Agency (EPA grant #EPA X 001840-01). Publication of this report does not signify that the contents necessarily reflect the views of the State of New York and Vermont, the Lake Champlain Basin Program, or the U.S.Environmental Protection Agency.

Geophysical Reconnaissance in the Mount Independence Area: Larrabee's Point to Chipman Point Lake Champlain.

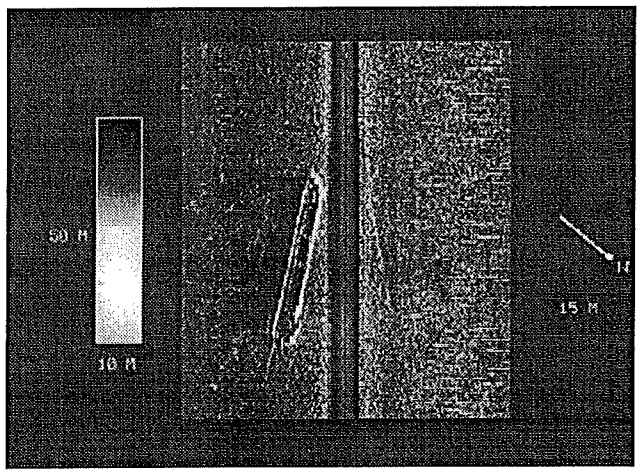

Prepared by Patricia L. Manley[†], Roger D. Flood[‡], Todd Hannahs[*]

[†]Geology Department, Middlebury College, Middlebury, VT 05753
[‡] Marine Science Research Center, State University of New York, Stony Brook, NY 11794-5000
[*]R.R. 2 Box 2301, Middlebury, VT 05753

Table of Contents

Introduction

Sediment bedforms are generated at the sediment water interface by the interaction of bottom water flow and bottom topography. Bedforms can be found in rivers, lakes and oceans. The dynamics of these sediment bedforms have been widely studied (Allen, 1985) such that it is possible to determine the direction and to some extent the magnitude of the bottom currents that formed them. Further information about sedimentation processes can be gleaned from analyzing sediments from these features.

A survey was conducted at the southern end of Lake Champlain; from Larabee's Point ferry crossing to Chipman Point. This survey was designed to locate cultural artifacts. Since submerged cultural artifacts represent obstructions to bottom water flow, they can be the cause of some sediment bedforms. Erosion and deposition processes which create sediment bedforms, might also have an effect on the management and preservation of submerged cultural resources in Lake Champlain. We utilized side-scan sonar, precision depth recorders, a magnetometer and sediment coring in identifying the orientation and location of all cultural artifacts and sediment bedforms. From our analysis, we inferred the average bottom water flow direction in this study region, discuss the nature and formation of the sediment bedforms, and assess the effects of erosion and deposition on the observed cultural artifacts.

Background

Geologic history of Lake Champlain

Lake Champlain is the sixth largest natural freshwater lake in the United States surpassed only by the five Great Lakes. It drains more than 8,000 square miles in portions of Vermont, New York and Quebec. Lake Champlain is commonly divided into five geographically distinct basins, each with their own characteristic hydrodynamic processes. The area studied in the 1992-93 survey, extending from Larabee's Point ferry crossing south to Chipman Point, is a section of the South Lake basin. South Lake extends from the mouth of the Poultney River north to Crown Point. This basin is generally narrow and shallow, and most places it is less than one mile across and less than fifty feet deep.

The development of modern Lake Champlain is a result of the last major glacial advance and isostatic rebound of the Champlain basin. The first stage in the development

of Lake Champlain was the formation of a pro-glacial lake known as Lake Albany (13 kabp - kabp means thousand years before present) which extended south of Glens Falls and drained out through the Hudson River. As the glacier continued to melt, it retreated northward and a larger region of the Champlain basin was covered by pro-glacial water known as Lake Coveville. Crustal rebound and denudation reduced the outflow to the southern outlet. Continued ice retreat finally closed the southern outlet and dammed the waters forming Lake Fort Ann, although there was still some overflow to the south into the Hudson River Valley (Teller, 1987). These two lakes (Lake Coveville and Lake Fort Ann) are often collectively known as Lake Vermont. By 12 kabp the ice margin had retreated far enough north so that a marine excursion replaced the fresh lake waters with saline waters. This period lasted about 2000 years and is known as the Champlain Sea. Present-day Lake Champlain began forming about 10.2 kabp when isostatic rebound uplifted the lands in the north, reducing the marine invasion and allowing the brackish water to freshen. Sediment deposited in all these stages, except Lake Albany, is preserved at the bottom of Lake Champlain (e.g. Chase and Hunt, 1972).

Geophysical techniques

Sonar

Sound has been proven a valuable tool for studying features underwater and in particular useful for mapping the lake bottom over a range of spatial scales. Depending on the size of feature on the lake bottom to be imaged, different acoustical devices can be employed to achieve the required data (vertical vs. horizontal image information) and resolution (or the minimum distance between adjacent features that can be resolved). For the purposes of this study, several different sound systems were used: a dual-frequency (100 and 500 kHz) short-range side-scan sonar and three echo-sounders, having a frequencies of 14 and 28 kHz, and 200 kHz.

All sonar systems use returned acoustic energy to form an image of the morphology of the bottom or sub-bottom. The sub-bottom profiler (often referred to as a PDR - precision depth recorder) transmits a sonar pulse in a conical beam. The energy is directed downwards where it is reflected off the lakebed (to obtain depth of water) as well as penetrating the sediments where it is reflected off acoustical impedance interfaces within the sediments. The reflected energy thus gives a vertical cross-section of the lakebed directly beneath the ship. The beam of energy is reflected back from a region of the lakebed ("footprint") which is proportional to the depth of water. In areas of water depths of 20 meters this region is approximately 2 m^2. The vertical resolution of such a system is

dependent on the frequency of the emitting pulse and the nature of the sediment. In the case of a 28 kHz pulse, one wavelength is 0.05 meters (2-3 inches). Depending then on the pulse width, it would only be able to resolve features on the order of 0.127 to 0.178 m (5 to 7 inches) apart.

A side-scan sonar unit transmits a fan-shaped sound beam to either side of the sonar fish instead of directing it downwards as in the case of conventional echo-sounders. Due to the high frequencies used (100 - 500 kHz) it only images the surface of the lake bottom and does not penetrate significantly into the sediment. This sideways oriented sound beam is narrow in the vertical direction and wide in the direction transverse to the sonar fish track. The strength of the returned sound beam is affected by topography of the sediment surface as well as by differing lithologies and bottom surface roughness. Objects which extend above the bottom having slopes facing the sonar fish will return stronger signals than those slopes which face away. Thus one can utilize this geometry to determine the height of an obstacle off the bottom. Depressions in the bottom would only have the back wall which would reflect energy back toward the sonar fish with a shadow zone in front.

A rougher surface will return more energy than a smoother surface. Hence a mud dominated surface will return less energy than one which contains sand or gravel sized material. Therefore a qualitative measurement of the sediment grain size can be determined by the strength of the return. Side-scan sonar records are not plan views of the sediment surface in their raw format, but simple mathematical algorithms can be used to convert the sonar record so they are close to plan view.

Magnetics

In addition to sound, looking at perturbations of the earth's magnetic field can help to locate anomalous metallic features. The earth's magnetic field is present all over the planet and a considerable distance into space. The strength and nature of this magnetic field has been extensively studied over the years (known as the ambient field). Ignoring small variations due to solar storms, the field remains stable and changes in the strength of the field occur in a predictable manner with geographic latitude and with time. The relative stability of the earth's magnetic field allows it to be used for the identification and delineation of local anomalies within the ambient field. Local anomalies originate from a variety of sources. Natural variations such as the existence of iron-rich mineral deposits or variations in the density of the substrate can produce changes in the local magnetic field that are large and intense. More commonly, however, it is the physical remains of human activities that produce the most intense fluctuations in the magnetic field because of the use of metals in man-made constructions. In water-covered areas, changes in the magnetic

field can be used to locate objects where visibility is poor and when objects have been covered with sediment.

The strength of the earth's magnetic field in the southern end of Lake Champlain is around 55,000 gammas (γ). To measure local variations, as small as a tenth of a gamma, a proton-precession magnetometer is used. The magnetometer is composed of two essential components: a sensor, which contains a fluid rich in hydrogen atoms, such as kerosene, surrounded by a coil, and a recording device. The sensor is towed through the water at least 2.5 boat lengths behind the vessel to remove any magnetic effects by the vessel. Within the sensor, hydrogen nuclei align parallel to the ambient geomagnetic field (earth's field). When a current is passed through the coil, a magnetic field is generated within the sensor which is 50 to 100 times larger than the earth's field and the hydrogen nuclei align themselves to this new field. Removing the current causes the nuclei to re-aligning with the earth's field, and as they do so, they precess. The frequency of the precession is determined and it gives a measure of the total geomagnetic field. By subtracting the ambient earth's field from the observed field, the anomalous field produced by an object(s) is determined.

The shape and strength of the anomalous signal (magnetic anomaly) can indicate the size and depth of burial for the object generating the anomalous field. The intensity of the magnetic anomaly drops off rapidly with increased distance from the source, allowing a reasonably accurate determination of the size of the object as well as its depth of burial. The physical extent of a magnetic anomaly can suggest what its origin may be. An anomaly which is kilometers in length is probably geologic in origin. One that is many hundreds of meters long may be man-made and is likely of recent origin (such as a drainage pipe or telephone cable). Small objects can have locally intense effects but are tightly circumscribed. A cannon ball can produce a field change in the hundreds of gammas but in an area of a few meters.

Magnetic material has both a positive and a negative pole. When the sensor passes within range of an object it records one or both poles of the anomalous field. A wholly positive or negative reading, referred to as a monopole, may indicate that only the edge of the anomaly has been recorded. The object causing the anomaly may be to one side or the other of the survey line, or less commonly it may be buried vertically in the sediments. When both the positive and negative readings are present (dipole), the sensor has passed in close proximity to the center of the object.

Another magnetic tool which aids in sediment core correlation is magnetic susceptibility. This method uses the principle of AC (alternating current) induction to

characterize the magnetic properties of the material. A low intensity alternating magnetic field is generated within the sensor. Any material brought within the influence of this field changes the oscillator frequency. This frequency change is converted to a value of magnetic susceptibility. Thus by passing sections of a sediment core through the sensor loop, a magnetic susceptibility profile of the core is made. High values of magnetic susceptibility indicate high magnetic material content and small values indicate lower amounts. For lake cores, higher susceptibility values are usually associated with soil erosion. Soil erosion increased dramatically with European settlement (circa 1760) as forests were cleared and subsequent grazing and cultivation occurred (King, et al., 1993). Also sewage, industrial wastes and fossil fuel combustion can enhance magnetic susceptibility values. As King et al. (1993) noted, we can use an increase in the susceptibility curve as a proxy dating tool to estimate sedimentation rates.

Radiometric Dating

^{210}Pb is a radionuclide which is naturally occurring and has a short half-life (22.6 years). This isotope is thus ideal for dating processes occurring over the last 100 years although it has a somewhat complex history. ^{210}Pb is generated as part of the ^{238} or ^{235}U decay series. Its parent is ^{222} Rn, a gas with a half life of 3.82 days. ^{222} Rn is present in the atmosphere and in lake water, and its parent is ^{226} Ra (half life of 1602 years). When ^{210}Pb is generated through decay of ^{222} Rn, it quickly becomes attached to particulates and is deposited on the lake bed. The sediments also contain ^{210}Pb generated through the decay of the ^{226}Ra (and subsequent decay of ^{222}Rn) that occurs in the sediment. Thus in sediments, ^{210}Pb consists of two components, one scavenged from lake water by settling particles (called unsupported ^{210}Pb) and the other from the decay of ^{226}Ra within the sediments (called supported ^{210}Pb). Analysis determines the total ^{210}Pb content. Therefore to get sedimentation rates, it is necessary to subtract the ^{226}Ra-supported fraction from the total activity to quantify the unsupported ^{210}Pb (Anderson et. al, 1993). Down core plots of unsupported ^{210}Pb can be used to calculate sedimentation rates.

Navigation

Navigation for the survey used either GPS or Loran-C systems. GPS (Global Positioning System) is a satellite-based radio navigation system which utilizes a constellation of satellites, some of which are visible at any time from any place on earth. The orbits of each satellite are precisely known, so that a GPS receiver measures the propagation time of signals transmitted from the satellites to accurately determine the latitude, longitude and elevation of the receiver. When GPS is in the selective availability mode available to non-government users, the precision is within 100 meters of the

receiver. In the configuration in place during the survey, the navigational precision was the same as the Loran-C system, on the order of 10 meters.

Loran-C utilizes the reception of radio signal from land based stations positioned in groups of 3 - 5 stations called a chain. A chain is established within specific geometric positions with one station designated as a master station and the others as secondary stations. The Loran-C receiver encodes the signals from the stations and computes the time delays (TD's) between signals arriving from the various stations. The intersection of two lines of constant time delay position (the Loran-C TD lines on navigation charts) is where the ship is located.

Shipboard Operations

Data were collected during a ten-day period in May 1992, between Larabee's Point and Chipman Point in the South Lake of Lake Champlain (Figures 1 and 2), and for two days in September 1993, near Fort Ticonderoga, NY and Mount Independence, VT. Two research vessels, *Neptune*, and Middlebury College's R/V *Baldwin* were used during this survey. Navigation on the R/V *Baldwin* was from Loran-C and GPS. Both recorded latitude and longitude of the ship's location approximately every four seconds onto the ship's computer. Only Loran-C was used on board the *Neptune* and its geographic position was logged every 8 seconds. This information was recorded and transferred to ARC/INFO Geographical Information Systems at Middlebury College where the ships' navigation tracks were plotted.

For the May 1992 survey, a dual frequency (100 and 500 kHz) Klein Digital Sonar System 590 (side-scan sonar) was used to cover 6 km^2 of the lake bottom to locate artifacts. Using a range of 37.5 m for each side, the total swath width was 75 m. The fish was towed approximately 5 to 10 meters behind the research vessel and the ship's speed was kept within 2 to 3.5 knots to maintain the fish's constant height, 4 meters, above the lake floor. These data were recorded on an TEAC RD-11T recorder, permitted replaying and post-processing of the data in digital format (see Flood, 1993).

The depth of the lake was determined every 2 seconds by a 200 kHz precision depth sounder; the average depth of the lake within the study area was 6.1 meters. The PDR data gathered on the R/V *Baldwin* was used to generate a three-dimensional model of the bathymetry of the entire survey area from Larabee's Point down to Chipman Point using Silicon Graphics' Interactive Surface and Volume Modeling program (Figure 5 in Hodson,

1993; 1995).

In addition to the side-scan sonar and PDR, a EG&G Geometrics 866 proton precession magnetometer was towed 33 meters (110 feet) aft of the navigation tracking antenna. It's depth was controlled by buoying the sensor to 3.05 meters (10 feet) below the water surface. The magnetometer's dual-trace analog print-out was operated on the 10/100 scale with readings taken every two seconds and automatically stored on a portable IBM compatible computer. All excess cabling for the sensor was coiled away from possible sources of electronic discharge, such as engines, other electronic cables, etc., to reduce background noise. Background noise was reduced below a ± 2 gamma variation. The short layback allowed the sensor depth to be tightly controlled.

One hundred transect lines, oriented predominantly north-south, imaged the study area (Figures 6-8 in Hodson, 1993; 1995). Some transect lines were repeated and some regions were imaged several times by overlapping track lines. This allowed cultural artifacts and sediment bedforms to be imaged at different angles permitting better interpretation of the bottom morphology as well as navigation correction.

For the two day field program in September 1993, five cores were taken on board the R/V *Baldwin* using a 3 meter Benthos piston corer. These cores were positioned using GPS and Loran-C. PDR profiles were collected at the piston core locations using three differing frequencies. Two echo-sounders were hull-mounted and had frequencies of 14 and 28 kHz. The third profiler, mounted along the side of the ship, was a 200 kHz narrow-beam, short-pulse echo-sounder. The 14 and 28 kHz profilers each had up to 10 meter penetration into the sediment whereas the 200 kHz system had 0.5 - 1 meter penetration. For all echo-sounding systems, no discernible subbottom reflectors were imaged, perhaps because of methane gas in the sediments.

Laboratory procedures on the cores included obtaining a magnetic susceptibility profile, after which they were split and described for color, grain size, and internal structure. All cores were X-rayed prior to splitting and the radiographs interpreted. One core (MIFT-05) was sampled in 2 cm intervals for the upper 50 cm and then in 5 cm intervals for the remainder of the core for radioisotope ^{210}Pb dating.

Observations

Side-scan sonar interpretation

A primary contribution of the side-scan sonar was locating and imaging numerous cultural artifacts (canal boats, drawboats, railroad trestle debris, Great Bridge caissons and iron cauldrons). Many of these observations are detailed in ancillary reports (Barranco, 1995; Cohn, 1995a; 1995b; Crisman, 1995). In addition, several significant bottom morphologies were identified: sediment waves, lineations, sediment furrows, and linear groups of pockmarks. For a complete summary of the side-scan interpretation see Hodson (1993, 1995).

Four sediment formations were identified within the survey area; these included pockmarks, lineations, sediment waves and sediment furrows. Each of these sediment structures has a distinctive image on the side-scan sonar records. Pockmarks are semi-circular depressions which are not created by an object protruding above the sediment. They image on a side-scan sonar as a circular or oblong shape with a semicircular band of black closest to the sonar fish (no acoustic energy being returned) next to a semicircular band of white farther from the sonar fish (acoustic energy returned from the farthest wall of the depression) (e.g. Figures 13-14). Lineations in sediments are formed by currents removing the finer-sized sediments and aligning the coarser sized material in the direction of the current. Lineations are imaged as parallel linear forms on side-scan records. Sediment furrows are long, narrow trough-shaped depressions that form parallel to the mean current direction (e.g. Figures 15-17). Sediment furrows differ from lineations in that they have sharp the well-defined trough walls. Sediment waves are regular undulations of the sediment surface which image as alternating dark and white areas on side-scan data. Sediment waves have wave crests and troughs which align perpendicular to the bottom current flow.

Most of the sediment waves are found in conjunction with the submerged cultural artifacts. Objects protruding from the lake floor, such as cultural artifacts, obstruct the normal bottom current and generate a flow which can create sediment waves. These waves are classified into two distinct groups by their size, orientation, and asymmetry. The height of the waves ranged from several centimeters to 0.5 meters, and the wavelength varied from 1 to 12 meters. The two groups had orientations of 65° and 175° (Plate B in Hodson, 1993; 1995). Some of the interpreted sediment waves may be acoustic artifacts from internal waves (see Figure 7 and discussion in digitized sonar images section below).

Around the inside bends of the lake surrounding navigational buoys 37 and 38, fields of sediment furrows have developed (Plate C in Hodson, 1993; 1995). They are approximately 15 to 50 cm deep, 2 meters wide, up to 600 meters long, and have an average spacing of 10 to 20 meters. Furrows are evidence of either a strong, stable bottom current in those regions or an strong, episodic current that erodes the bottom sediment. Like sediment waves, furrow can be used to determine the orientation of the bottom current flow. Two furrows often join to form one (termed a tuning fork) in the direction of the bottom flow responsible for furrow formation.

Along the underwater slopes of the lake there is evidence of either slumping or pockmarks. Pockmarks were imaged along a linear trend on the eastern slope of the lake, north of Mt. Independence. This northeast trend could be related to a subsurface fault that facilitates the upwelling of biogenic gas or groundwater into the lake (Plate D in Hodson, 1993; 1995). Several small gas vents (probably biogenic methane), were identified in the reprocessed sonar images (see Figure 21). However, no evidence of gas upwelling was documented coming from these pockmarks (see Figures 13-15) which suggests that these features may be formed by groundwater discharge into the lake.

From the orientations of the sediment bedforms, the direction of the bottom currents in the study area was estimated (Plate E in Hodson, 1993; 1995). The average bottom current movement in the southern section of Lake Champlain is to the north, following the local bathymetry (T. Manley, per. comm.). However, both sediment waves and furrows suggest bi-directional currents, as well as episodic events that are characterized by an increase in current speed. The cause of these stronger, bi-directional currents is unknown, but we speculate that it is either related to the main lake's internal seiche (Manley et al., 1993), or to the dynamics of the water where it flows around a bend in the lake, or a combination of the two processes.

Digitized sonar images

Selected side-scan sonar records were digitized and enhanced using image-processing techniques to better display both artifacts and natural features imaged by the sonar. Such image enhancement techniques permits sonar data to be interpreted more easily, allow more details to be resolved and therefore provides a better understanding of both artifacts and natural features on the lake bottom. The images displayed have strong returns as white or lighter color and acoustic shadows are dark. This is opposite from the paper field records. Compare Figure 16 (photograph of a field image) in Hodson (1993; 1995) to Figure 5 (Image 3 - digitized record) of this report.

Data acquisition and processing

Sonar acquisition and processing followed procedures similar to those utilized by Flood (1993) to image the bed of the Hudson River. Side-scan sonar data was recorded on magnetic tape using an 8-channel TEAC RD-11T tape recorder. This recorder digitizes 8 input channels at a frequency of 12 kHz per channel at 16-bit resolution for a frequency response of 0-5 kHz per channel. The digitized signal data is written on tape. When the tape is replayed, the recorded digital data is re-constituted into the eight analog signals. Six of these recorder channels were used. Recorded channels include 100 kHz sonar data (port and starboard channels), 500 kHz sonar data (port and starboard channels), the trigger signal, and an annotation channel. Selected portions of the recorded sonar data were replayed and digitized by a 12-bit digitizer board at a frequency of 11,905 Hz installed in a PC computer. The 12-bit digitized data is then reduced to 8-bit data as the digital sonar image is constructed. Both the 100 kHz and 500 kHz sonar data were digitized for the selected stations. The 100 kHz data provided the best image of the bottom during this survey, thus only the 100 kHz data are shown in this report.

The digitized sonar data were decimated using a median filter to reduce speckle noise and thus enhance sonar targets. Resolution of the image after decimation is approximately 0.24 m per image pixel in both the along-track and across-track directions. This resolution is adequate for resolving sonar targets with dimensions of 0.5 m and larger. Side-scan sonar data often displays a cross-track variation in signal intensity related to the beam pattern of the sonar and the changing angle at which sound reflects off the bottom. A correction (termed a "shading correction") was made for these systematic changes in signal levels by averaging the sonar data in the along-track direction and thus sonar targets (man-made and natural) are enhanced. No slant-range correction was applied to the sonar images to remove the effects of the water column on the sonar image. This correction is sometimes applied to sonar data when height of the sonar fish above the bottom is large and variable. For these images, fish height is not large enough in relation to swath width to warrant correction. Also, several of the sonar targets of interest rise significantly above the lake bed, and thus a slant-range correction will not make the image easier to interpret.

The digitized sonar data were merged with available navigation data to determine the approximate position of the sonar images in the lake and the speed over the ground. This speed information is needed to produce a sonar image where scales in the along-track and across-track direction are the same. Our processing efforts focused on a portion of an individual sonar swaths (with dimension of 75 m wide by about 50 to 100 m long) that

showed distinct features.

To process the images, navigation data were converted to a local coordinate system determined as distance in feet north and east of 43° N, 74° W.

North distance = (Latitude - 43) * 364,560 feet/degree
East distance = (Longitude - 74) * 364, 560 feet/degree * cos (43.8°)

No corrections have been applied to the Loran-C navigation data to correct for any local offsets between Loran-C and actual positions.

A total of 24 images have been produced from 23 record sections. Table 1 lists the times and locations of the sonar images. Figures 1 and 2 show the location of the sonar images along with relative shoreline positions. The sonar images themselves are shown in Figures 3 to 26. Two copies of sonar Image 24 are shown (Figures 25 & 26). Figure 26 shows the data as processed by the techniques described above. Additional processing was applied to the same sonar record to minimize the importance of black streaks caused by digitization errors (Figure 25). The format of each image is the same. The processed sonar record is shown in the center of the figure with the ship-track in the center of the image. The direction of ship motion is from the bottom to the top of the image. The along-track and across-track scales are the same for all images. To the left of the sonar record is a gray scale. Strong sonar returns are shown as white on these images and weak sonar signals (including sonar shadows) are shown as dark or black. The gray scale has a scaled width of 10 m and length of 50 m. To the right of the image is a line that represent the local north direction. This direction was determined from the navigation data, and the arrow represents a line 15 m long.

Images 1- 9 (Figures 3 - 11) are in the vicinity of the row of caissons that anchored the "Great Bridge" from Mount Independence, VT to Fort Ticonderoga, NY. Images 16-19 (Figures 18-21) are in the vicinity of the Addison Company railroad trestle which connected Vermont and New York. Images 10-15 (Figures 12-17) are located between these two locations and Images 21-24 (Figures 23-26) are south of the caissons near to navigational buoy 40.

Sonar image processing has substantially increased the quality of the sonar images analyzed. Comparing analog records with the digitized processed ones, a better discrimination is made between man-made artifacts, natural features, and disruptions

caused by sound diffraction in the water column. The following comparisons can be made between the figures shown here and those of Hodson (1993; 1995).

Analog (Hodson; 1993; 1995)	Digitized	Feature imaged
Figure 10b	Figure 19 (Image 17)	Broken piece of 1888 drawboat
Figure 10a	Figure 20 (Image 18)	Broken 1888 drawboat sections stacked
Figure 11	Figure 12 (Image 10)	Canal boat
Figure 16	Figure 5 (Image 3)	Caissons
Figure 21	Figure 13 (Image 11)	Pockmarks
Figure 26	Figure 16 (Image 14)	Furrows

Features observed on the images include both man-made artifacts and natural features. Caissons are observed in Figures 3-6 and 8-11 (Images 1-4 and 6-9). Sunken canal boats are observed in Figures 12, 22, and 24-26 (Images 10, 20 and 22-24; Images 22, 23 and 24 are of the same canal boat). Figure 22 (Image 20), located south of Larabee's Point at Beadles Cove, shows two canal boats situated side by side. Due to the orientation of the towed sonar fish to these vessels, the image seems to show only one distinctive feature. Debris associated with the railroad crossing is observed in Figures 18-21, including the sections of the 1888 floating drawboat (Figures 19 and 20; see Barranco, 1995 for full discussion). Several mounds are seen in this area that may have been related to the railroad trestle, and there is debris in some areas (e.g. Figures 18 and 21). Natural features observed include pockmarks (depressions in sediment often associated with the venting of fluids or gas; Figures 13-14 and 23, furrows (linear bedforms thought to be developed as currents flow through the lake (Figure 14-17), and local and regional changes in sediment reflectivity probably related to grain-size changes (e.g., Figure 17 shows a boundary between higher and lower reflectivity sediments). Features are also observed in the water column, possibly gas venting from the sediments, although not from pockmarks, in Figure 21. Gas vents are characterized by strong reflections in the water column and prominent shadows cast on the lake bed behind the gas-charged water. The images in many areas are somewhat distorted by sound diffraction's by internal waves (e.g., Figure 7). These wave patterns, caused by irregular temperature (and thus sound velocity) changes in the water column,

produce an imprint over reflectivity patterns from sediments and/or artifacts.

Image descriptions

Image 1 (Figure 3) shows the Vermont end of the row of caissons. The reflective zone in the southern portion of the image is the shallow zone near the shore. Two caissons (Caisson 2 and 3 described by Crisman, 1995) about 5-8 m on a side are observed trending to the north. The center of the image shows a reflective zone in the water column that casts a prominent shadow. This is probably a series of 5 large upright logs (up to 3.8 m above the mudline) identified ~20 m south of Caisson 2 (Crisman, 1995).

Image 2 (Figure 4) shows a north-south row of 5 caissons (Caissons 2 - 5; Crisman, 1995) near the Vermont shore of the lake. Shadows behind the caissons suggesting that they protrude above the bottom. The weak "diamond" pattern near the edge of the image is probably due to sound refraction in the water column.

Image 3 (Figure 5) shows a north-south row of 4 caissons (Caissons 5 - 8; Crisman, 1995). Some of the caissons (Caissons 7 and 8) have no shadows, suggesting that they have little relief. Crisman (1995) found for these two caissons that ballast rocks protruded up to 91 cm above the sediment. Caisson 8 appeared tipped with the south side 1.2 m above the mudline. A reflection is also observed about 50 m to the southwest of the southernmost Caisson 5. This target is also observed on Image 2, suggesting that the southern two caissons of Image 3 are the same as the northern two caissons of Image 2. The lineated north-south reflections are probably due to sound diffraction in the water column.

Image 4 (Figure 6) shows a north-south row of 3 caissons. While the precise location of this image is uncertain, the image appears to show the same caissons as Image 3 (Caissons 5 - 7, Crisman, 1995). However, the most northern caisson is obscured by a prominent reflection that appears to be caused by sound diffraction within the water column.

Image 5 (Figure 7) collected southwest of and immediately before Image 4 shows a prominent field of northeast-southwest lineations. Because of the association with the features in Image 4, these lineations appear to be caused from internal waves in the water column and are not sediment waves on the lake bottom.

Image 6 (Figure 8) shows a north-south row of 4 or perhaps 5 caissons which have little relief. These caissons are located north of those in Images 3 and 4. Most likely these

correspond to Crisman's caisson numbers 10 - 13. Caisson 10 has all 4 sides exposed above the lake bottom whereas caissons 11 - 13 only have ballast stones above the mudline (Crisman, 1995).

Image 7 (Figure 9) also shows 4 caissons (Caissons 11 - 14; Crisman, 1995). A prominent, thin shadow zone occurs at the western end of the most northern caisson. Diver verification of this caisson documented three unattached logs, one of which was jammed diagonally into the lake bottom and protruding ~ 5m of its length above the sediment. It is possible that this log is producing the shadow zone near the northern caisson on the side-scan image.

Image 8 (Figure 10) shows 4 caissons (Caissons 14 - 17; Crisman, 1995) near the northern end of the row. The caisson immediately south of the center of the image appears to have two parts. Lake sediment has covered the central section of the caisson. Crisman (1995) noted that Caisson 15 consisted of two separate piles of ballast rocks with mud between them. Caissons 16 - 17 only showed a few ballast stones above the lake bottom and hence appear less reflective. The wave-like features on the northern edge of the image may be caused by sound diffraction in the water column.

Image 9 (Figure 11) is near the New York shore. Other irregular targets associated with the nearshore sediments and the shoreline are observed. Three caissons were imaged and most likely correspond to Caissons 19 - 21 (Crisman, 1995).

Image 10 (Figure 12) shows a canal boat resting on the lake bed. The shadow zone shows that the boat extends above the lake bed. Some of the internal structures of the boat are also seen.

Image 11 (Figure 13) shows a row of pockmarks near the western shore of the lake. No evidence of gas venting is seen. This row of pockmarks may be associated with the edge of the finer-grained sediments in the lake.

Images 12 and 13 (Figures 14 and 15) Image 12 is continuous with Image 13 which is the more northerly of the two. Image 12 (Figure 14) shows a row of pockmarks north of Image 11 (Figure 13). Lineated sedimentary features extend northeast-southwest near these features. These features become better defined on Image 13 (Figure 15) as furrows. Three pockmarks seem to be located in the trough of a furrow on Image 13. A strong reflection with a diffraction pattern on the southern side of Image 13 is navigational buoy 38.

Image 14 (Figure 16) shows northeast-trending furrows along the western side of the lake. Two furrows join to form one (termed a tuning fork) towards the northeast. Studies in other areas have suggested that furrows join in the direction of the bottom flow responsible for furrow formation (Flood, 1983). This suggests dominant flows to the northeast at this site. The change in sediment reflectivity from high in the northwest to low in the southeast is probably related to finer sediments accumulating in the central portion of the lake here.

Image 15 (Figure 17) also shows furrows near the western shore of the lake.

Image 16 (Figure 18) is at the New York end of the Addison Company railway. There is a shallow area at the western edge of the image near the shore, and a mound is present at the middle of this shallow area. This mound may have been used to anchor the railroad trestle. Other debris can be observed on the bottom. In particular, a log-shaped feature is present in the southeast part of the image.

Image 17 (Figure 19) contains a section of the 1888 floating drawboat associated with this railway (see Barranco, 1995). Some of the internal structure of the trestle can be observed sticking out of the mud. A more reflective part of the image west of the track is a mound possibly associated with this drawboat system. This portion of the 1888 drawboat lies within the former draw opening.

Image 18 (Figure 20) is the larger section of the 1888 drawboat (see Barranco, 1995). The broken sections of the drawboat are stacked upon each other. A dark streak trending to the east in the center of the image may be caused by gas venting from the lake bed.

Image 19 (Figure 21) shows a mound on the western portion of the image (related to the railway) along with several clearly defined gas plumes. As with other images, these gas plumes do not appear to be associated with pockmarks.

Image 20 (Figure 22) is north of the railway near the north point of Beadles Cove on the Vermont shore. This target has been confirmed to be two canal boats resting side by side (Barranco, 1995). The aspect angle the sonar fish had with respect to these canal boats was such that they were not well distinguished. The bright targets to the west of the track appear to be caused by internal waves diffractions.

Image 21 (Figure 23) is from the western shore of the lake to the south of the caisson area. A prominent row of pockmarks is present here, again apparently at the edge of the potentially finer-grained sediments that fill the central portion of the lake. The along-track banding observed on this and Images 22-24 (Figures 24-26) apparently is instrument noise.

Image 22 (Figure 24) is of a canal boat partially buried in the sediment. This boat is about the same width but appears shorter than the boat in Image 10. The difference in length may be in part due to inaccuracies in navigation. Image 22 is the same boat found in Images 23 and 24.

Images 23 and 24 (Figures 25 and 26) are the same image with different levels of processing applied. Image 24 is processed identically to Images 1 - 22, although additional steps have been used on Image 23 to remove the horizontal black lines that result from improper tape replay on Image 24. This replay problem only affected this image and not the other images displayed. Both images are included here because Image 24 shows more detail in the boat even though the image has missing data. Some of the internal structure of the vessel can be observed. The boat appears wider here than on Image 22 due to navigational uncertainties.

Magnetics

The magnetic survey done within the project region shows the bottom of Lake Champlain to be magnetically complex. Sixty-six anomalies were determined within the survey region (Table 2). While some regions of the survey were entirely devoid of anomalies, other areas showed magnetic signatures, both monopole and dipole, indicative of significant cultural artifacts. Of the magnetic anomalies identified, only those with values which deviated from the ambient field by more than 100 γ appear associated with large cultural artifacts (canal boats, drawboats, railroad trestles - Table 2). The smaller anomalies (< 100 γ) often can not be correlated with any significant object(s) in the side-scan sonar records. It should be noted that low or the absence of anomalies are not a guarantee of the absence of cultural resources. The magnitude and polarity of the magnetic signature is dependent on the distance and orientation of the transects to the cultural object(s). Also, a cultural object(s) composed of material having little or no magnetic character would not produce a magnetic anomaly.

Canal boats are easily identified by magnetic anomalies (Table 2, Figures 27-28). Figure 27 shows two magnetic transects near the canal boat imaged by side-scan sonar (Figure 12). One survey was taken from southwest to northeast along the center line of

Figure 12 (Image 10) and the other was located 10 m to the west of this line. These two transects show dissimilar magnetic anomaly signatures. This is due to the distance and orientation of the transects to the canal boat. Similarly, another submerged canal boat, located south of navigational buoy 39 (Figure 24 - Image 22) shows a even different magnetic signature (Figure 28). In both cases the magnitude of the anomalies (100 -160 γ) clearly identify the canal boats whereas, the magnetic anomaly shape indicates that there is a concentration of magnetic material at one end of the vessel. In the case of the canal boat of Image 10, the magnetic content appears to be concentrated at the northern end of the vessel near the bow. For the canal boat of Image 22 the magnetic content is located at the eastern end also at the bow. This magnetic concentration may correlate to the windlass which was used to haul up the anchor at the bow of the canal boats (Cohn, pers. comm., 1995).

The magnetic survey near the Addison Company railroad crossing (Barranco, 1995), gave a more complex pattern (Figure 29). This transect followed the railway right of way and defined its salient features. Magnetic material (presumably iron) is scattered along its length in small concentrations. The areas with the greatest amount of iron are located near each shore, where numerous debris has been identified by side-scan sonar. The large anomalies near the western end of the transect, can be correlated with the locations of the broken 1888 drawboat sections and a 9 m^2 timber crib associated with the trestle. The middle of the channel is relatively free of magnetic material. This seems consistent with the use of this right of way having a fixed wooden railroad trestle with a moveable wooden drawboat portion (Barranco, 1995).

Four iron cauldrons (large enough for a diver to stand inside) were found near the Ticonderoga Creek delta. Original located by side-scan sonar by as a strong hyperbolic signal, the identification of them could only be done by a diver (Cohn, 1995a). These cauldrons showed a very abrupt and strong magnetic signature (Figure 30) only when the magnetic sensor was extremely near to these features. These cauldrons produced the largest magnetic anomaly (800 γ) seen in the survey area.

The magnetic survey line located 10 meters north of the "Great Bridge" is generally devoid of anomalies (Figure 31) until close to the western (New York) shoreline. Numerous N-S crossings were made near the caissons of the "Great Bridge" and usually there was associated with the caisson a small anomaly (~30-50 γ - Table 2). This reflects the relative paucity of iron used in the construction of the individual caissons. However a few large anomalies (> 293 γ) were associated with some of these caissons. Iron anchors were found caught on several of the submerged caissons (Crishman, 1995). Those caissons

which were associated with large magnetic anomalies had anchors and anchor chains located near them. A large magnetic anomaly (400 γ) at the western end of the "Great Bridge" survey (Figure 31) occurs near Caisson 19. This caisson had a large wooden-stocked iron anchor as well as an unidentifiable iron object (2' X 1.5'X 2"~dimensions) near it (Crisman, 1995).

Cores

Core description

Five piston cores were taken in a transect starting from the Vermont shore towards the central channel near the caissons (Figure 1). The cores varied from 113 cm to 214 cm in length (Figures 32-41). Magnetic susceptibility profiles were run on the whole cores and then they were split and visually described (Figures 32-41). No significant layering was observed though there were three dominant color changes. All cores contained sections of olive gray color (5 Y 4/1), dark greenish gray color (5 GY 4/1) and in the near surface, laminae of olive black color (5 Y2/1). Silt-sized material existed throughout the cores with the exception of layers of organic material (MIFT-02, 46 cm downcore; MIFT-03, 12 cm downcore -pine needles), wood chips (MIFT-02, 90 cm downcore; MIFT-05, 165-210 cm downcore) and spent-fuel clinkers (MIFT-03, 3-9 cm; MIFT-04, 30-41 cm; 49-64 cm downcore). All cores showed signs of bioturbation and contain sediment only from the recent Lake Champlain period (10.2 kabp to present). Radiographs of cores (Figures 33, 35, 37, 39, 41) show bioturbation throughout most of the core. However a distinct interval of laminations exists in all cores, approximately 15 cm thick. These laminations were not easily recognized (or seen at all) in the visual inspection of the cores. Individual laminations are ~3-5 cm thick and alternate from dark to light color on the radiograph. The significance of these laminations is discussed later.

Radiometric Dating

Core MIFT-05 was analyzed for ^{210}Pb activity to derive a sedimentation accumulation rate (Table 3, Figures 42 and 43). This core was located near Caisson 2 on the Vermont side of the survey region and was sectioned in 2 cm intervals for the upper 50 cm, and then in 5 cm intervals to the base of the core at 200 cm. Wet and dry weights were obtained from the sectioned intervals and porosity was calculated from these measurements using an assumed sediment grain density of 2.5 g/cm^3. Sediments were analyzed for ^{210}Pb by alpha spectrometry as well as selected samples for ^{230}Th activity. Measurement of the activity of ^{230}Th in 4 samples was determined to additionally estimate the amount of supported ^{210}Pb activity.

To resolve the total ^{210}Pb activity into its supported and unsupported components, we assumed that the ^{226}Ra was uniform with depth. Thus the ^{210}Pb activity deep in the core should be in equilibrium with ^{226}Ra. This value was determined to be 2.2± 0.1 dpm/g (dpm - disintegration's per minute). The ^{230}Th activities ranged between 2.1 and 2.3 dpm/g, and are consistent with the deep ^{210}Pb levels. Subtracting this ^{210}Pb activity, determined deep in the core, from the measured values gave the unsupported ^{210}Pb activities (Table 3). With the removal of the supported ^{210}Pb from the total ^{210}Pb analyzed, core MIFT-05 had extremely low unsupported ^{210}Pb activity. In comparison, the ^{210}Pb activities in Canadian Shield lake studies were two times larger (Anderson et al., 1987). The low ^{210}Pb inventory in the Lake Champlain core is due to either 1) lost of the surficial sediments in coring, 2) the sediment mass accumulation rate here is extremely large (R.A. Anderson, LDEO, per. comm., 1994) or 3) sediment has been lost by winnowing and transport elsewhere.

Besides having a low inventory, the unsupported ^{210}Pb profile is concave downward, which is opposite of the curvature normally observed in ^{210}Pb profiles. As the biota homogenize the sediment, the unsupported ^{210}Pb is spread out through a mixed layer. This combined with a decrease in porosity with depth causes the ^{210}Pb profile to decrease less steeply near the top of the core than at depth resulting in a profile that is concave upward. In the MIFT-05 core, the steepest decrease is near the top suggesting that either sediment mass accumulation rates have been declining over the past decade or that there was compression of the deeper sediments during the coring procedure (R.A. Anderson, LDEO, per. comm., 1994). Of interest, the International Paper company constructed a modern mill between Crown Point and Ticonderoga in 1968. The effluent, which was discharged into the Ticonderoga Creek (slightly south of survey area) since the 1880's, is now located to the north nearer Crown Point. It has been estimated that ~1,236,000 m^3 of paper waste was discharged into the Ticonderoga Creek (King, et al., 1993). Thus there has been a decrease in input to this area over the last 20 years which appears to be reflected in the concave profile.

Using measured porosity and assuming a sediment density of 2.5 g/cm^3, the inventory of unsupported ^{210}Pb is 14.5 dpm/cm^2. Under steady state conditions this is equivalent to a flux of ^{210}Pb from the atmosphere of 0.45 $dpm/cm^2/yr$. This is half of what should be expected for the atmospheric flux of ^{210}Pb in this geographic region (R.A. Anderson, LDEO, per. comm. 1994). Once again, this implies that the coring failed to recover the surface-most sediments or that the site has lost some of its sediment by winnowing and transport elsewhere.

The derived sediment accumulation rates from this data have some uncertainty due to the low unsupported ^{210}Pb activity. Since the derived sediment accumulation rate is sensitive to the amount of supported ^{210}Pb activity, a series of slightly differing values for supported ^{210}Pb were used (Figure 44). Annual rate of accumulation is obtained by taking the decay constant of ^{210}Pb (3.11×10^{-2}/yr) and dividing by the slope of the best fit line of the ln (^{210}Pb) vs. depth plot (Figure 44). These calculations assume a constant accumulation rate or a constant flux of ^{210}Pb. The accumulation rate, as determined from MIFT-05, was 0.7± 0.2 cm/yr. A higher accumulation rate of 0.93 cm/yr is determined for a supported ^{210}Pb level of 2.1 dpm and a lower accumulation rate of 0.55 cm/yr is determined for a supported 2.3 dpm. Using this information with the magnetic susceptibility data (section below), an average value of 0.5 cm/yr has been used for this core.

Magnetic susceptibility and Core Interpretation

Calculating the downcore depth for MIFT-05 using 0.5 cm/yr gives an age of 1780 for the kick in the magnetic susceptibility profile at 105 cm and the change of slope at ~100 cm for the total supported ^{210}Pb profile (Figures 41 and 42). This agrees well with the European settlement of this area ~ 1760. Work by King et al. (1993) on other cores from Lake Champlain, show that the magnetic susceptibility increases dramatically when settlement began in the Champlain basin. This is due to the deforestation and increased erosion which subsequently occurred. In addition, magnetic susceptibility decreases after the 1900's as local forest clearance ceases and a higher organic input occurs into Lake Champlain (King et al. ,1993).

Using an accumulation rate of 0.5 cm/year, we can estimate dates for specific patterns seen in the magnetic susceptibility profiles (Figures 41 and 45). At 167-190 cm downcore, the magnetic susceptibility profile of MIFT-05 shows a slight increase. This increase relates to a time period from approximately 1600 to 1700. The core material in this section is a silty sand and has a higher percentage of rock fragments. The increase of quartz, sand-size minerals and rock fragments suggests a period of increased erosion. The Little Ice Age, a climatic fluctuation occurring between 1600-1800, is a period of enhanced erosion which may have caused more rock fragments to be deposited within Lake Champlain. An alternate hypothesis for this layer is that this unit (23 cm thick), is some form of mass wasting event (slump, etc.) The radiograph of MIFT-05, shows a sharp contact for the top of this feature at 167 cm (Figure 41). The only other core which was long enough to reach this layer was near the central channel, MIFT-04 (Figure 39 and 45). At 178 cm downcore, a 5 cm layer is found which also contains an increased amount of rock fragments. This suggests

that if this was a mass wasting event, it dissipated as it worked its way out into the central region of the area, depositing a smaller layer.

Radiographs have shown a laminated section present in all cores. The laminations are approximate 3-5 cm thick alternating from dark to light, and occur in a ~15 cm layer which was consistently located ~40 cm above the 1780 interface (Figure 45). Using a 0.5 cm/yr accumulation rate, this layer was deposited over a time period of 20-25 years. The layer seems to correlate to a time period of 1860 to 1880 for MIFT-05.

We can correlate the five cores by using the magnetic susceptibility profiles (Figure 45). Using the characteristic increase in magnetic susceptibility, which corresponds to the early settlement of the Champlain basin circa 1780, we observe that this age horizon is nearer the sediment-water interface in some cores than others. It is apparent that significant portions of the sediment column above 5 cm in MIFT-03 are missing. This may indicate that sediment is being removed through erosion or lower sedimentation rates have occurred here. The MIFT-03 core is near the central channel within the lake and near Caisson 12 (Crisman, 1995), where a diver experienced water movement along the lake bottom caused by the wake of a passing motor boat. This suggests that within the central channel lower sedimentation rates may occur due to enhanced sediment movement due to surficial boat traffic or natural processes.

The only other cores to show significant increases in magnetic susceptibility are MIFT-03 and MIFT-04. A large increase in magnetic susceptibility occurs at 3-9 cm downcore in MIFT-03 and 30-41 cm, 49-64 cm in MIFT-04. Radiographic images for both cores show an increase number of fragments in these intervals. In both cores within these intervals, spent fuel known as *clinkers* was found. Clinkers are generally associated with the steam driven vessels which dominated on Lake Champlain during the 1800's. Using the same accumulation rate as determined from MIFT-05 (0.5 cm/yr), the clinker layer dates around 1860-1880 for the lower clinker layer in both cores. This is consistent with the period of most common steamboat traffic occurring on Lake Champlain. The occurrence of the 1880 interface within 5 cm of the lakebed surface in MIFT-03 suggests that post 1880's sedimentation rates are variable. The shallower clinker layer in MIFT-04 (30-41 cm), correlates to a time period in the early 1920's. In cores MIFT-03 and MIFT-04, the laminated section directly underlies the lowermost clinker layer. Since the cores are bioturbated above and below this section, this laminated region suggests that the benthic community was dramatically reduced or absent or that very high sedimentation rates occurred such that the benthic community did not disturb the laminae. A few burrow tracks are seen within the laminated section. The varved nature of this layer suggest that climatic control

also may be a an important factor. The correlation of the laminae layer between cores (Figure 46), suggests a uniform sedimentation prior to 1880, and one which was highly variable after 1880 particularly those cores in the central portion of the channel. Heavy boat traffic through the central section of the channel may have affect the sedimentation rates for this period of time.

Conclusions

Reconnaissance of the south lake between Larabee's and Chipman Points has shown that significant cultural artifacts can be located using geophysical techniques. Insights into lake bed processes can also be gained through this type of study. Thus we have augmented our understanding of the cultural and geologic history for this region of Lake Champlain. With the use of the side-scan sonar and magnetometer, cultural artifacts were systematically located and identified within a 6 km^2 region. Man-made artifacts whose images have been enhanced by this study include caissons, railroad bridge artifacts (drawboats) and sunken canal boats. Several other less well resolved targets (e.g., the feature in the southern corner of Figure 5 (Image 3), probably represent buried features. The existence of enhanced images of these man-made artifacts and of natural features in this part of the lake will significantly increase the scientific and public awareness of the significance of this kind of environment.

In addition to the discovery of several significant historical wrecks (see Barranco, 1995; Cohn, 1995a; Crisman, 1995), the bottom morphology of this region was mapped and interpreted. With the absence of hydrographic monitoring, we can use sedimentary bedforms, which have developed with respect to long term dominant bottom flow conditions, to determine flow patterns. Specific bedforms identified within the survey area include sediment waves, sediment furrows, pockmarks and lineations. Analysis of these features suggest that this part of the south lake is dominated by a south to north flow but that there is a strong southerly component as well. This southerly component we interpret as being the internal sieche which exists and dominates within the main lake (Manley et al., 1993; Manley and Manley, 1993; Saylor et al., 1993). The cultural artifacts themselves appear to be catalysts for the initiation of some sediment bedforms as sediment waves appear most developed around them and bend around them.

Large pockmarks appear near the edges of the lake bed, suggesting that possible sediment deformation associated with compaction may have helped to localize them in this area. Pockmarks found within this region maybe groundwater conduits since these features do not show any signs of gas venting. Possible gas venting is observed on several images. This gas is most likely methane produced during the decay of organic matter. The

localized venting suggests that studies of gas flux to the atmosphere based on water-samples alone may have underestimated the flux of this important green-house gas to the atmosphere. Venting of gas also suggests gas-charged sediments. This would be consistent with the lack of good subbottom profile data in this are because gas-charged sediments stop sound penetration before subbottom layers can be detected.

Core analysis shows that the sampled material is confined to recent sedimentation. The accumulation rate within this region is approximately 0.7± 0.2 cm/yr. A rate of 0.5 cm/yr seems to be most consistent with the likely age of the clinker layers (MIFT-03 & MIFT-04) and the onset of European settlement. Using this rate, two cores sampled material dating back into the 1600's (MIFT-04 & MIFT-05). This rate appears to be uniform up until the 1880's and then becomes more variable. This change in sedimentation rate may be related to an increase in lake traffic with the opening of the canals to the north and south of Lake Champlain. Increased boat traffic may reduce sedimentation accumulation in the central channel as sediment is disturbed by passing boats. These cores also provide us information about past conditions during the early stages of European settlement. Two cores have retrieved sediments dated tentatively around 1600. Cores such as these or longer may allow us to investigate further back in time.

The implications for cultural artifacts in this region is that these significant historical locations will continue to affect the bottom flow conditions until they are covered by sediments. The timing of their coverage is speculative but assuming a constant rate of 0.5 cm/year, this implies that in 200 years, 1 meter (3 feet) of sediment will have been deposited. Thus it will be on the order of 500 to 1,000 years before the largest artifacts will be covered by natural sedimentation. Those artifacts which are located in regions of active bottom currents or in high boat traffic areas will require a longer time period.

References

Anderson, R. F., S. L. Schiff and R. H. Hesslein, 1987. Determining sediment accumulation and mixing rates using ^{210}Pb, ^{137}Cs and other tracers: Problems due to post depositional mobility or coring artifacts. *Canadian J. of Fisheries and Aquatic Sci.*, v. 44 Supplement 1, p. 231-250.

Anderson, R. F., W. Q. Fleisher and P.L. Manley, 1993. Uranium-series tracers of mud wave migration in the Argentine Basin. *Deep-Sea Research. II*, v. 40, p. 889-909.

Barranco, Jr., A. Peter, 1995. Ticonderoga's floating drawbridge: 1871-1920. Lake Champlain Basin Program, Demonstration report 4E.

Chase, J. S. and A. S. Hunt, 1972. Sub-bottom profiling in central Lake Champlain - A reconnaissance study. *Proc. 15th Conf. Great Lakes Res.*, p. 317-319.

Cohn, A., 1995a. The Fort Ticonderoga - Mount Independence 1992 submerged cultural resource survey: Executive summary. Lake Champlain Basin Program, Demonstration Report 4A.

Cohn, A., 1995b. The Great Bridge "From Ticonderoga to Independence Point". Lake Champlain Basin Program, Demonstration Report 4C.

Crisman, K., 1995. The 1992 Mount Independence underwater archaeological survey. Lake Champlain Basin Program, Demonstration report 4B.

Flood, R. D., 1993. Sediment data from the Hudson River between Bakers Falls and Lock 5. for *Hudson River PCB Reassessment RI/FS, EPA Work Assignment 013-2N84, EPA Contract No. 68-S9-2001,* for *TAMS Consultants, Inc., TAMS Subcontract NO. 5213-01,* September, 1993.

Flood, R. D., 1983. Classification of sedimentary furrows and a model for furrow initiation and evolution. *Geological Society of America Bulletin*, v. 94: 630-639.

Hodson, H., 1993. Bottom morphology and boundary currents of southern Lake Champlain: Larabee's Point to Chipman Point: Unpublished senior thesis, Middlebury College, Middlebury, VT, 51p.

Hodson, H., 1995. Bottom morphology and boundary currents of southern Lake Champlain: Larabee's Point to Chipman Point: Lake Champlain Basin Program, Demonstration report 4F.

King, J., E. Mecray, P. Gangemi, C. Gibson, A. Hunt, P. Appleby, and J. Boucher, 1993. The History of trace metal and nutrient contamination recorded in the sediments of Lake Champlain. Technical Report - University of Vermont, 74p.

Manley, P. L. and T. O. Manley, 1993. Sediment - current interactions at Valcour Island, Lake Champlain - A case of helical flow in the bottom boundary layer. *Northeastern section GSA* March 1993, p. 36.

Manley, P.L., L. Fuller, and J.K. Singer, 1992. Bottom morphology and environmental implications for the Buffalo Lake: Evidence from side-scan sonar. *International Association for Great Lakes Research, Program and Abstracts.*

Manley, T. O., P. L. Manley, J. Saylor, and K. L. Hunkins, 1993. Lake Champlain hydrodynamic monitoring program - An overview. *Northeastern section GSA* , March 1993, p. 61.

Saylor, J., T. O. Manley, P.L. Manley and J. Miller, 1993. Physical processes driving high-speed currents in Lake Champlain bottom water. *Northeastern section GSA* , March 1993, p. 76.

Teller, J. T., 1987. Proglacial lakes and the southern margin of the Laurentide Ice Sheet, in Ruddiman, W. F., and Wright, H. E., Jr., North America and adjacent oceans during the last deglaciation. Geological Society of America, *The Geology of North America,* Boulder, Colorado, v. K-3., p. 39-69.

Table 1

Location of Processed Sonar Images and Core Locations

Image Number	Date	Time† (hhmn:ss)	Local Coordinate* (East)	(North)	Latitude+ (North)	Longitude+ (West)	Course‡
1	20 May 92	1117:22	162645	304656	43°50.14'	73°22.91'	225
2	20 May 92	1124:34	162694	305023	43°50.20'	73°22.90'	055
3	20 May 92	1151:52	162666	305287	43°50.24'	73°22.91'	235
4	19 May 92	1724:45	162380	305063	43°50.21'	73°22.97'	045
5	19 May 92	1723:51	162156	304820	43°50.17'	73°23.02'	040
6	20 May 92	1519:54	162539	305710	43°50.31'	73°22.94'	230
7	20 May 92	1532:36	162553	305756	43°50.32'	73°22.93'	060
8	20 May 92	1554:42	162498	305913	43°50.35'	73°22.95'	230
9	20 May 92	1609:15	162486	305874	43°50.34'	73°22.95'	060
10	20 May 92	1146:36	163916	306159	43°50.39'	73°22.62'	225
11	20 May 92	1133:02	164773	306729	43°50.48'	73°22.43'	060
12	20 May 92	1612:22	163306	306549	43°50.45'	73°22.76'	050
13	20 May 92	1613:04	163559	306731	43°50.48'	73°22.70'	050
14	20 May 92	1712:37	163700	307038	43°50.53'	73°22.59'	000
16	20 May 92	1700:49	164006	309173	43°50.88'	73°22.60'	355
17	20 May 92	1746:03	164477	309220	43°50.89'	73°22.49'	190
18	20 May 92	1808:52	164732	309407	43°50.92'	73°22.44'	355
19	20 May 92	1807:50	164752	309011	43°50.86'	73°22.43'	000
20	20 May 92	1922:24	164689	310296	43°51.07'	73°22.45'	320
21	22 May 92	1237:42	158801	298831	43°49.18'	73°23.79'	020
22	22 May 92	1308:59	161892	296646	43°48.82'	73°23.08'	140
23	22 May 92	1621:52	162216	296673	43°48.83'	73°23.01'	070
24	22 May 92	1621:52	162216	296673	43°48.83'	73°23.01'	070
Cores							
MIFT 01	16 Sept. 93	1010:00	162787	304833	43°50.17'	73°22.88'	---
MIFT 02	16 Sept. 93	1112:00	162874	304954	43°50.19'	73°22.86'	---
MIFT 03	16 Sept. 93	1305:00	162655	305562	43°50.29'	73°22.91'	---
MIFT 04	16 Sept. 93	1357:00	162743	305684	43°50.31'	73°22.89'	---
MIFT 05	16 Sept. 93	1458:00	162918	304894	43°50.18'	73°22.85'	---

†calculated for approximate center of image displayed.

*Local coordinates are in feet North of 43° N and East of 74° W for approximate center of image.

+Position in Loran-C coordinates. No correction made for any possible Loran-C offset.

‡Course calculated from navigation data.

Table 2

Magnetic Anomalies

Line #	Duration *	Length (M)	Field strength ‡ (γ)	Description	Notes
1	11:12:21 - 11:12:33	21.6	+54	Monopole	
	11:16:49 - 11:17:47	104.4	-358/+29	Dipole	nearshore (Figure 3)
2	11:24:07 - 11:24:51	79.2	+389/-34	Dipole	Caisson 2 (Figure 4)
3	11:46:57 - 11:47:29	57.6	-50	Monopole	canal boat (Figure 12)
5	15:17:01 - 15:17:11	18	+25	Monopole	
	15:22:35 - 15:23:03	50.4	-56/+156	Dipole	
6	15:39:05 - 15:39:15	18	+13	Monopole	
7	15:48:47 - 15:48:59	21.6	-6/+25	Dipole	
8	16:09:53 - 16:10:19	46.8	-30	Monopole	Caissons 19 - 21(Figure 11)
9	17:01:15 - 17:01:35	36	+59/-59	Dipole	Off Ticonderoga Light
10	17:13:05 - 17:13:31	46.8	-12/+18	Dipole	
	17:20:43 - 17:20:53	18	-6/+11	Dipole	
	17:22:03 - 17:22:15	21.6	+24	Monopole	
11	17:37:33 - 17:38:05	57.6	+162/-185	Dipole	railroad debris
12	17:46:07 - 17:46:27	216	-39/+12	Dipole	drawboat (Figure 19)
13	18:08:13 - 18:08:27	25.2	+20	Monopole	railroad mound (Figure 21)
	18:09:11 - 18:09:47	64.8	+87/-235	Dipole	stacked drawboat (Figure 20)
14	18:19:11 - 18:19:31	36	-17	Monopole	railroad debris
	18:20:33 - 18:21:01	50.4	+35	Monopole	railroad mound (Figure 21)
	18:48:17 - 18:48:37	36	+13/-17	Dipole	railroad debris
15	18:55:45 - 18:56:16	54	-10	Monopole	railroad debris
16	19:19:37 - 19:19:49	21.6	+10/-20	Dipole	railroad debris
	19:22:49 - 19:23:13	43.2	+166/-38	Dipole	canal boats (Figure 22)
17	11:15:24 - 11:15:46	39.6	+343/-86	Dipole	canal boats (Figure 22)
	11:19:12 - 11:19:22	18	+17	Monopole	
18	11:44:32 - 11:45:04	57.6	-51	Monopole	
	11:58:26 - 11:59:10	79.2	+905/-284	Dipole	navigation buoy 37
22	13:20:00 - 13:20:10	18	+7	Monopole	
24	14:47:24 - 14:47:36	21.6	-10/+38	Dipole	
25	15:19:26 - 15:19:42	28.8	+12/-5	Monopole	
26	15:32:18 - 15:33:02	79.2	-71/+54	Dipole	
27	16:01:00 - 16:01:14	25.2	+7/-4	Dipole	
	16:05:16 - 16:05:38	39.6	-80/+50	Dipole	
28	16:29:10 - 16:29:26	28.8	+27	Monopole	
	16:39:36 - 16:39:46	18	+10	Monopole	
30	17:11:02 - 17:11:18	28.8	+26	Monopole	
32	17:49:22 - 17:49:44	39.6	-28/+10	Dipole	near iron cauldrons
	17:50:50 - 17:51:04	25.2	-8/+4	Dipole	

33	18:07:24 - 18:07:30	10.8	+17	Monopole	
34	09:48:37 - 09:49:07	54	+61/-40	Dipole	
	09:49:41 - 09:50:57	118.8	+56/-53	Dipole	
	09:51:13 - 09:51:27	27	-42/+20	Dipole	
38	10:52:09 - 10:52:31	39.6	+19	Monopole	
	10:56:07 - 10:56:23	28.8	+94	Monopole	
42	13:09:21 - 13:09:41	36	-40	Monopole	
43	13:26:17 - 13:26:23	10.8	+14	Monopole	
44	13:49:49 - 13:49:59	18	-6/+11	Dipole	
49	16:06:47 - 16:06:59	21.6	+14	Monopole	
50	16:16:19 - 16:16:25	10.8	-5/+10	Dipole	
73	14:20:42 - 14:21:00	32.4	+27/-13	Dipole	
74	14:31:08 - 14:31:18	18	+18	Monopole	
77	15:01:34 - 15:01:42	14.4	-21	Monopole	
79	15:51:02 - 15:51:12	18	+25	Monopole	
80	16:10:28 - 16:10:48	36	-76	Monopole	
82	16:50:44 - 16:51:00	28.8	+23/-44	Dipole	
83	17:21:00 - 17:21:12	21.6	+15	Monopole	
86	12:17:50 - 12:17:58	14.4	+15	Monopole	
89	12:55:26 - 12:55:38	39.6	-6/+15	Dipole	
93	16:27:41 - 16:27:59	32.4	-19	Monopole	
94	16:59:17 - 16:59:39	39.6	+20/-7	Dipole	
	17:02:39 - 17:07:13	493.2	+790	Monopole	near shore (NY)
95	17:19:11 - 17:22:35	367.2	+469	Monopole	near shore (NY)
97	17:41:39 - 17:41:47	14.4	+66	Monopole	
98	09:29:39 - 09:30:05	46.8	-72/+73	Dipole	railroad debris
	09:48:13 - 09:48:39	46.8	+293	Monopole	directly over Caisson 2
	09:49:11 - 09:49:33	39.6	+250	Monopole	near shore(VT) cannon area

66 anomalies
Longest in physical duration 137 readings/274 seconds/493.2 meters
Greatest intensity +905/-284 γ
*one second equals an average distance of 1.8 meters
‡deviation from ambient field

Table 3

Supported ^{210}Pb = 2.2±0.1 dpm/g

Sample Depth (cm)	Total ^{210}Pb (dpm/g)	Sigma Total ^{210}Pb (dpm/g)	Unsupported ^{210}Pb (dpm/g)	Sigma Unsupported ^{210}Pb (dpm/g)	Porosity (ϕ)	^{230}Th (dpm/g)
0-2	4.741	0.075	2.553	0.126	0.837	
2-4	3.256	0.075	1.060	0.125	0.813	
4-6	3.142	0.060	0.947	0.117	0.787	2.342±0.49
8-10	2.827	0.047	0.630	0.111	0.789	2.324±0.057
10-12	2.904	0.054	0.706	0.114	0.790	
12-14	2.924	0.047	0.727	0.111	0.780	
16-18	2.699	0.040	0.502	0.108	0.766	
18-20	2.552	0.057	0.353	0.115	0.759	
26-28	2.544	0.060	0.345	0.117	0.769	
34-36	2.414	0.050	0.215	0.112	0.755	
42-44	2.427	0.049	0.228	0.112	0.767	
55-60	2.359	0.043	0.159	0.109	0.757	2.148±0.057
70-75	2.203	0.035	0.003	0.106	0.755	2.104±0.051
85-90	2.116	0.042	-0.084	0.109	0.750	
115-120	2.240	0.048	0.040	0.111	0.812	
145-150	2.204	0.049	0.004	0.112	0.804	
175-180	2.054	0.041	-0.147	0.108	0.772	
205-210	1.803	0.037	-0.399	0.107	0.761	

Figure Captions

Figure 1. Location of the re-processed side-scan sonar images north of the "Great Bridge" caissons. Numbers relate to the images described in the text and shown in Figures 3 to 26. Location of the cores are indicated by star and appropriate core label. Local coordinates are in feet north and east of 43° N and 74° W.

Figure 2. Location of re-processed side-scan sonar images for the entire survey region. Numbers relate to the Images described in the text for those occurring near navigational buoy 40. Local coordinates are in feet north and east of 43° N and 74° W.

Figure 3. Digital sonar Image 1 displaying the Vermont end of the row of caissons. The reflective zone in the southern portion of the image is the shallow zone near the shore. Two caissons (Caissons 2 and 3; Crisman, 1995) about 5-8 m on a side are observed trending to the north. The center of the image shows a reflective zone in the water column that casts a prominent shadow. This is caused by a series of 5 large upright logs (up to 3.8 m above the mudline) identified ~20 m south of Caisson 2 (Crisman, 1995).

Figure 4. Digital sonar Image 2 shows a north-south row of 5 caissons (Caissons 2 - 5; Crisman, 1995) near the Vermont shore. Shadows are often observed behind the caissons suggesting that they protrude above the bottom. The weak "diamond" pattern near the edge of the image is probably due to sound refraction in the water column.

Figure 5. Digital sonar Image 3 shows a north-south row of 4 caissons (Caissons 5-8; Crisman, 1995). Some of the caissons (Caissons 7 and 8) have no shadows, suggesting that they have little relief. A reflection is also observed about 50 m to the southwest of Caisson 5. This target is also observed on Image 2, suggesting that the southern two caissons of Image 3 are the same as the northern two caissons of Image 2. The lineated north-south reflections are probably due to sound diffraction in the water column.

Figure 6. Digital sonar Image 4 shows a north-south row of 3 caissons (probably Caissons 5-7; Crisman, 1995). While the precise location of this image is uncertain, the image appears to show the same three caissons as Image 3. However, the most northern caisson is obscured by a prominent reflection that appears to be a sound diffraction within the water.

Figure 7. Digital sonar Image 5 collected immediately southwest of and immediately before Image 4 (Figure 6) shows a prominent field of northeast-southwest lineations. Because of the association with the features in Image 4, these lineations appear to be caused from internal waves in the water column and are not sediment waves on the lake bottom.

Figure 8. Digital sonar Image 6 shows a north-south row of 4 or perhaps 5 caissons which have little relief. These caissons are located north of those in Images 3 and 4. Most likely these correspond to Caissons 10 - 13 (Crisman, 1995). Caisson 10 has all 4 sides exposed above the lake bottom whereas Caissons 11 - 13 only have ballast stones above the mudline (Crisman, 1995).

Figure 9. Digital sonar Image 7 shows 4 caissons (Caissons 11 - 14; Crisman, 1995). A prominent, thin shadow zone occurs at the western end of the most northern caisson. Diver verification of this caisson documented three unattached logs, one of which was jammed diagonally into the lake bottom and protruding ~ 5m of its length above the sediment. It is possible that this log is producing the shadow zone near the northern caisson on the side-scan image.

Figure 10. Digital sonar Image 8 shows 4 caissons (Caissons 14 - 17; Crisman, 1995) near the northern end of the row. The caisson immediately south of the center of the image appears to have two parts. Lake sediment appears to have covered the central section of the caisson. Crisman (1995) noted that Caisson 15 consisted of two separate piles of ballast rocks with mud between them. Caissons 16 - 17 only showed a few ballast stones above the lake bottom. The wave-like features on the northern edge of the image may be caused by sound diffraction in the water column.

Figure 11. Digital sonar Image 9 is near the New York shore. Other irregular targets associated with the nearshore sediments and the shoreline are observed. Three caissons were imaged and most likely correspond to Caissons 19 - 21 (Crisman, 1995).

Figure 12. Digital sonar Image 10 shows a canal boat resting on the lake bed. The shadow zone shows that the boat extends above the lake bed. Some of the internal structures of the boat are also seen.

Figure 13. Digital sonar Image 11 shows a row of pockmarks near the western shore of the lake. No evidence of gas venting is seen. This row of pockmarks may be associated with the edge of the finer-grained sediments in the lake.

Figures 14. Digital sonar Image 12 shows a row of pockmarks to the north of Image 11. Lineated sedimentary features extend northeast-southwest near these features. These features become better defined on Image 13 (Figure 15) as furrows.

Figure 15. Digital sonar Image 13 has three small pockmarks located in the trough of a furrow. A strong reflection with a diffraction pattern on the southern side of Image 13 is navigational buoy 38. This image is a continuation of Figure 14.

Figure 16. Digital sonar Image 14 shows northeast-trending furrows along the western side of the lake. Two furrows join to one (termed a tuning fork) towards the northeast. Studies in other areas have suggested that furrows join in the direction of the bottom flow responsible for furrow formation (Flood, 1983). This suggests dominant flows to the northeast at this site. The change in sediment reflectivity from high in the northwest to low in the southeast is probably related to finer sediments accumulating in the central portion of the lake here.

Figure 17. Digital sonar Image 15 also shows furrows near the western shore of the lake.

Figure 18. Digital sonar Image 16 is at the New York end of the Addison Company railway. There is a shallow area at the western edge of the image near the shore, and a mound is present at the middle of this shallow area. This mound may have been used to anchor the railroad trestle. Other debris can be observed on the bottom. In particular, a log-shaped feature is present in the southeast part of the image.

Figure 19. Digital sonar Image 17 contains a section of the 1888 floating draw boat associated with the railway (see Barranco, 1995). Some of the internal structure of the trestle can be observed sticking out of the mud. A more reflective part of the image west of the track is a mound possibly associated with this drawboat system. This portion of the 1888 drawboat lies within the former draw opening.

Figure 20. Digital sonar Image 18 shows the larger section of the 1888 drawboat (see Barranco, 1995). The broken sections of the draw boat are stacked upon each other. A dark streak trending to the east in the center of the image may be caused by gas venting from the lake bed.

Figure 21. Digital sonar Image 19 shows a mound on the western portion of the image (related to the railway) along with several clearly defined gas plumes. As with other images, these gas plumes do not appear to be associated with pockmarks.

Figure 22. Digital sonar Image 20 is north of the railway near the north point of Beadles Cove on Vermont shore. This target is confirmed to be two canal boats resting side by side (Barranco, 1995). The aspect angle the sonar fish had with respect to these canal boats was such that they were not well distinguished. The bright targets to the west of the track appear to be caused by internal waves diffractions.

Figure 23. Digital sonar Image 21 is from the western shore of the lake (NY side), south of the caisson area. A prominent row of pockmarks is present here, again apparently at the edge of the potentially finer-grained sediments that fill the central portion of the lake. The along-track banding observed on this and Figures 24 - 26 (Images 22 - 24) apparently is instrument noise.

Figure 24. Digital sonar Image 22 is of a canal boat partially buried in the sediment. This boat is about the same width but appears shorter than the boat in Image 10. The difference in length may be in part due to inaccuracies in navigation. Image 22 is the same boat found in Images 23 and 24 (Figures 25 and 26).

Figure 25. Digital sonar Image 23 has had additional processing to remove the horizontal black lines that result from lost data on tape replay seen on Image 24 (Figure 26). Some of the internal structure of the vessel can be observed. The boat appears wider here than in Figure 24 (Image 22) due to navigational uncertainties.

Figure 26. Digital sonar Image 24 is identical with Image 23 (Figure 25). Some data was lost on tape replay.

Figure 27. a) Magnetic survey line from south to north paralleling the canal boat imaged by side-scan sonar (Figure 12 - Image 10). Dipole field is present. b) Magnetic survey line from south to north 10 meters west of the transect displayed in Figure 27a. Largest concentration of magnetic material is located at the northern end (bow) of the vessel.

Figure 28. a) Magnetic survey line from northwest to southeast paralleling the canal boat imaged by side-scan sonar (Figure 24 - Image 22). b) Magnetic survey line from southeast to northwest 10 meters off the transect done displayed in Figure 29a. Largest concentration of magnetic material is located at the eastern end (bow) of the canal boat.

Figure 29. Magnetic survey line from west to east along the Addison Company railway path. The transect clearly shows the presence of magnetic material along its entire length. The greatest concentrations of magnetic material is seen close to each shore whereas the middle of the channel is relatively free of magnetic material. The largest anomalies appear to be associated with the 1888 drawboat sections and a 9 m^2 timber crib.

Figure 30. Magnetic survey line from north to south over the side-scan sonar hyperbolic target at Ticonderoga Creek delta. The high and close nature of the magnetic anomaly indicates are very distinct object. Diver verification showed this object to be four iron cauldrons (three sitting upright and one on its side) which were large enough for the diver to stand in.

Figure 31. Magnetic survey line from west to east, 10 meters north of the "Great Bridge" caissons. The large anomaly at the western end of the transect may be associated with a large wooden-stocked iron anchor and large (2' X 2' X 2") unidentified iron object near Caisson 19.

Figure 32. Geological sample data sheet for core MIFT-01.

Figure 33. Core description of MIFT-01.

Figure 34. Geological sample data sheet for core MIFT-02.

Figure 35. Core description of MIFT-02.

Figure 36. Geological sample data sheet for core MIFT-03.

Figure 37. Core description of MIFT-03.

Figure 38. Geological sample data sheet for core MIFT-04.

Figure 39. Core description of MIFT-04.

Figure 40. Geological sample data sheet for core MIFT-05.

Figure 41. Core description of MIFT-05.

Figure 42. Graph of Total ^{210}Pb versus depth for MIFT-05 core (linear scale).

Figure 43. Graph of unsupported ^{210}Pb with error bars versus depth for MIFT-05 core. 2.2 ± 0.1 dpm/g was used for the supported ^{210}Pb activity. The concave profile suggests that compaction of the upper sediment layers occurred for this core or that sedimentation rates have declined in the last 20 years.

Figure 44. Log graph of unsupported ^{210}Pb vs depth for varying supported ^{210}Pb activities (2.1, 2.2, and 2.3 dpm/g). Each line represents a regression from which sediment accumulation rates were calculated. Sedimentation rates range from 0.55 cm/yr to 0.76 cm/yr.

Figure 45. Graph of the magnetic susceptibility for the five cores taken. Cores are in order showing an increase in distance from the Vermont shoreline from left to right; MIFT-05 is closest to the shore, MIFT-03 and MIFT-04 are out in the central channel. Using the kick in magnetic susceptibility as a 1780 age marker (determined form ^{210}Pb dating on MIFT-05), correlation is made for all cores. A laminated layer (~15 cm thick) occurs approximately 40 cm above the 1780 marker and can also be correlated between cores. Clinkers gave large susceptibility peaks in MIFT-03 and MIFT-04; approximate dates for those clinkers - 1880's. MIFT-05 and MIFT-04 show increased susceptibility between 150 and 200 cm depth; approximate dates of 1590 to 1690.

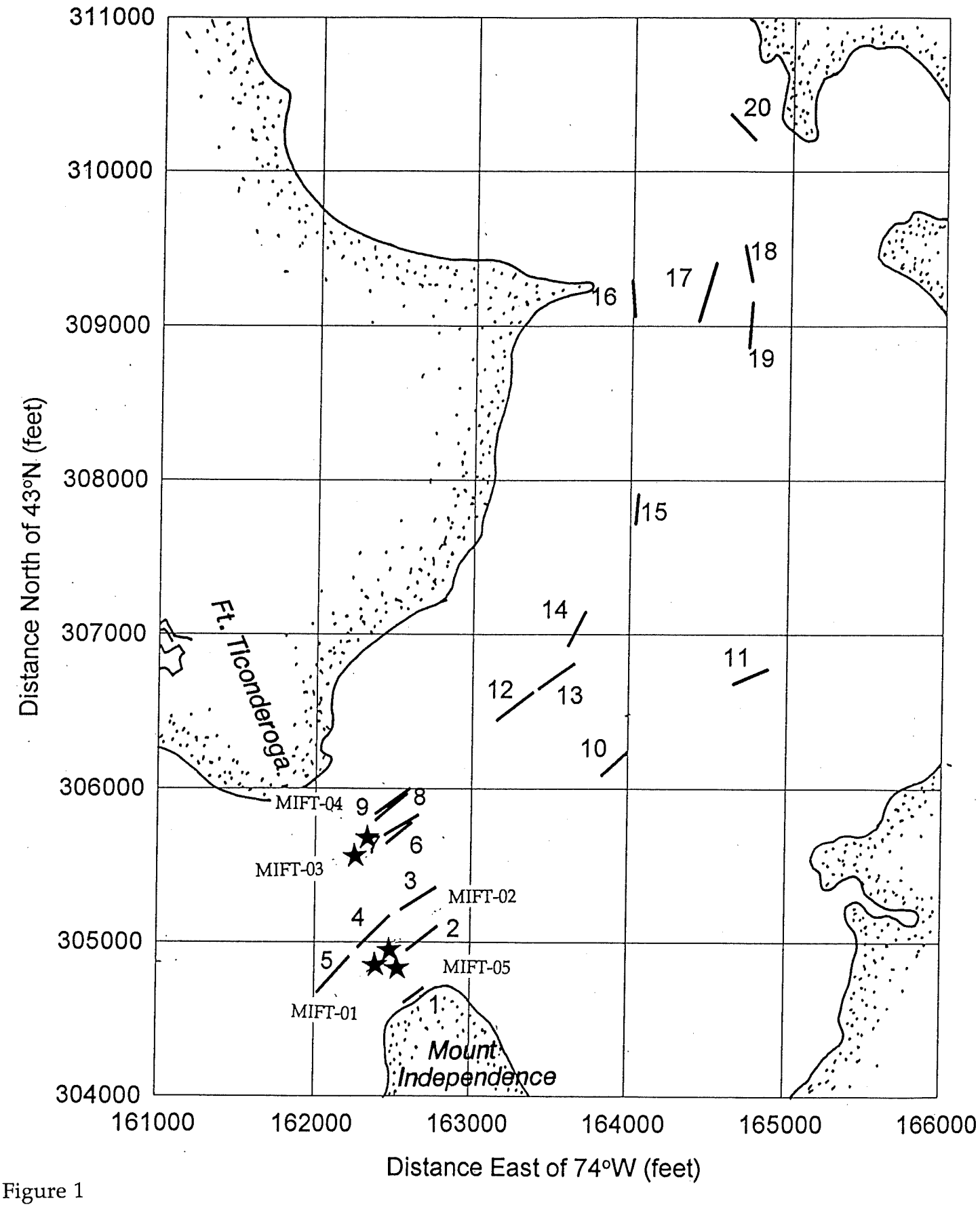
Fort Ticonderoga Sonar Images (Northern Area)
311000
310000
309000
308000
307000
306000
305000
304000
161000
162000
163000
164000
165000
166000
Distance North of 43°N (feet)
Distance East of 74°W (feet)
Ft. Ticonderoga
Mount Independence
MIFT-01
MIFT-02
MIFT-03
MIFT-04
MIFT-05
1
2
3
4
5
6
7
8
9
10
11
12
13
14
15
16
17
18
19
20

Figure 1

Fort Ticonderoga Sonar Images (Entire Area)

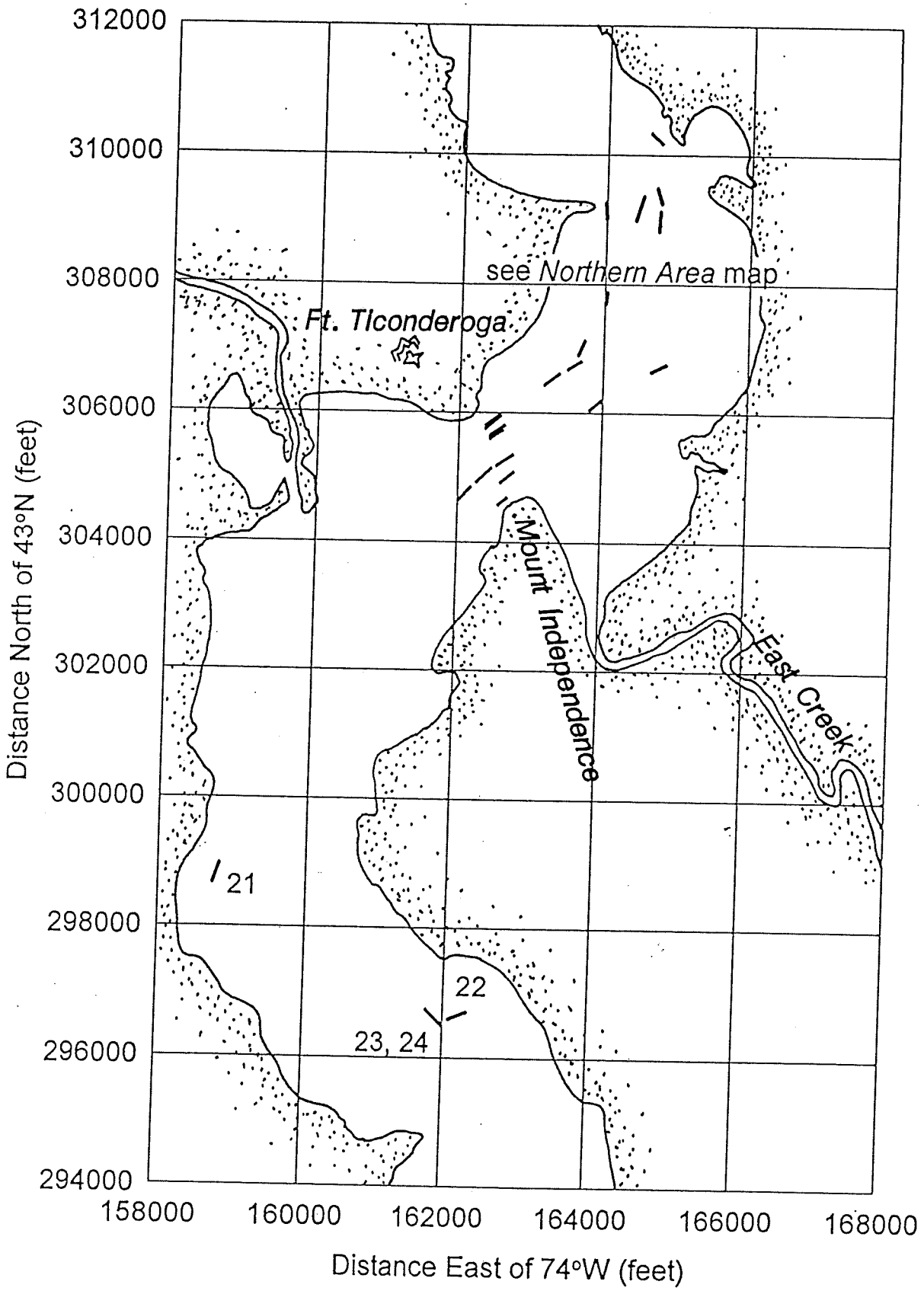

Figure 2

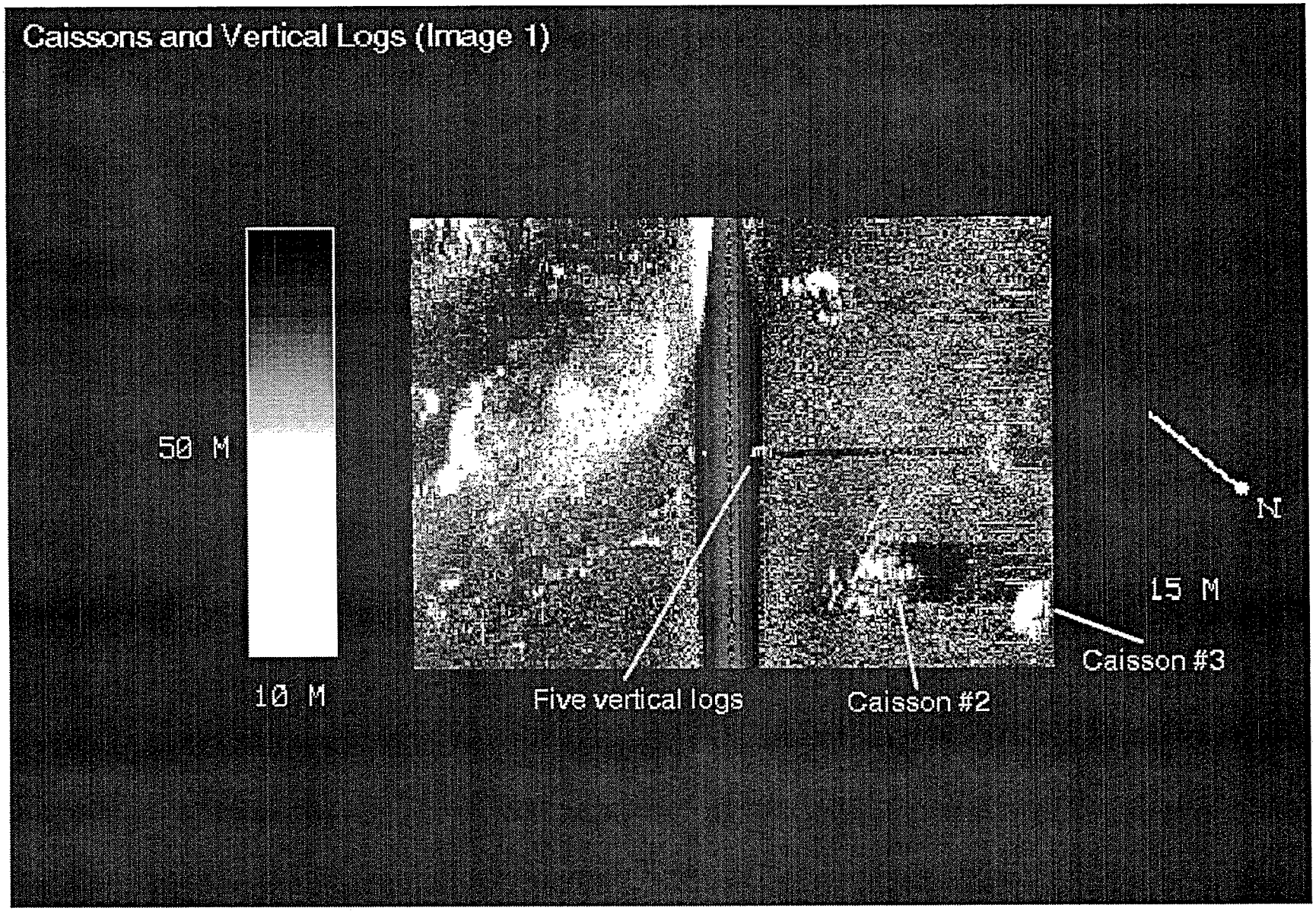
Caissons and Vertical Logs (Image 1)
50 M
10 M
Five vertical logs
Caisson #2
Caisson #3
15 M
N

Figure 3

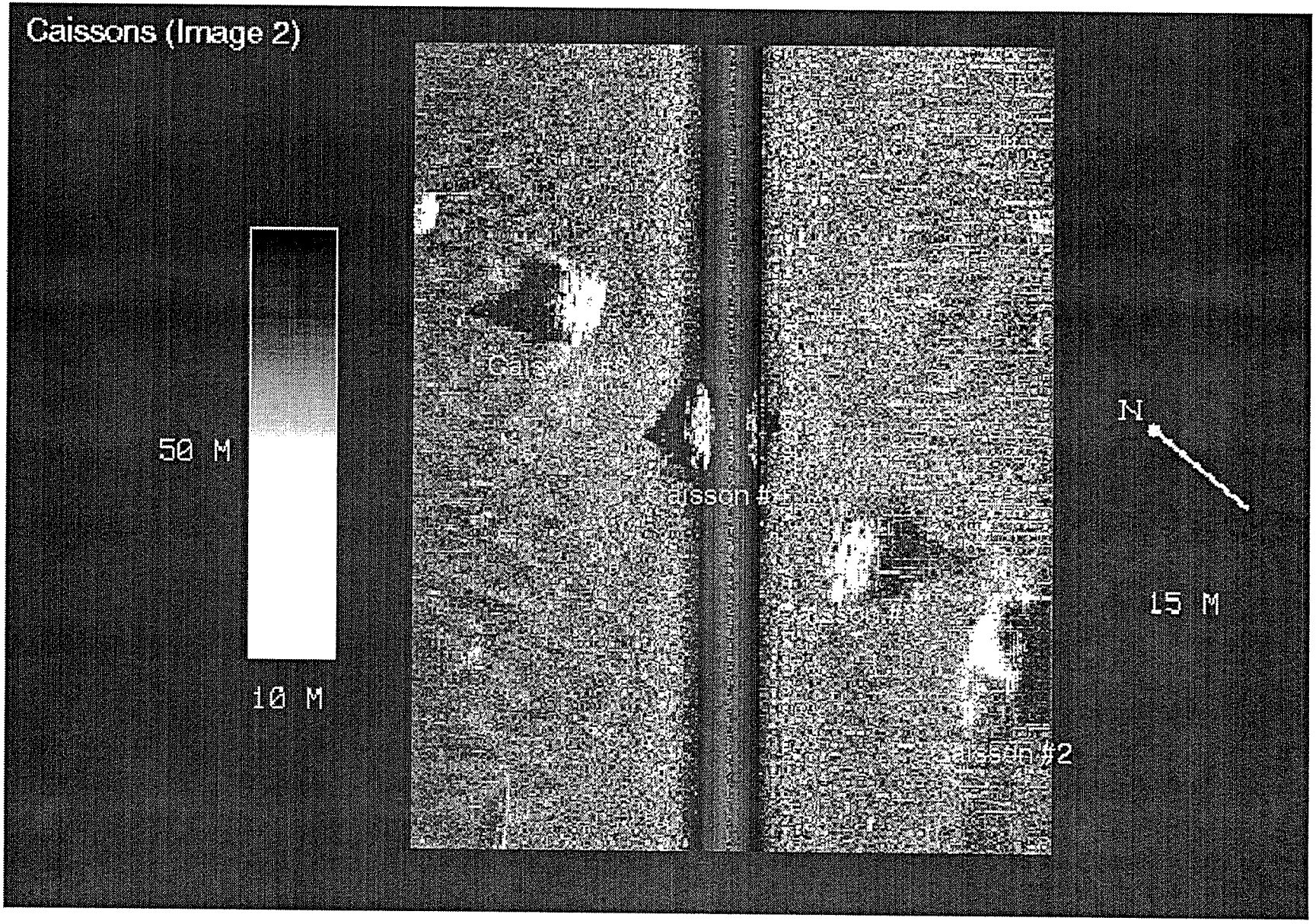

Figure 4

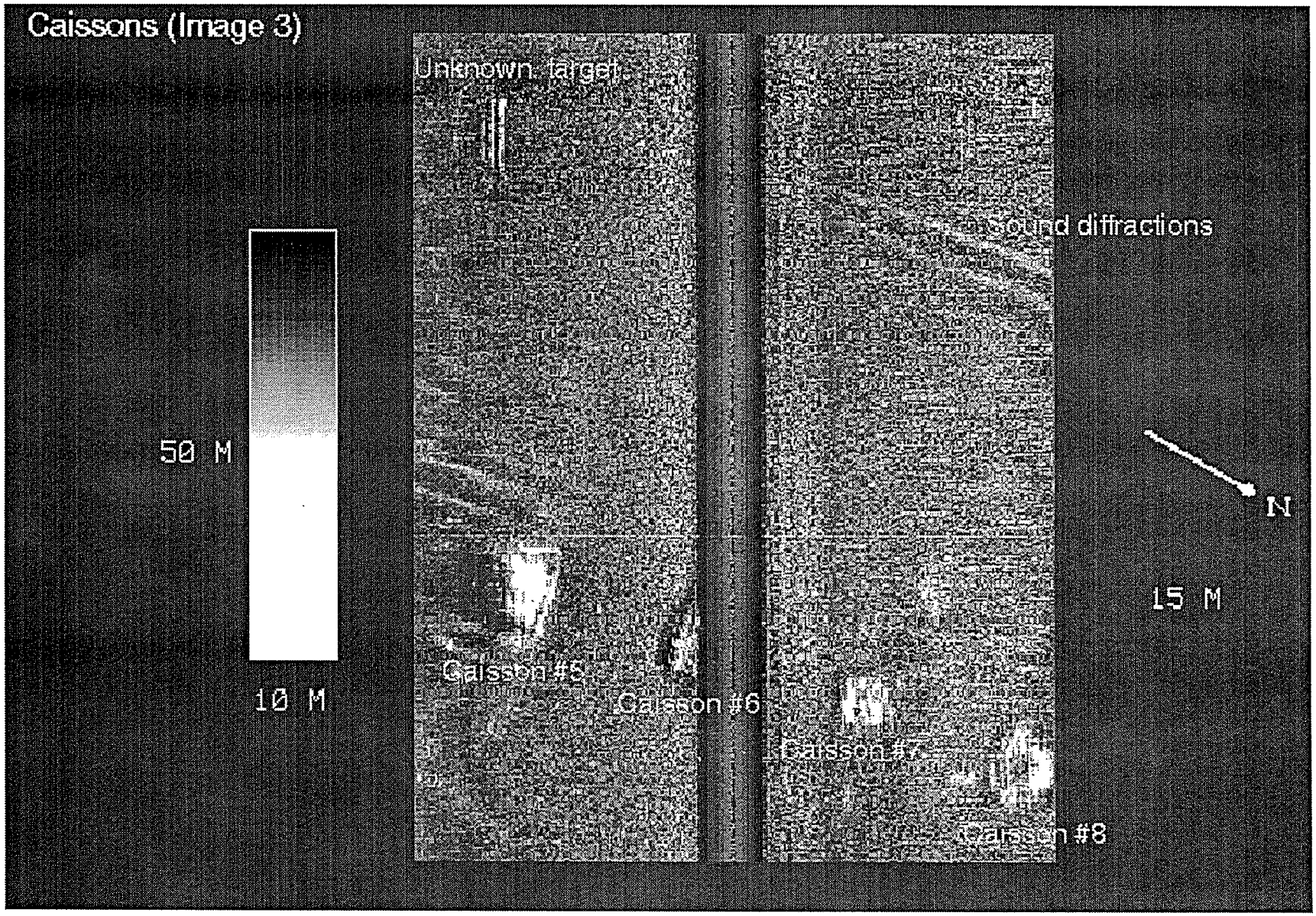
Caissons (Image 3)
Unknown target
Sound diffractions
50 M
10 M
N
15 M
Caisson #5
Caisson #6
Caisson #7
Caisson #8

Figure 5

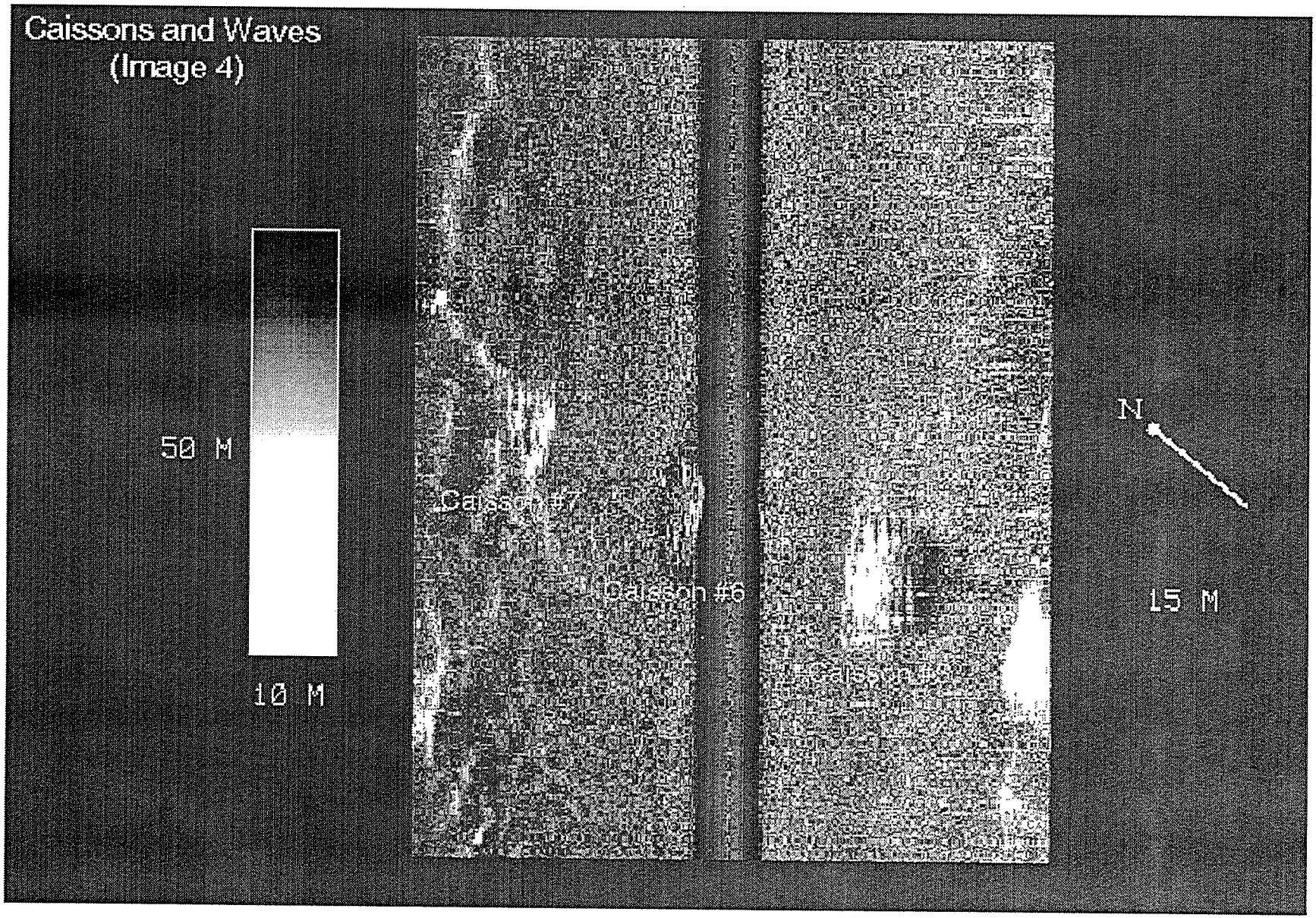

Figure 6

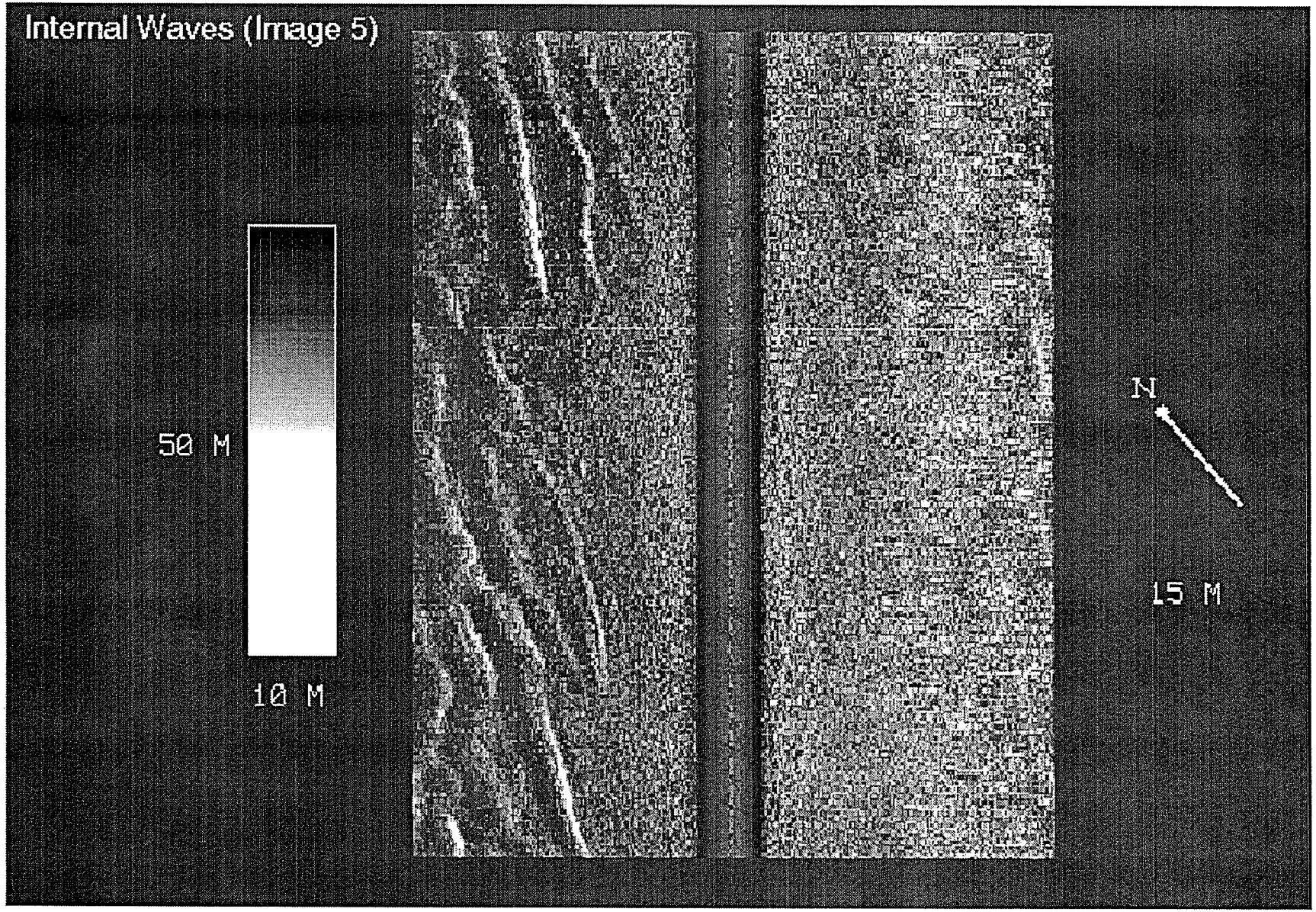

Figure 7

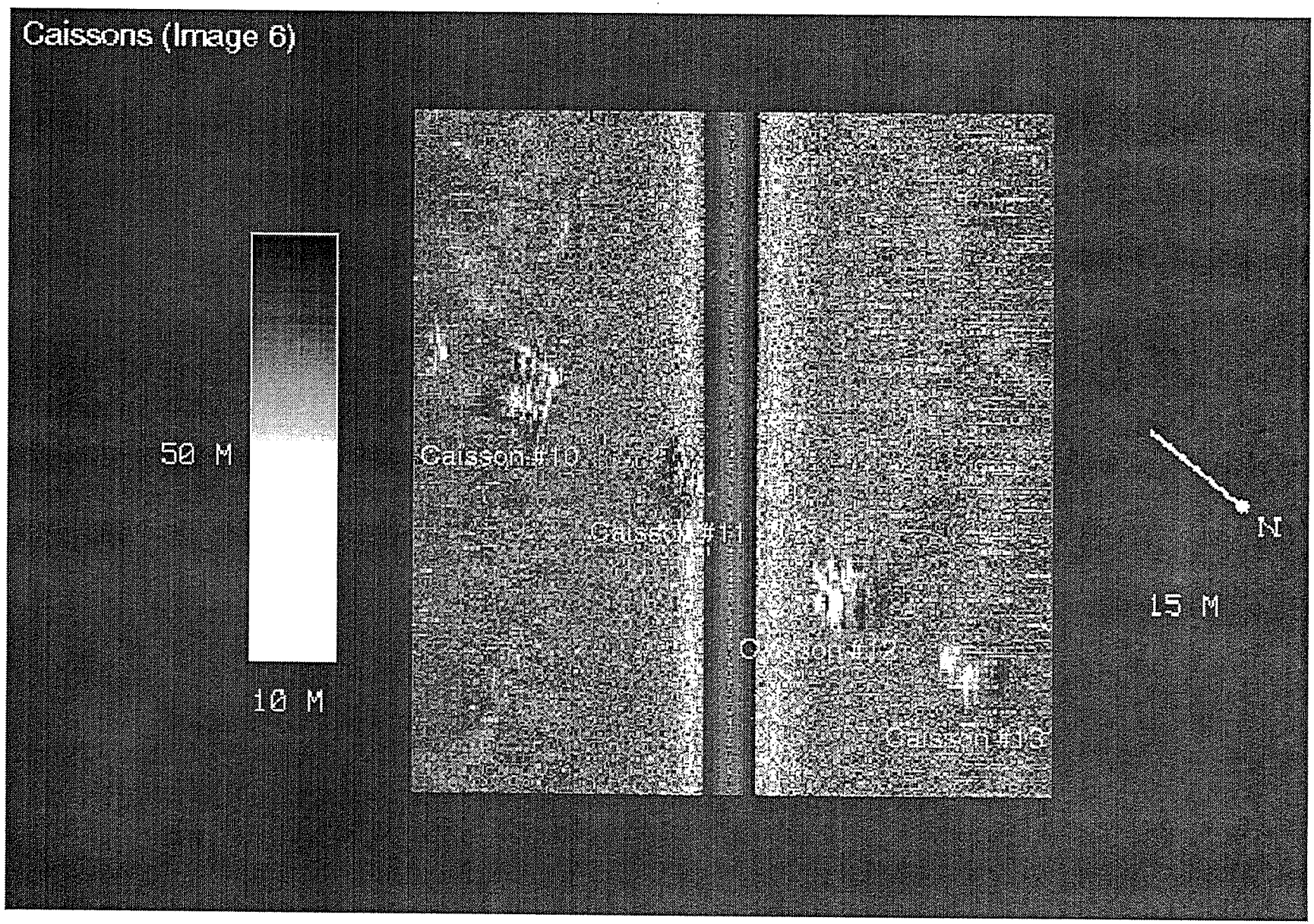
Caissons (Image 6)
50 M
10 M
Caisson #10
Caisson #11
Caisson #12
Caisson #13
N
15 M

Figure 8

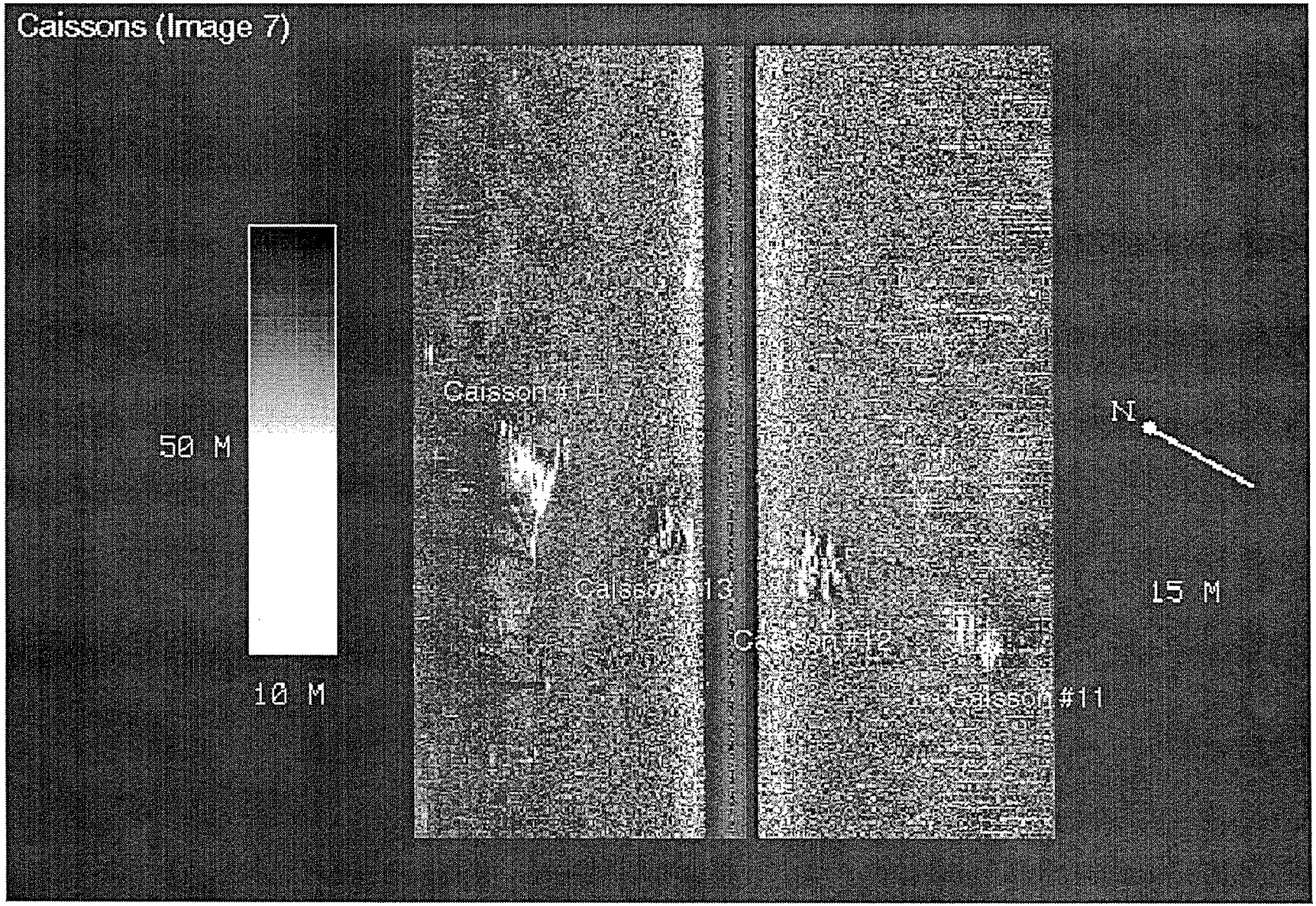

Figure 9

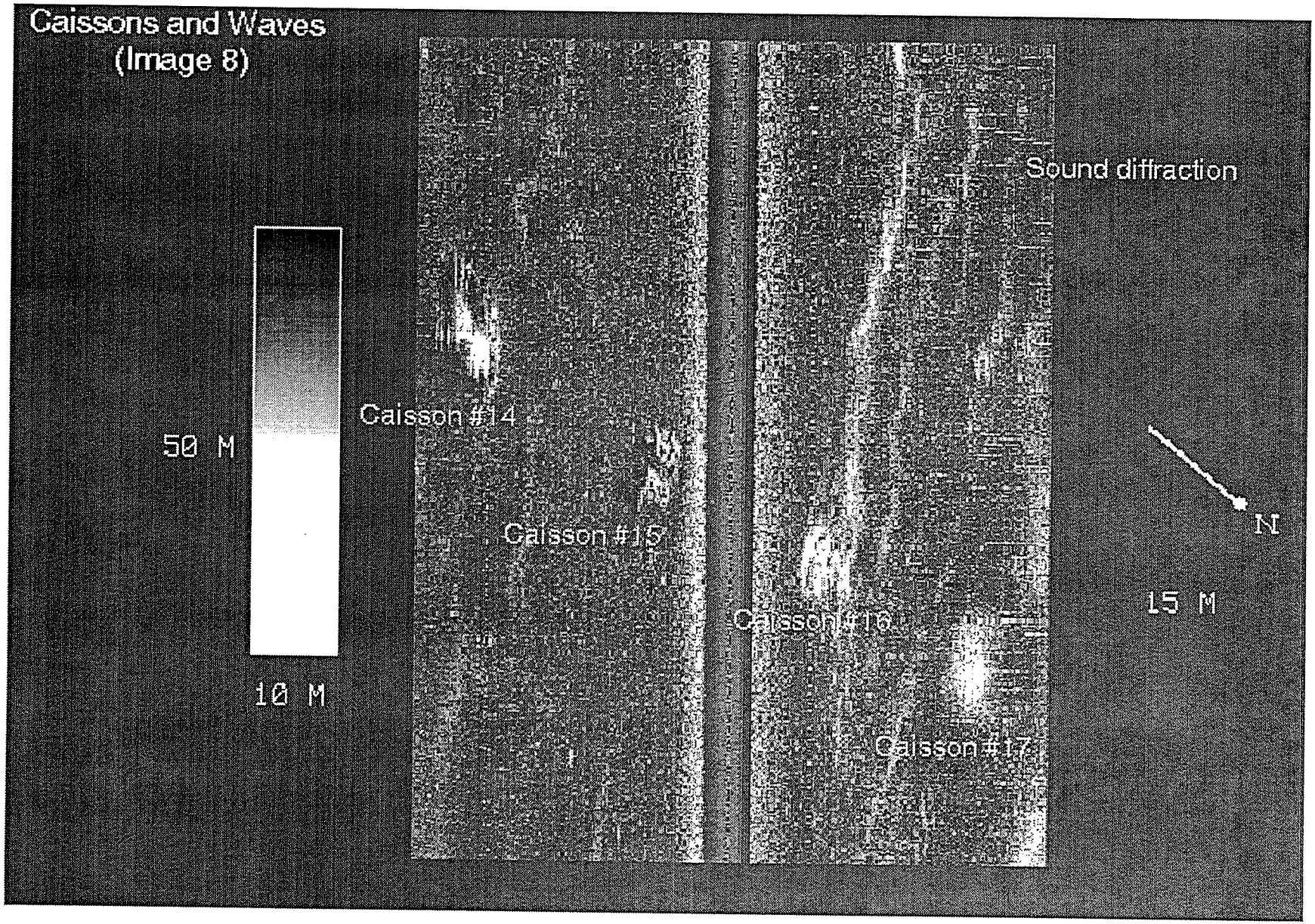
Caissons and Waves
(Image 8)
Sound diffraction
50 M
10 M
Caisson #14
Caisson #15
Caisson #16
Caisson #17
N
15 M

Figure 10

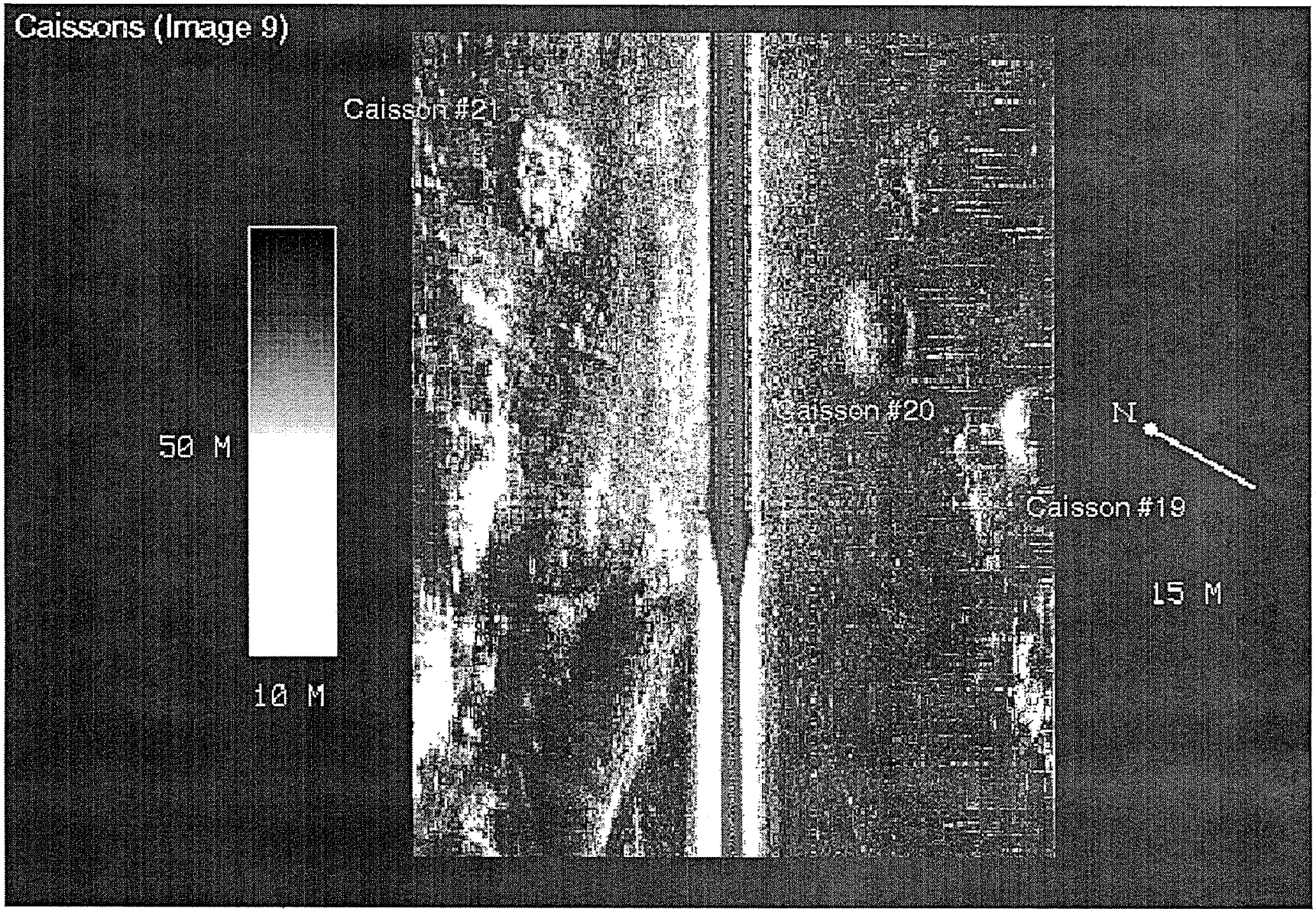
Caissons (Image 9)
Caisson #21
Caisson #20
Caisson #19
50 M
10 M
N
15 M

Figure 11

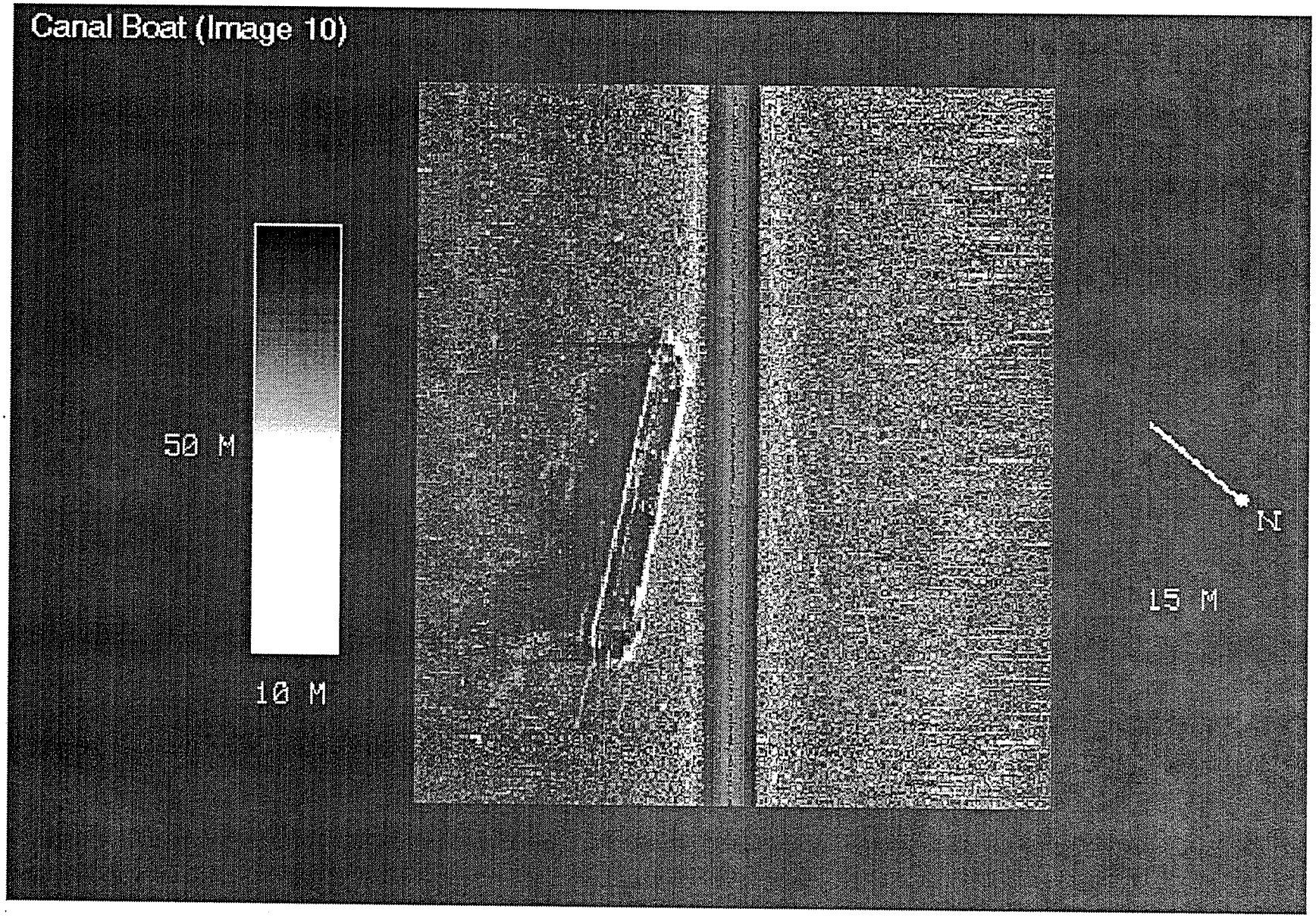

Figure 12

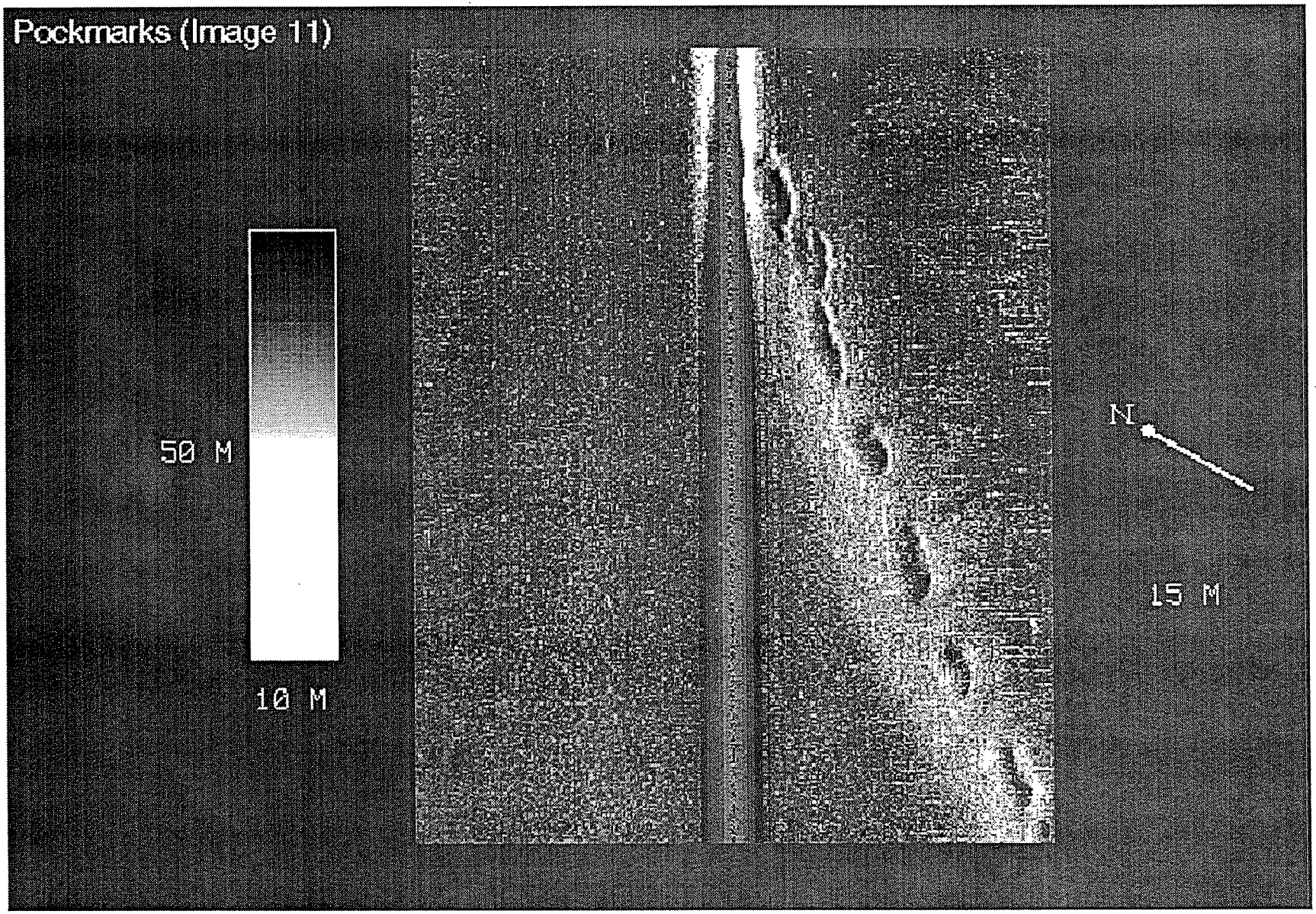

Figure 13

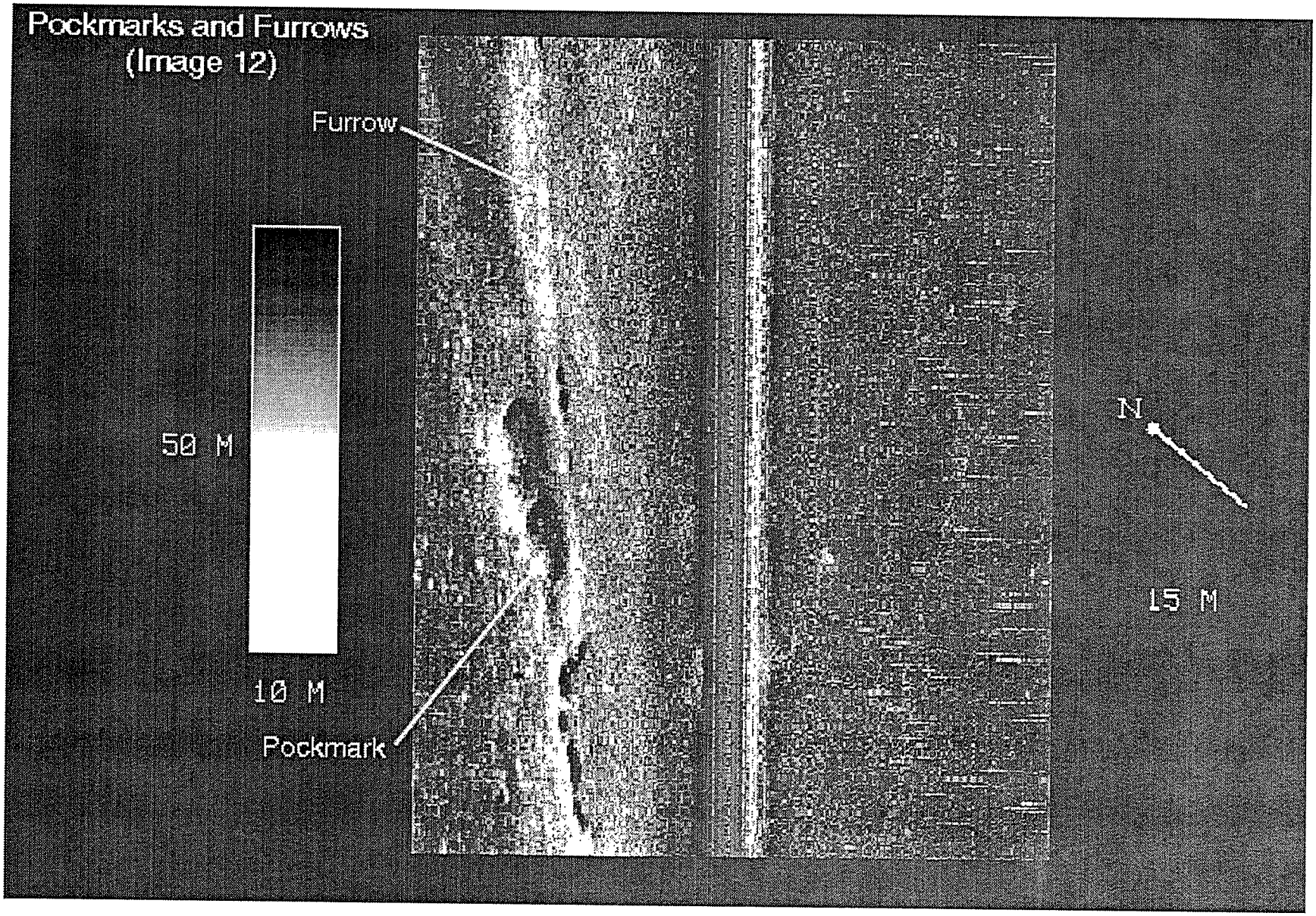
Pockmarks and Furrows
(Image 12)
Furrow
50 M
10 M
Pockmark
N
15 M

Figure 14

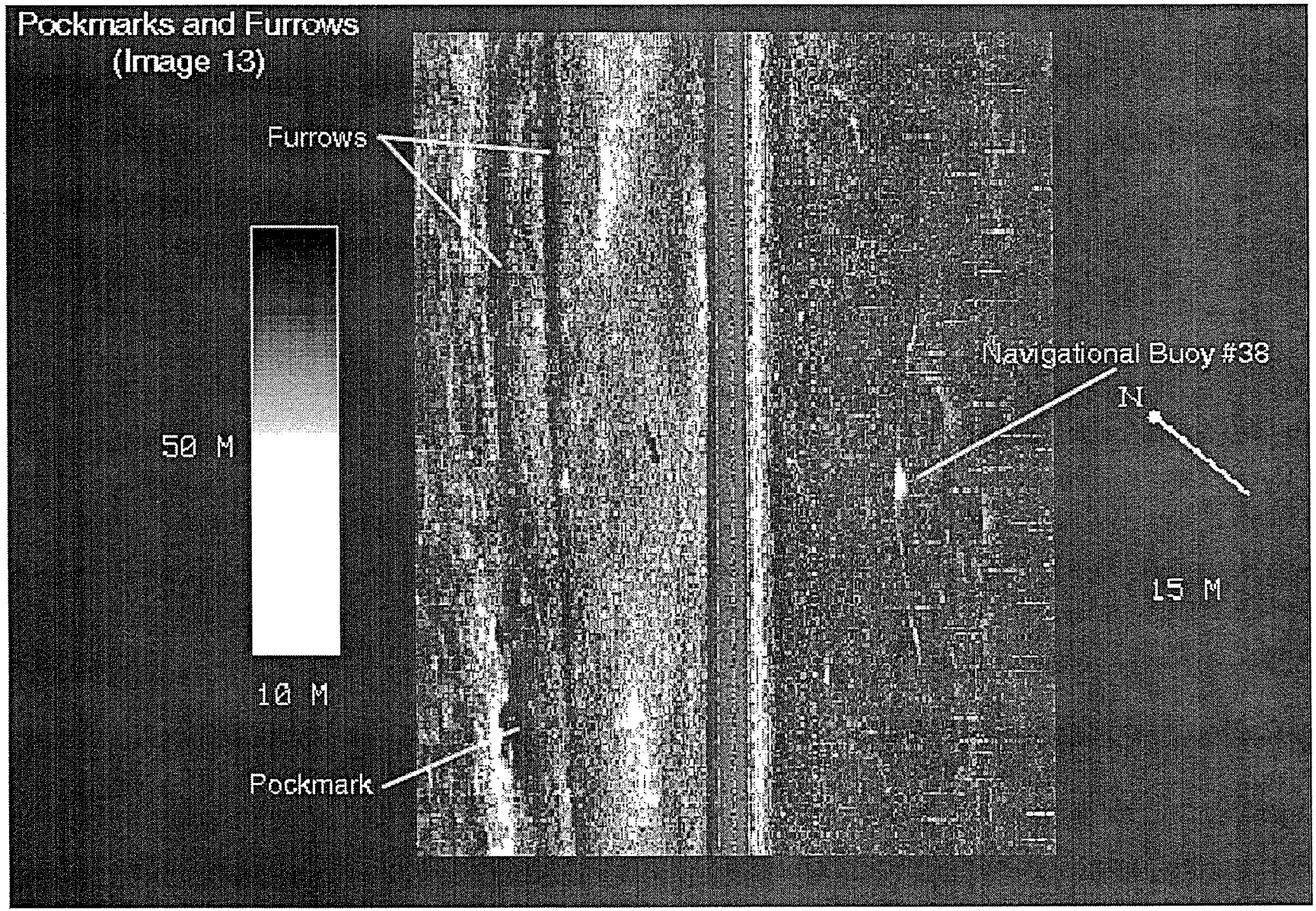
Pockmarks and Furrows
(Image 13)
Furrows
50 M
10 M
Navigational Buoy #38
N
15 M
Pockmark

Figure 15

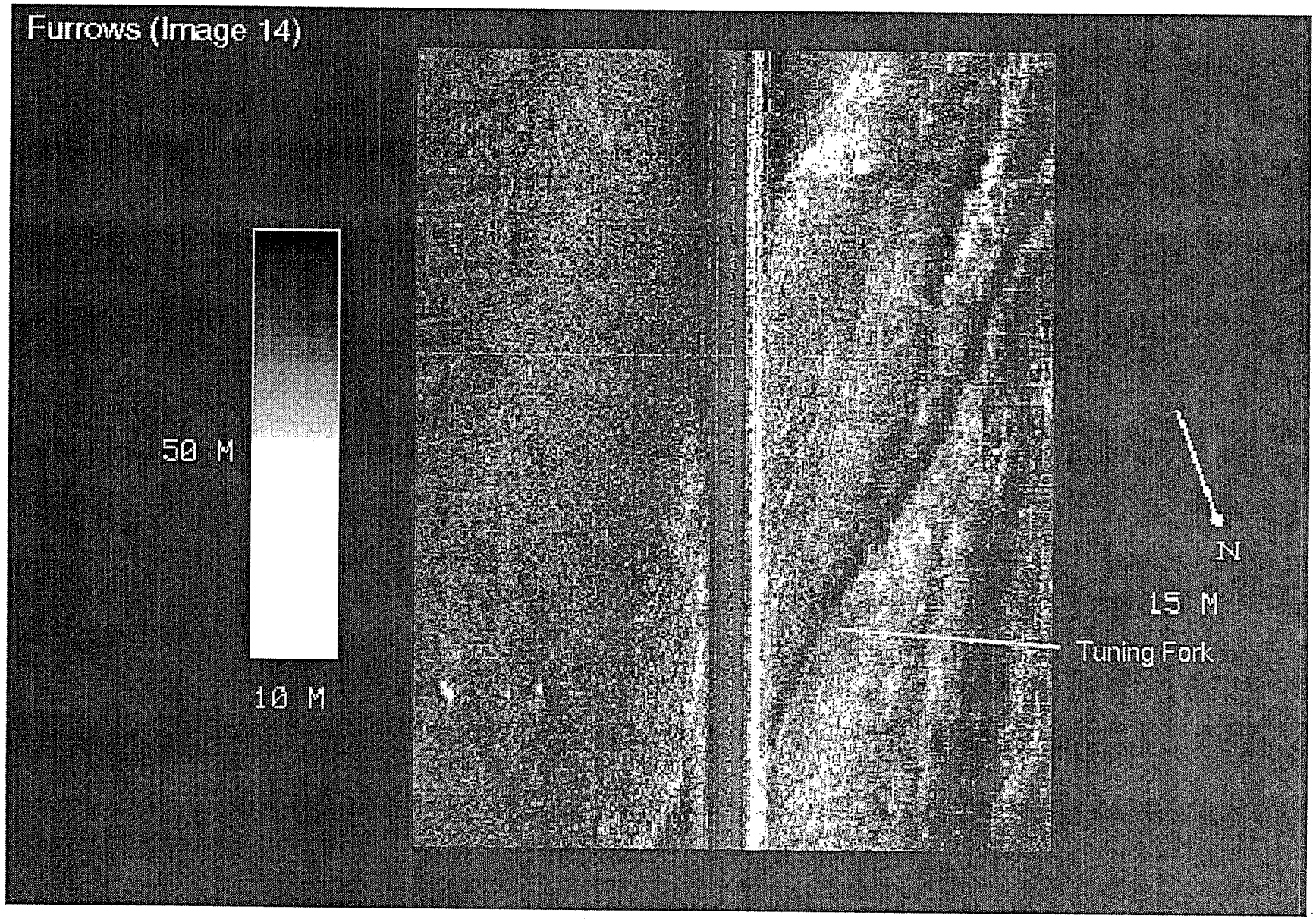

Figure 16

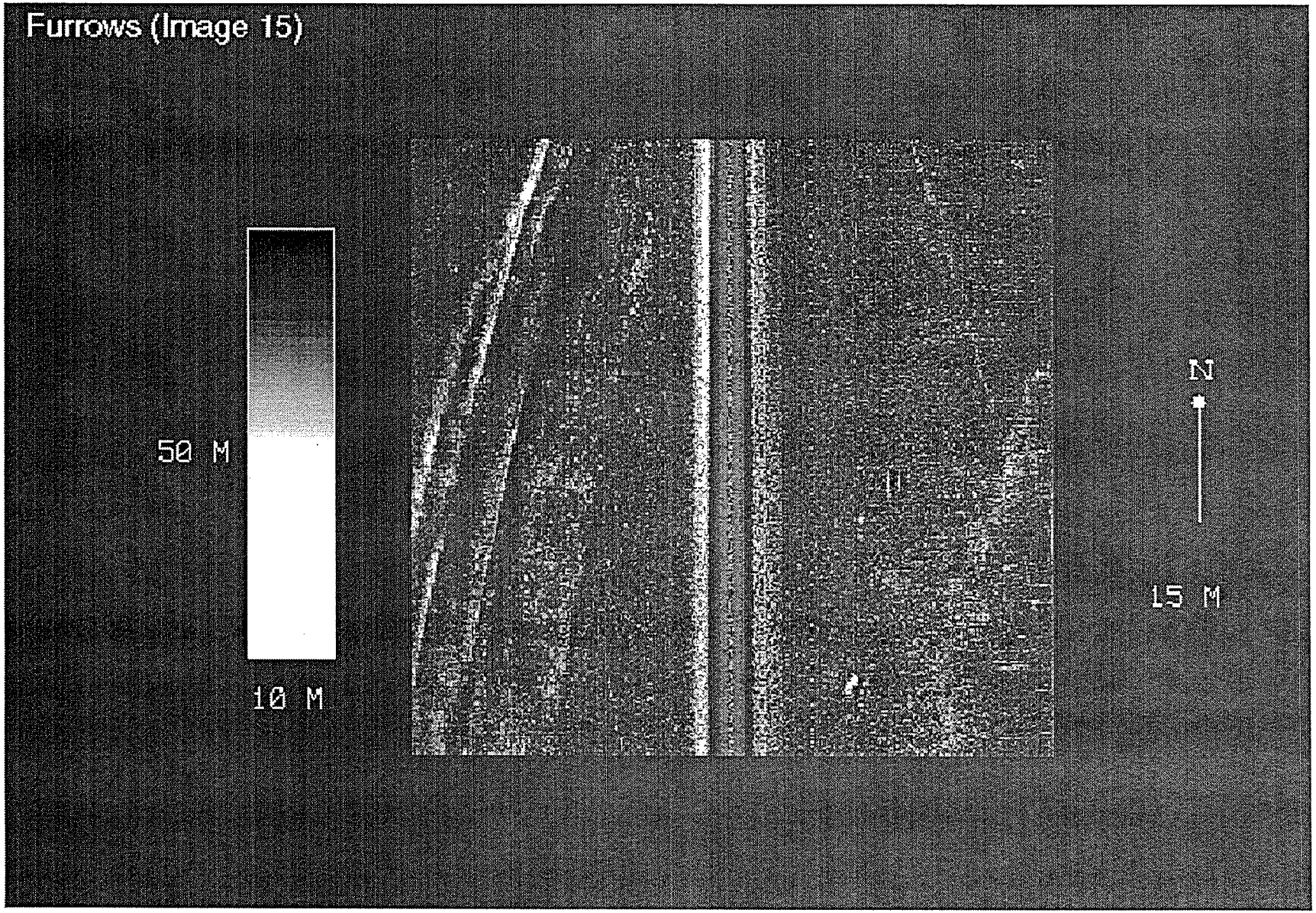

Figure 17

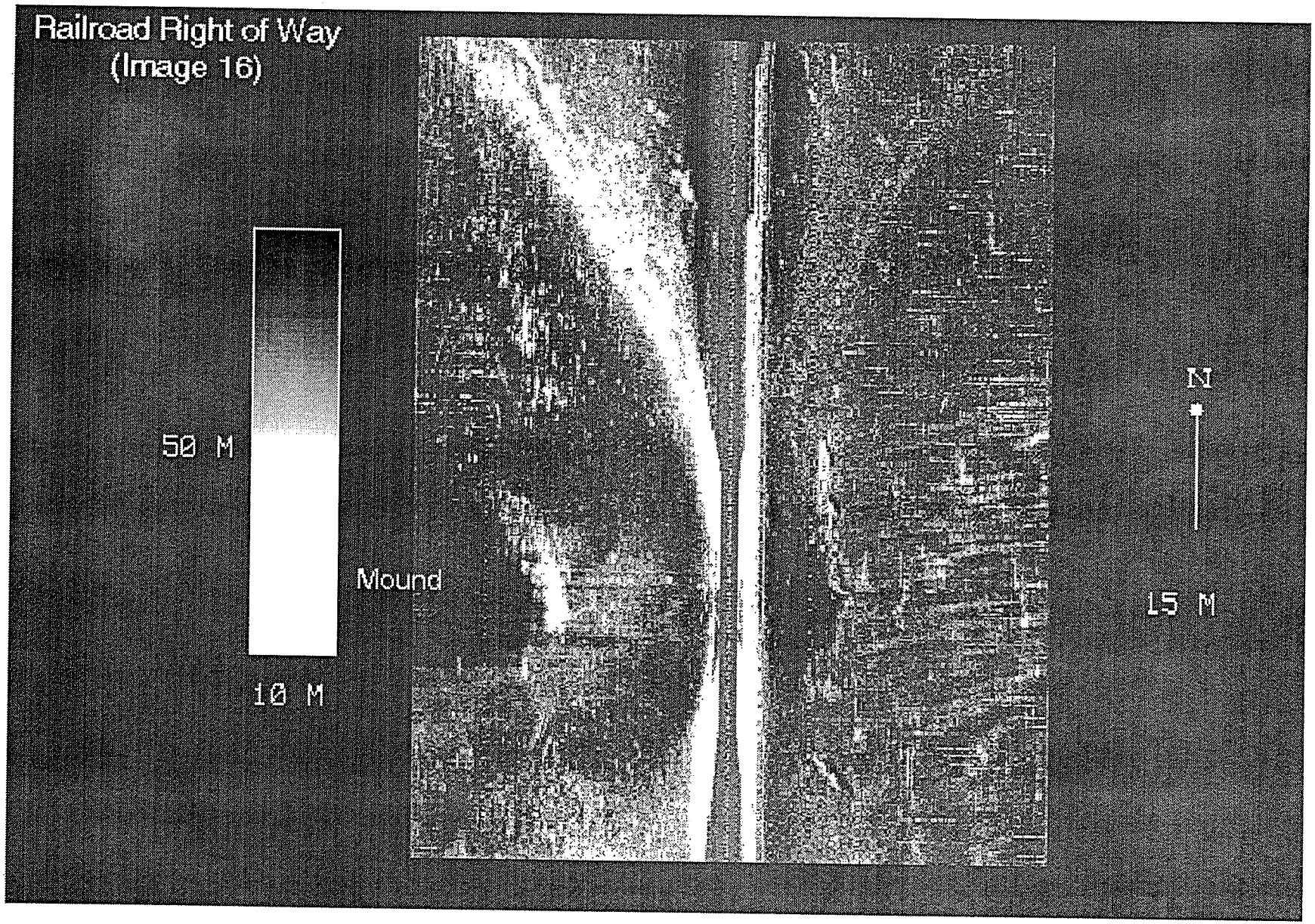

Figure 18

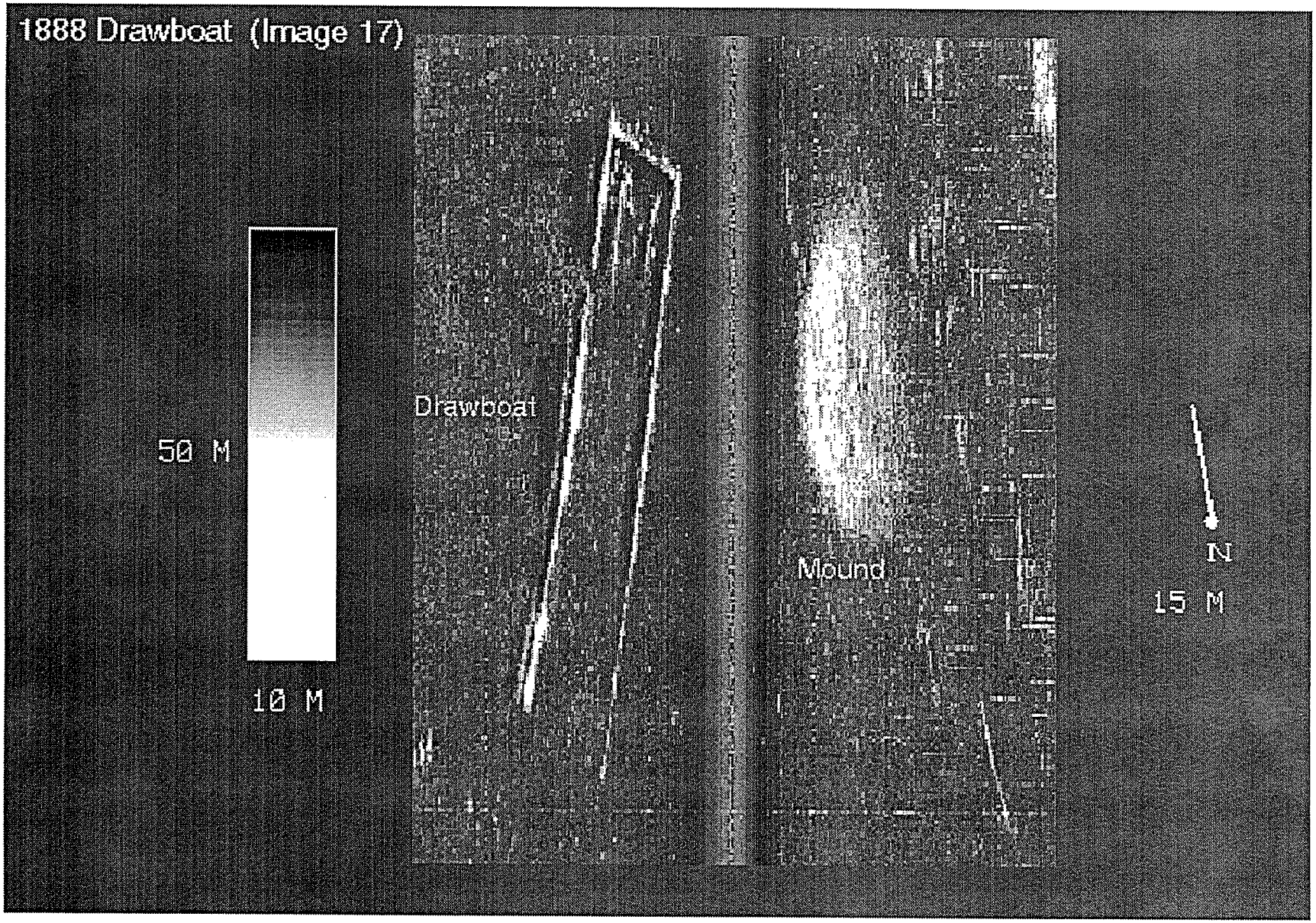

Figure 19

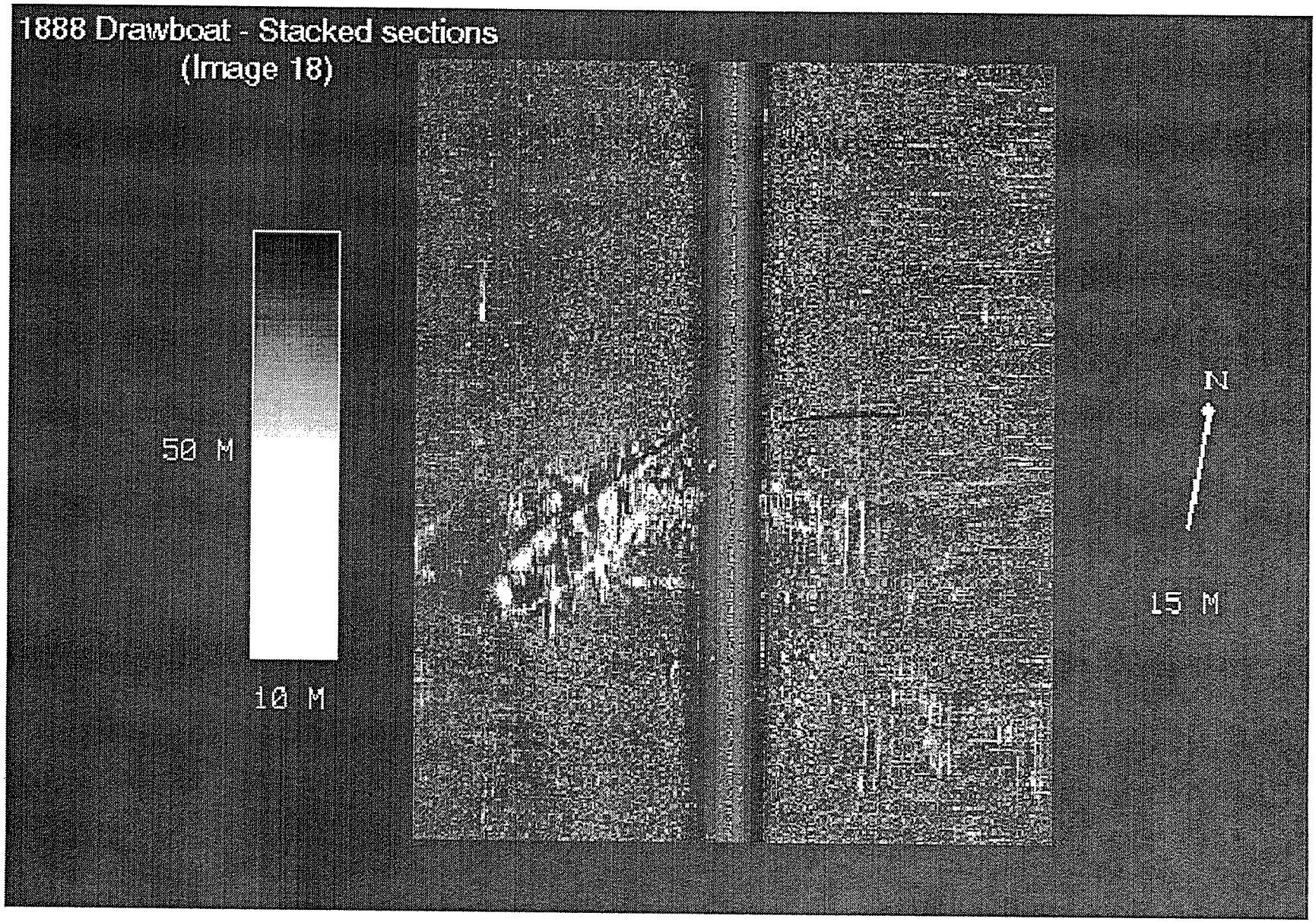

Figure 20

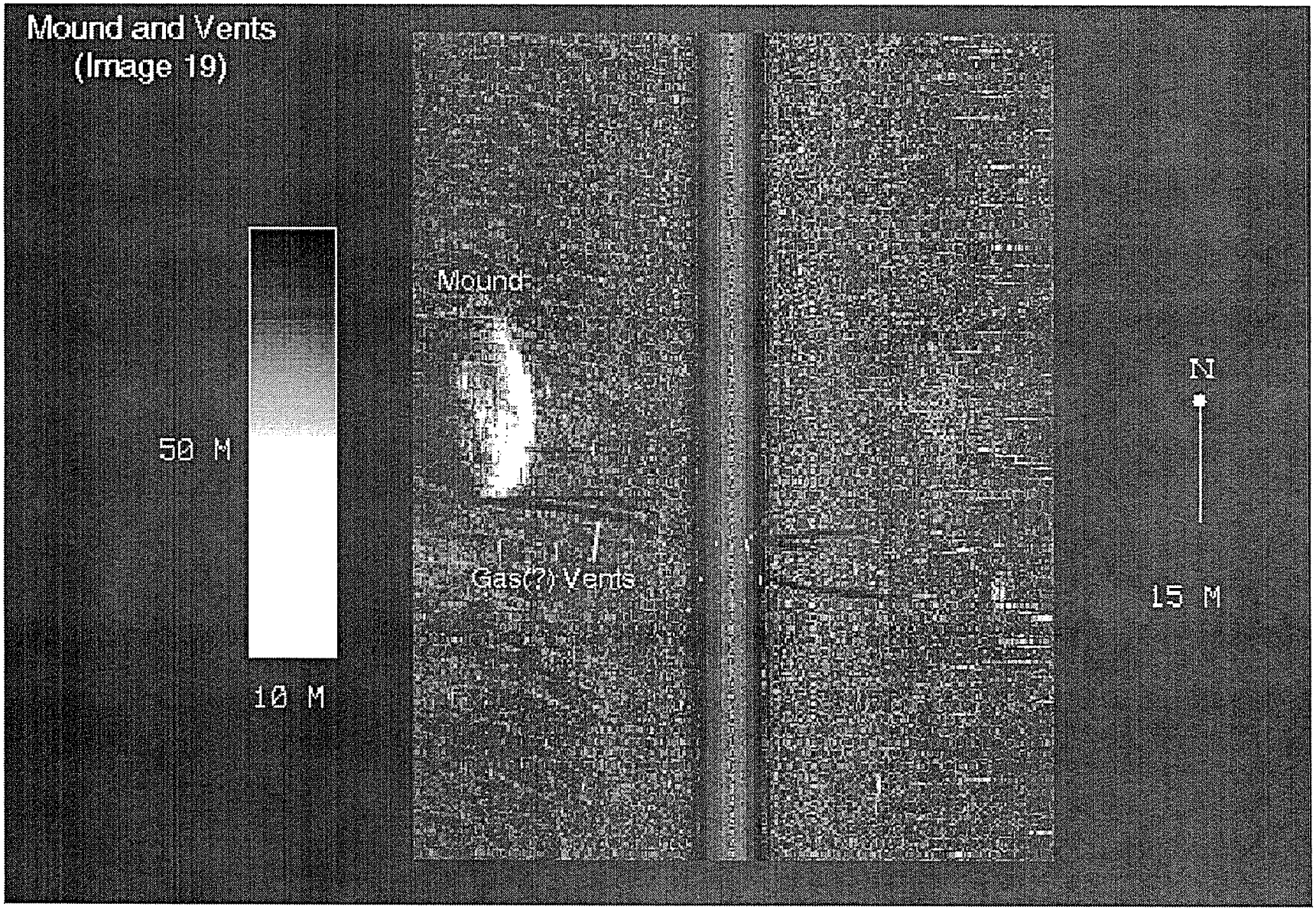

Figure 21

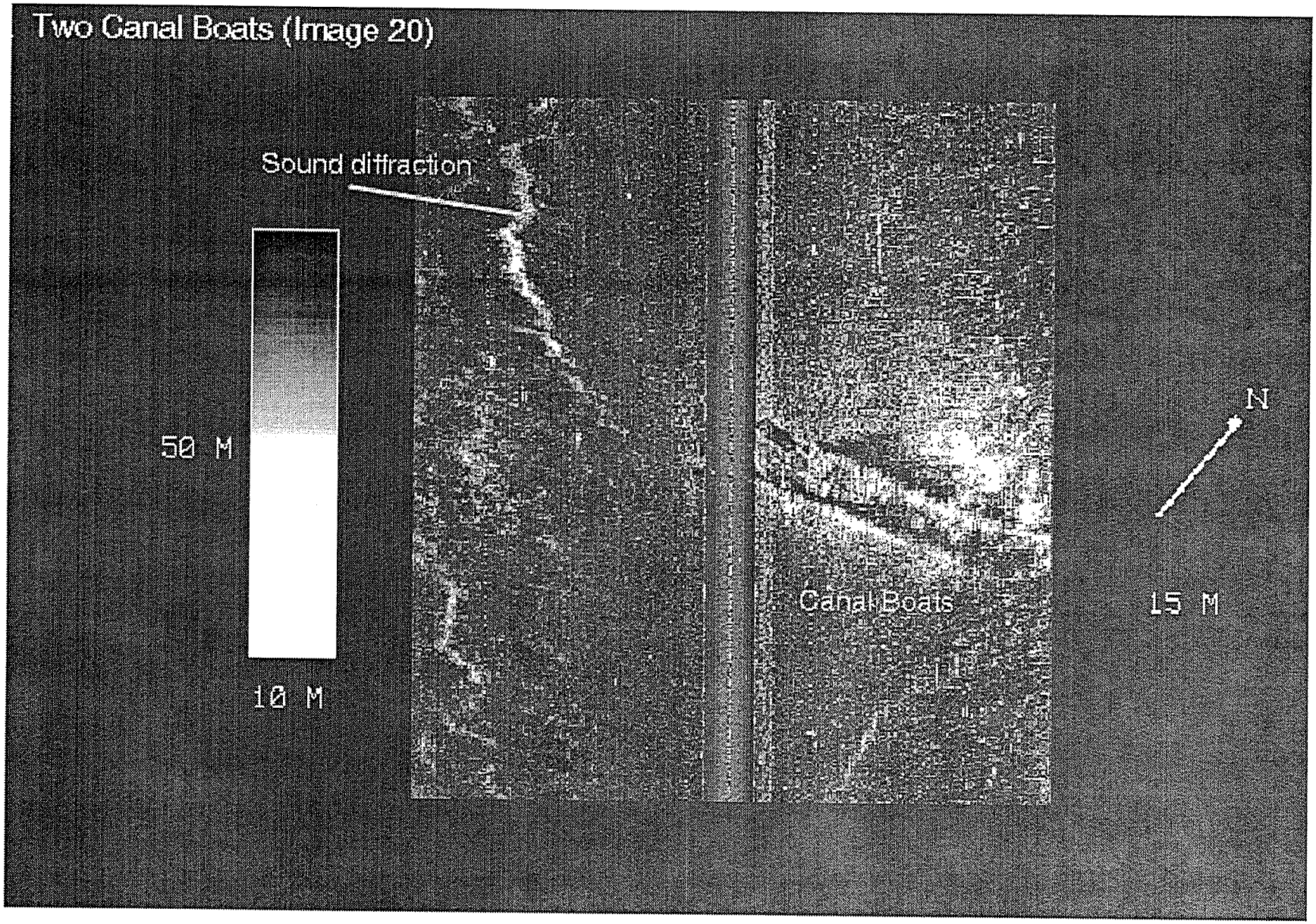
Two Canal Boats (Image 20)
Sound diffraction
50 M
10 M
Canal Boats
N
15 M

Figure 22

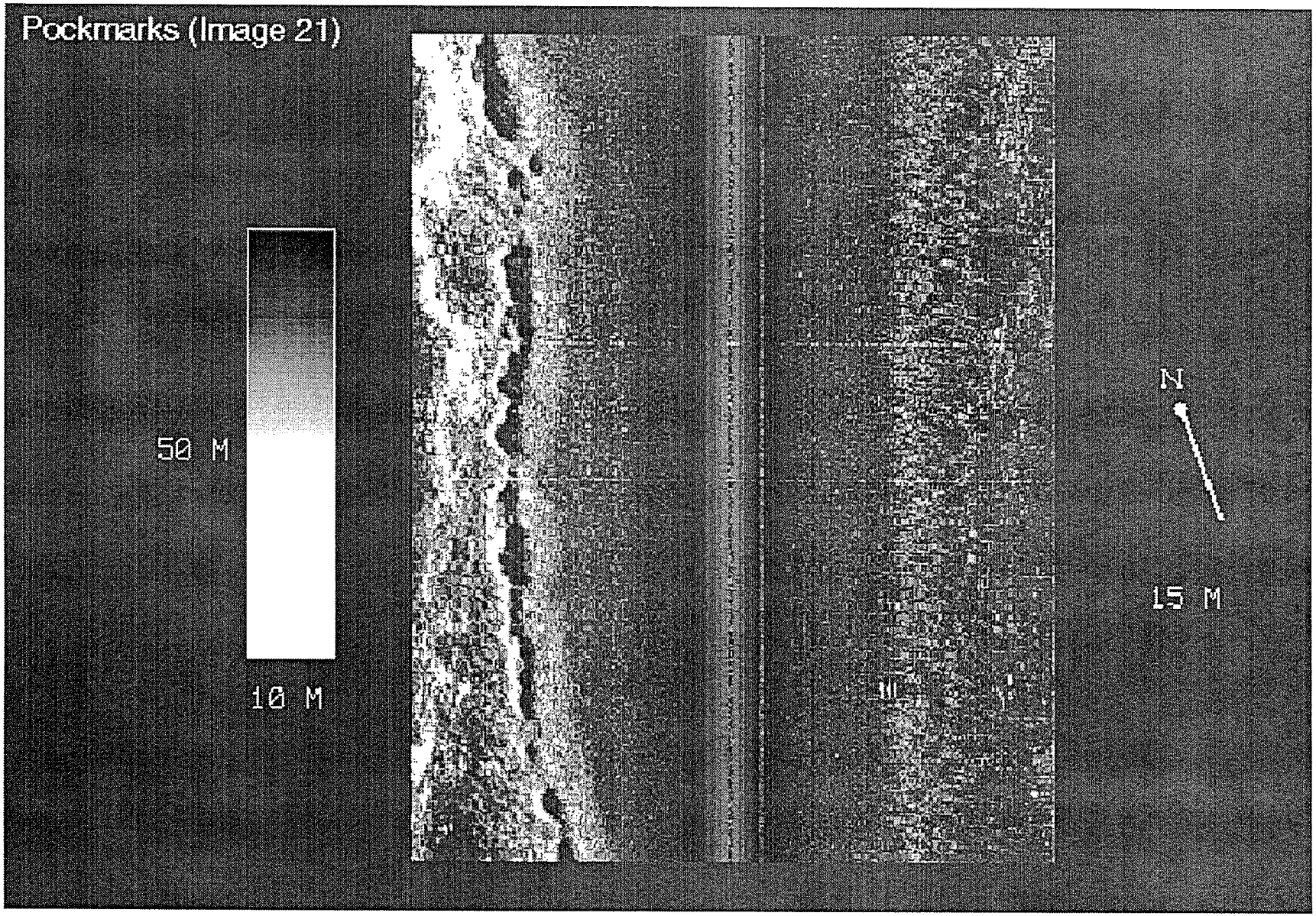

Figure 23

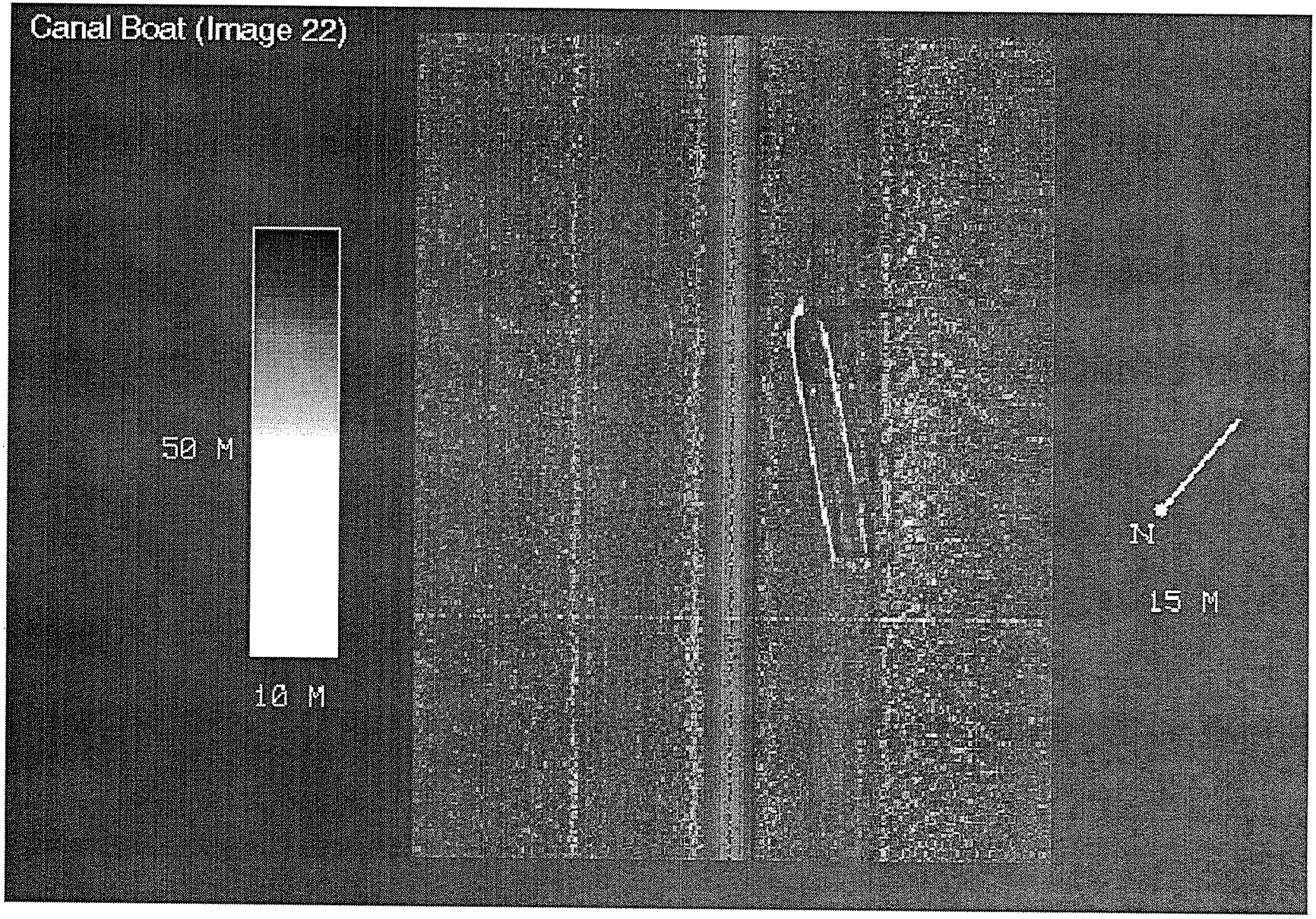

Figure 24

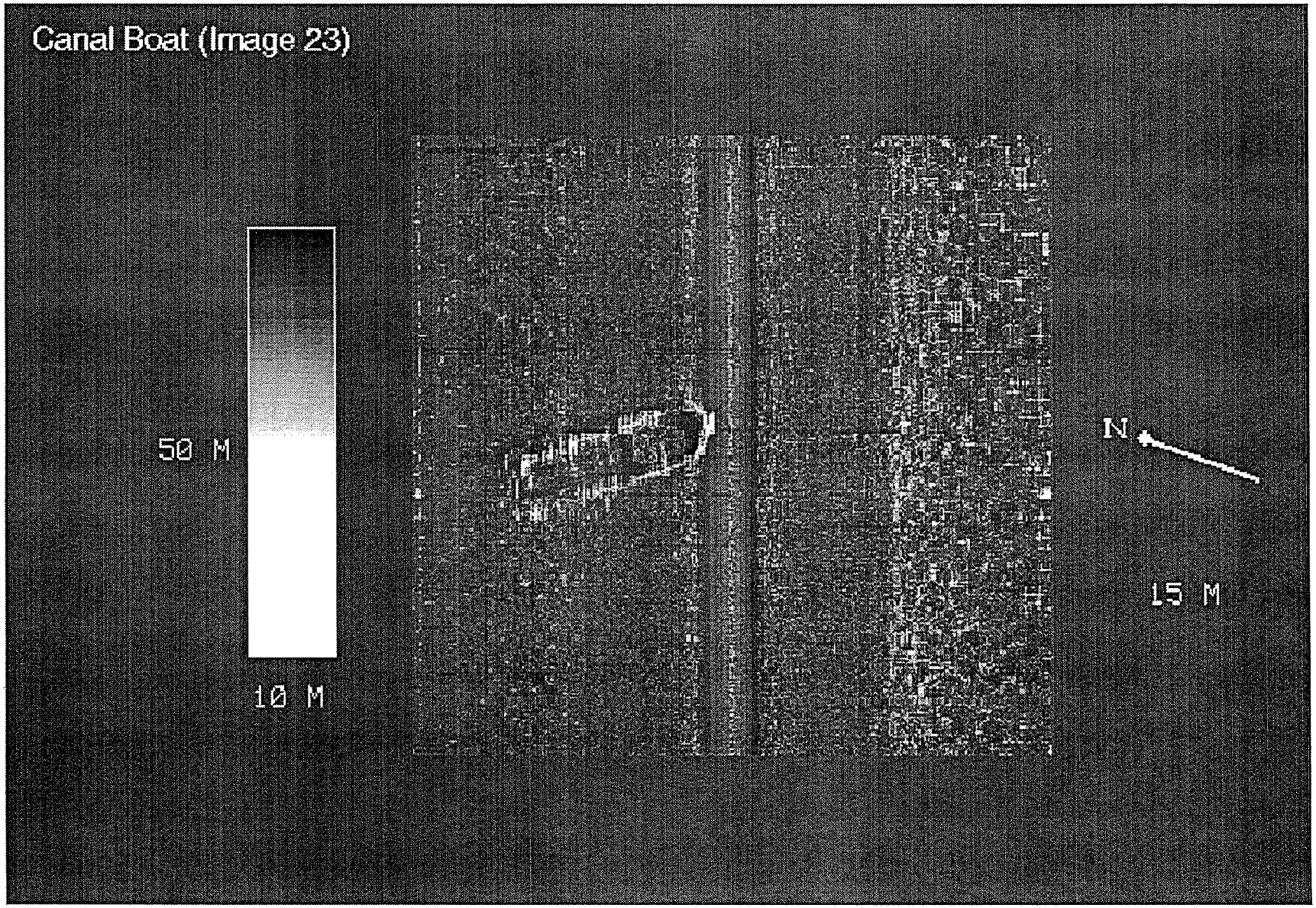

Figure 25

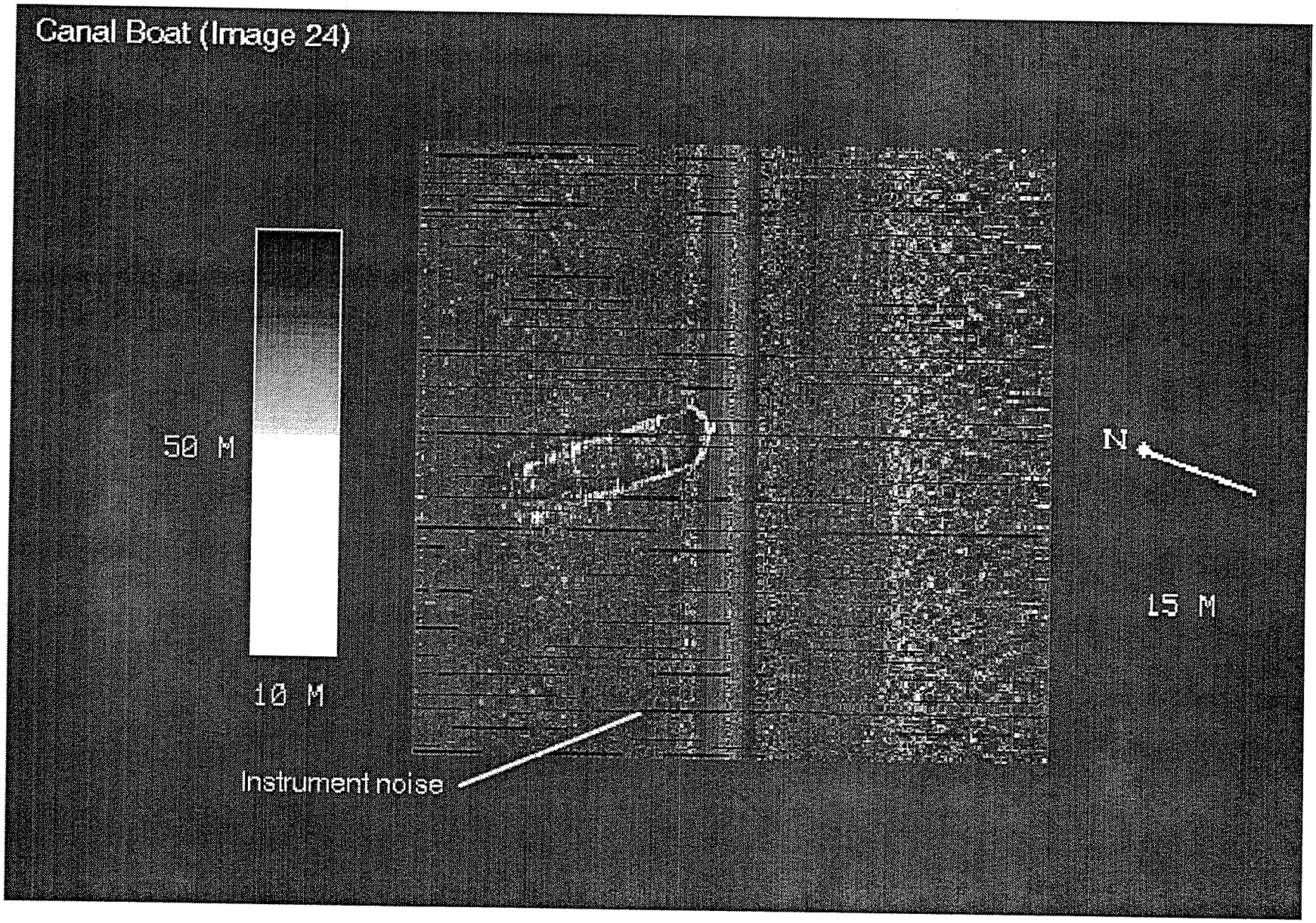

Figure 26

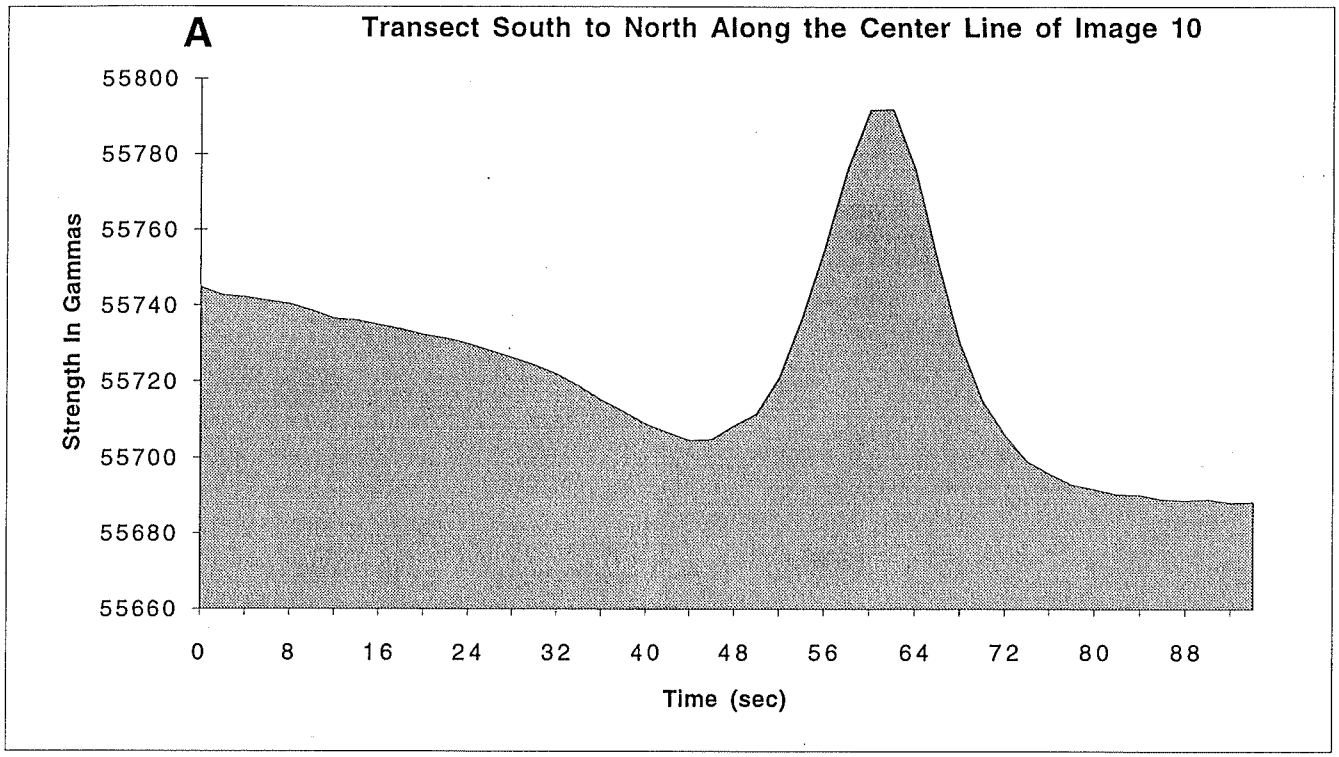
A
Transect South to North Along the Center Line of Image 10
55800
55780
55760
55740
55720
55700
55680
55660
Strength In Gammas
0
8
16
24
32
40
48
56
64
72
80
88
Time (sec)

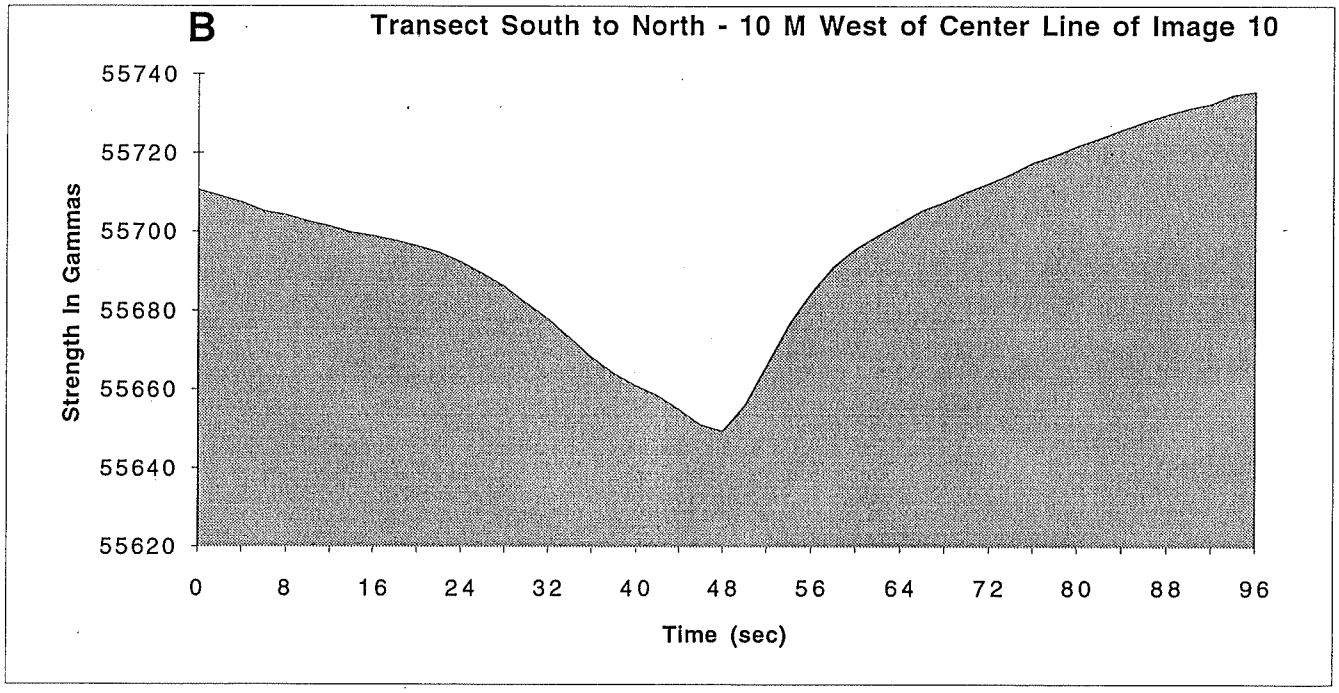
B
Transect South to North - 10 M West of Center Line of Image 10
55740
55720
55700
55680
55660
55640
55620
Strength In Gammas
0
8
16
24
32
40
48
56
64
72
80
88
96
Time (sec)

Figure 27

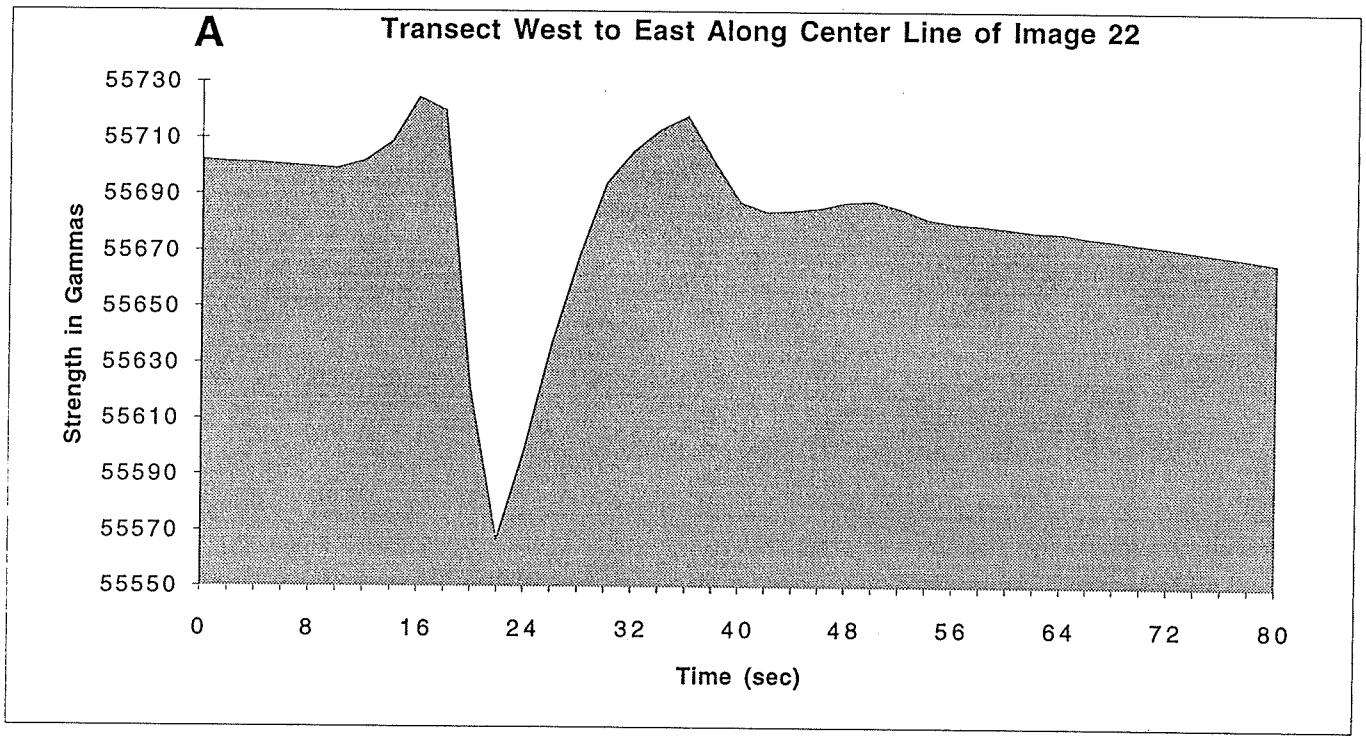
A
Transect West to East Along Center Line of Image 22
Strength in Gammas
55730
55710
55690
55670
55650
55630
55610
55590
55570
55550
0
8
16
24
32
40
48
56
64
72
80
Time (sec)

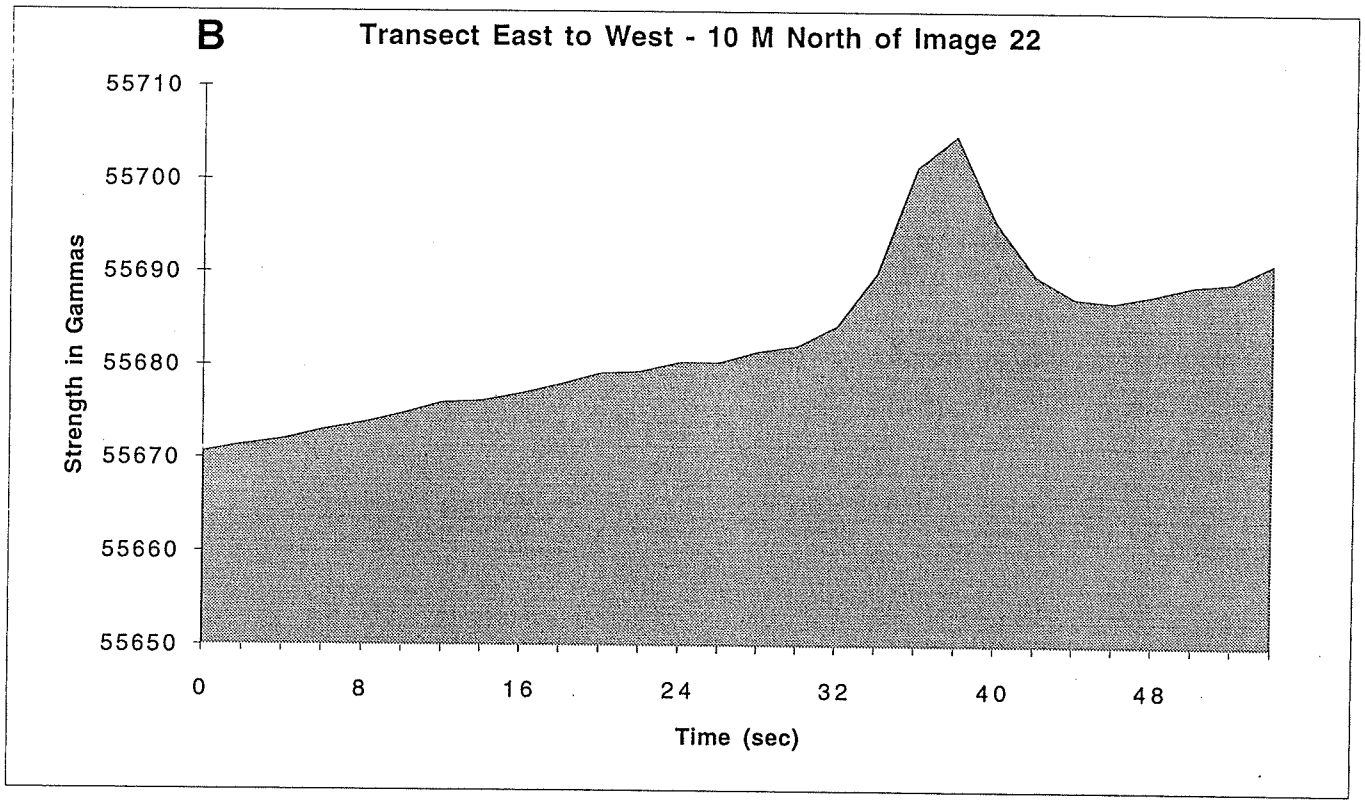
B
Transect East to West - 10 M North of Image 22
Strength in Gammas
55710
55700
55690
55680
55670
55660
55650
0
8
16
24
32
40
48
Time (sec)

Figure 28

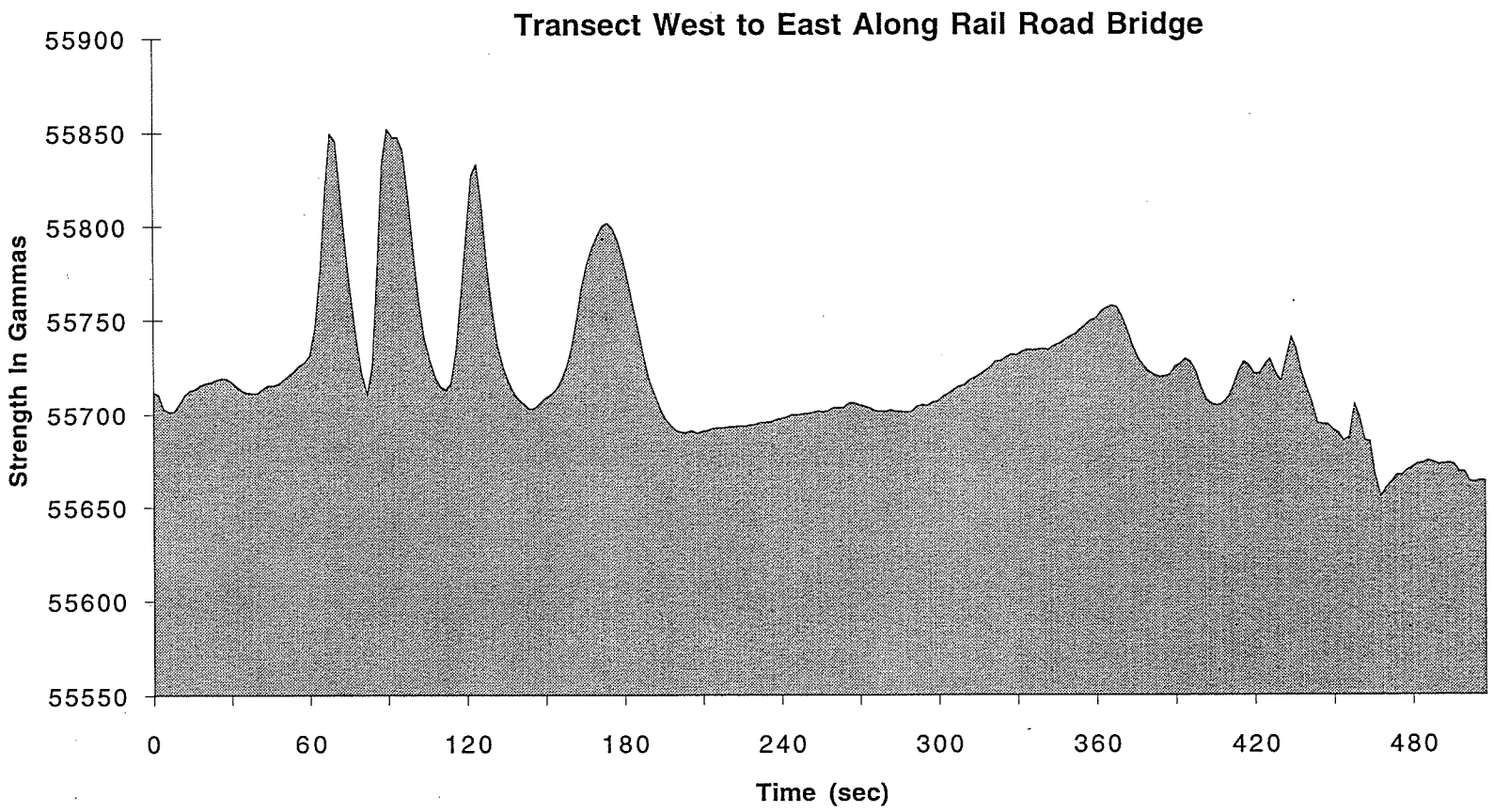
Transect West to East Along Rail Road Bridge
Strength In Gammas
55900
55850
55800
55750
55700
55650
55600
55550
0
60
120
180
240
300
360
420
480
Time (sec)

Figure 29

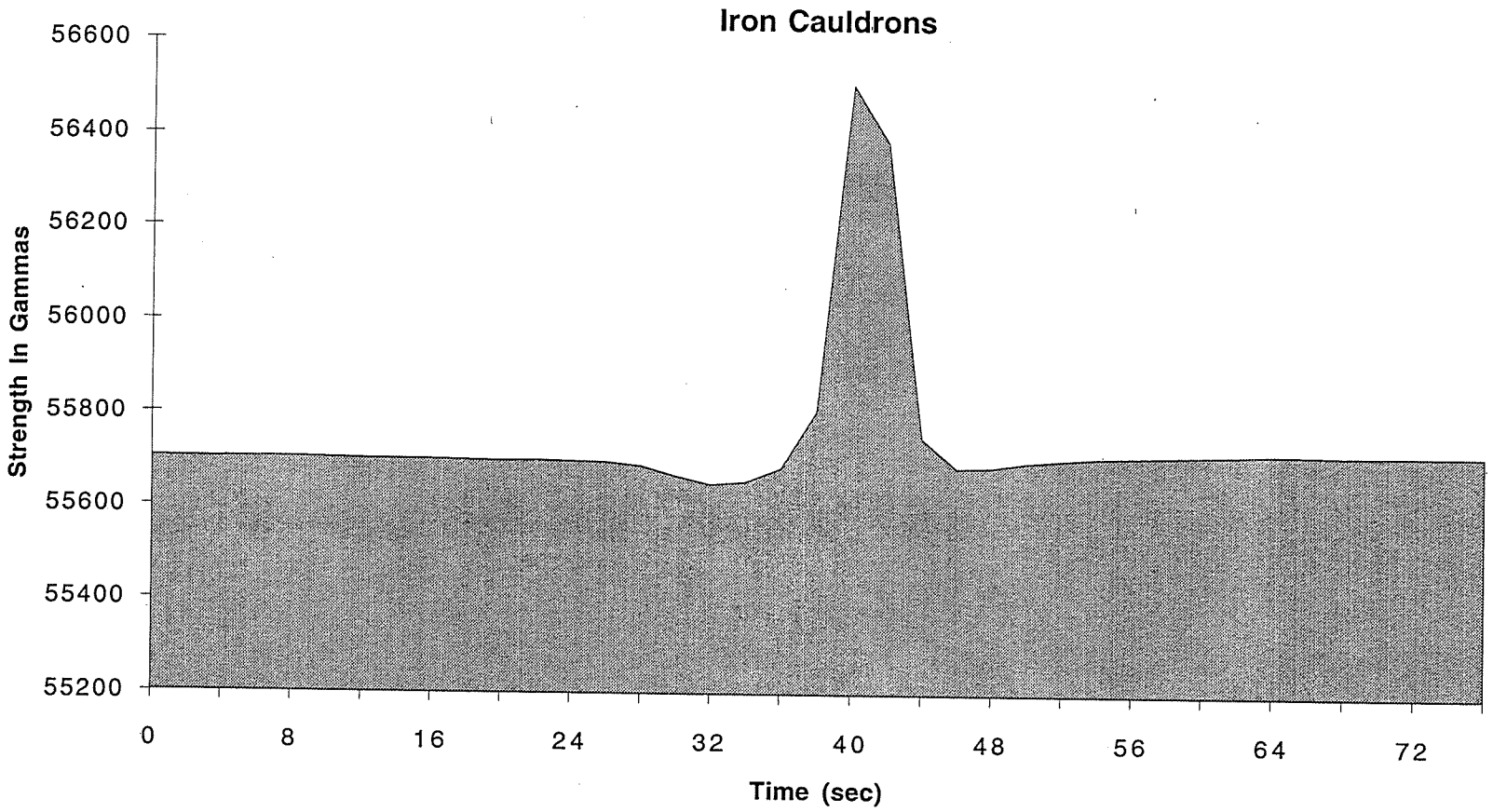
Iron Cauldrons
56600
56400
56200
56000
55800
55600
55400
55200
Strength In Gammas
0
8
16
24
32
40
48
56
64
72
Time (sec)

Figure 30

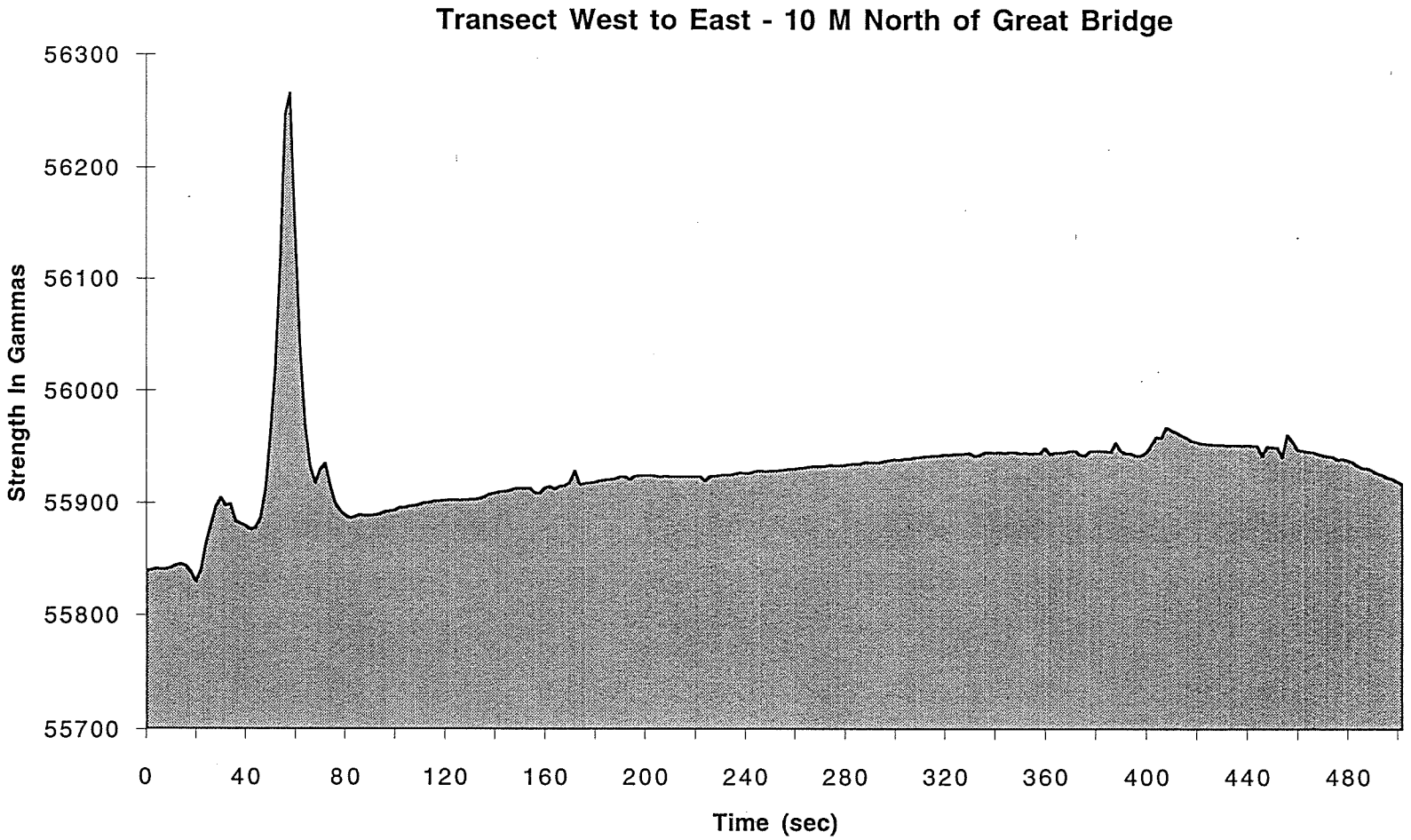
Transect West to East - 10 M North of Great Bridge
Strength In Gammas
56300
56200
56100
56000
55900
55800
55700
0
40
80
120
160
200
240
280
320
360
400
440
480
Time (sec)

Figure 31

MIDDLEBURY COLLEGE MARINE SCIENCES

Geological Sample Data Sheet

Vessel & Cruise: Baldwin Leg: B93-01

Station: 1 Date (DY/MO/YR): 16-09-93

General Location: Northeast caisson #2

Bottom Topography: flat Sediment Thickness: N/A (sec)

☑ Core ☐ Ponar# MIFT-01 Len. of corer: 7 ft Chief Scientist: Pat Manley

Personnel: Tom Manley /Art Cohen /Fred Fayette /C. Goodrich /

/ / / / /

	START	ON BTM	END
Time:	10:10 22:10(com.)		
Depth :	20.2 ft		
GPS			
Lat.:	43° 50.2'	43° 50.17'	
Long.:	73° 22.876'	73° 22.88'	
LORAN-C			
Lat. :			
Long.:			

Weight on Corer: 20 (kg) Trigger length: 15 (ft)

Free fall length: 60 (in) Dist btwn TW /cutter: 56 (in)

Optimum for 7 foot core: 40 kg on corer, Trigger length 18 feet, Dist btwn TW and cutter 102 in

Length of core: 185 cm

Brief Description:

Mud on outer weight

No noticable horizons on PDR

Addition Station Work at same location:

Remarks:

Sketch:

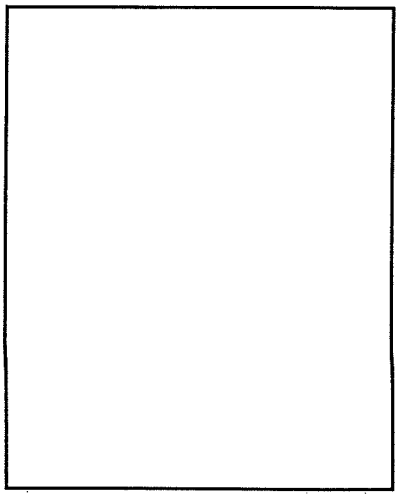

Figure 32

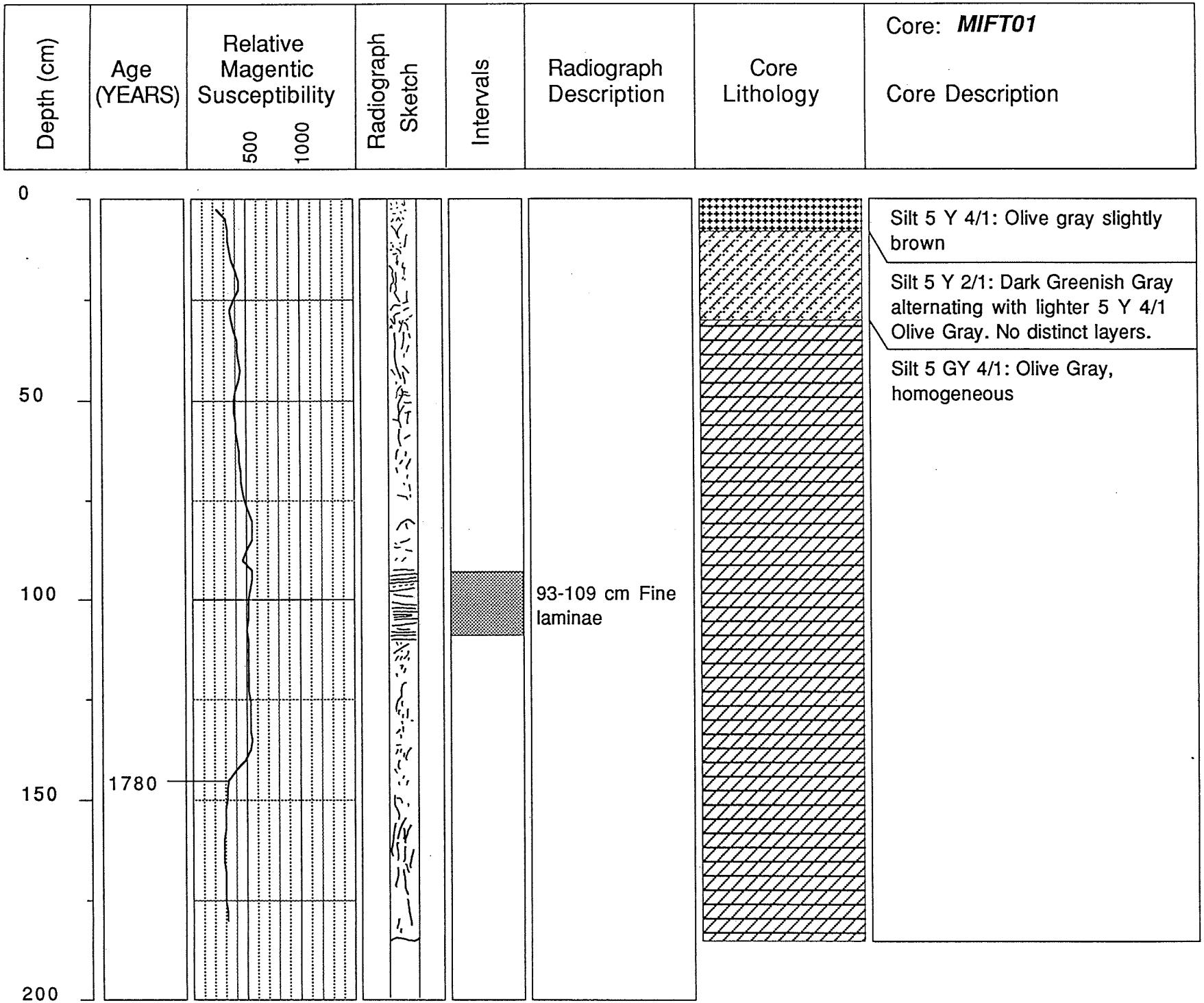
Depth (cm)
Age (YEARS)
Relative Magentic Susceptibility
500
1000
Radiograph Sketch
Intervals
Radiograph Description
Core Lithology
Core: MIFT01
Core Description
0
50
100
150
200
1780
93-109 cm Fine laminae
Silt 5 Y 4/1: Olive gray slightly brown
Silt 5 Y 2/1: Dark Greenish Gray alternating with lighter 5 Y 4/1 Olive Gray. No distinct layers.
Silt 5 GY 4/1: Olive Gray, homogeneous

Figure 33

MIDDLEBURY COLLEGE MARINE SCIENCES

Geological Sample Data Sheet

Vessel & Cruise: Baldwin Leg: B93-01

Station: 1 Date (DY/MO/YR): 16-09-93

General Location: Northeast caisson #2

Bottom Topography: flat Sediment Thickness: N/A (sec)

☑ Core ☐ Ponar# MIFT-02 Len. of corer: 7 ft Chief Scientist: Pat Manley

Personnel: Tom Manley /Art Cohen /Fred Fayette /C. Goodrich /

/ / / / /

	START	**ON BTM**	**END**
Time:	11:12		
Depth :	20 ft		
GPS			
Lat.:	43° 50.227'	43° 50.194'	
Long.:	73° 22.882'	73° 22.86'	
LORAN-C			
Lat. :			
Long.:			

Weight on Corer: 20 (kg) Trigger length: 14 (ft)

Free fall length: 72 (in) Dist btwn TW /cutter: 44 (in)

Optimum for 7 foot core: 40 kg on corer, Trigger length 18 feet, Dist btwn TW and cutter 102 in

Length of core: 124 cm

Brief Description:

Mud on core barrel below core head

No noticable horizons on PDR

Trigger not so noticable .

Addition Station Work at same location:

Remarks:

Sketch:

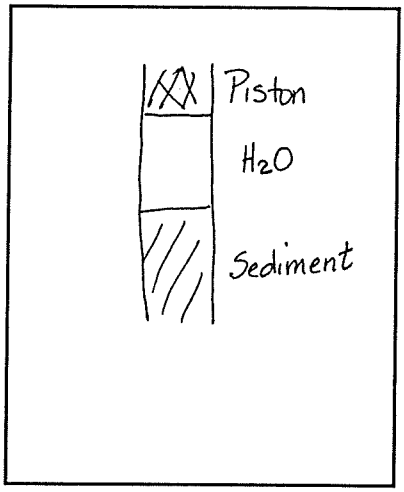

Figure 34

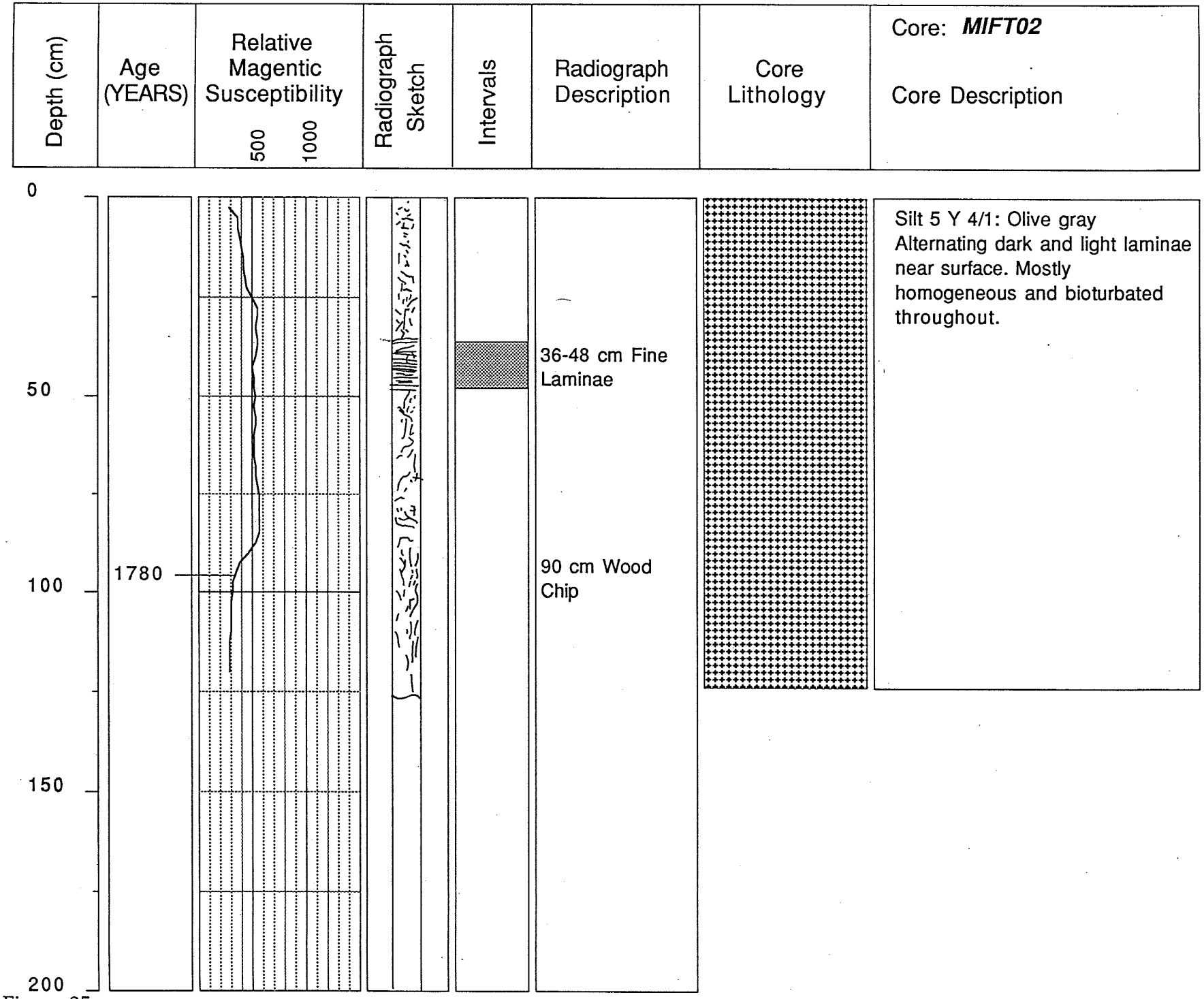
Depth (cm)
Age (YEARS)
Relative Magentic Susceptibility
500
1000
Radiograph Sketch
Intervals
Radiograph Description
Core Lithology
Core: MIFT02
Core Description
0
50
100
150
200
1780
36-48 cm Fine Laminae
90 cm Wood Chip
Silt 5 Y 4/1: Olive gray
Alternating dark and light laminae near surface. Mostly homogeneous and bioturbated throughout.

Figure 35

MIDDLEBURY COLLEGE MARINE SCIENCES
Geological Sample Data Sheet

Vessel & Cruise: Baldwin Leg: B93-01
Station: 1 Date (DY/MO/YR): 16-09-93
General Location: Center channel south of caissons
Bottom Topography: flat Sediment Thickness: N/A (sec)
☑ Core ☐ Ponar# MIFT-03 Len. of corer: 7 ft Chief Scientist: Pat Manley
Personnel: Tom Manley /Art Cohen /Fred Fayette /C. Goodrich /
/ / / / /

	START	ON BTM	END
Time:	12:57	1:05	
Depth :	21.1 ft		
GPS			
Lat.:	43° 50.290'	43° 50.292'	
Long.:	73° 22.910'	73° 22.909'	
LORAN-C			
Lat. :			
Long.:			

Weight on Corer: 20 (kg) Trigger length: 18 (ft)
Free fall length: 37.2 (in) Dist btwn TW /cutter: 102 (in)

Optim. for 7 ft core: 40 kg on corer, 20 kg on trigger, Trig len. 18 feet, Dist btwn TW and cutter 102cm

Brief Description:
Mud on core barrel above knuckle
No noticable horizons on PDR
Good Trigger

Addition Station Work at same location:

Remarks:
No sediment in the core catcher

Length of core: 113 cm

Sketch:

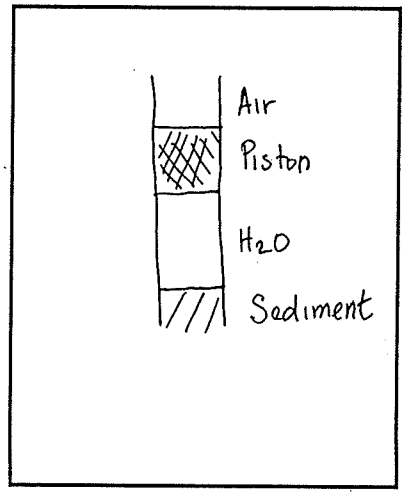

Figure 36

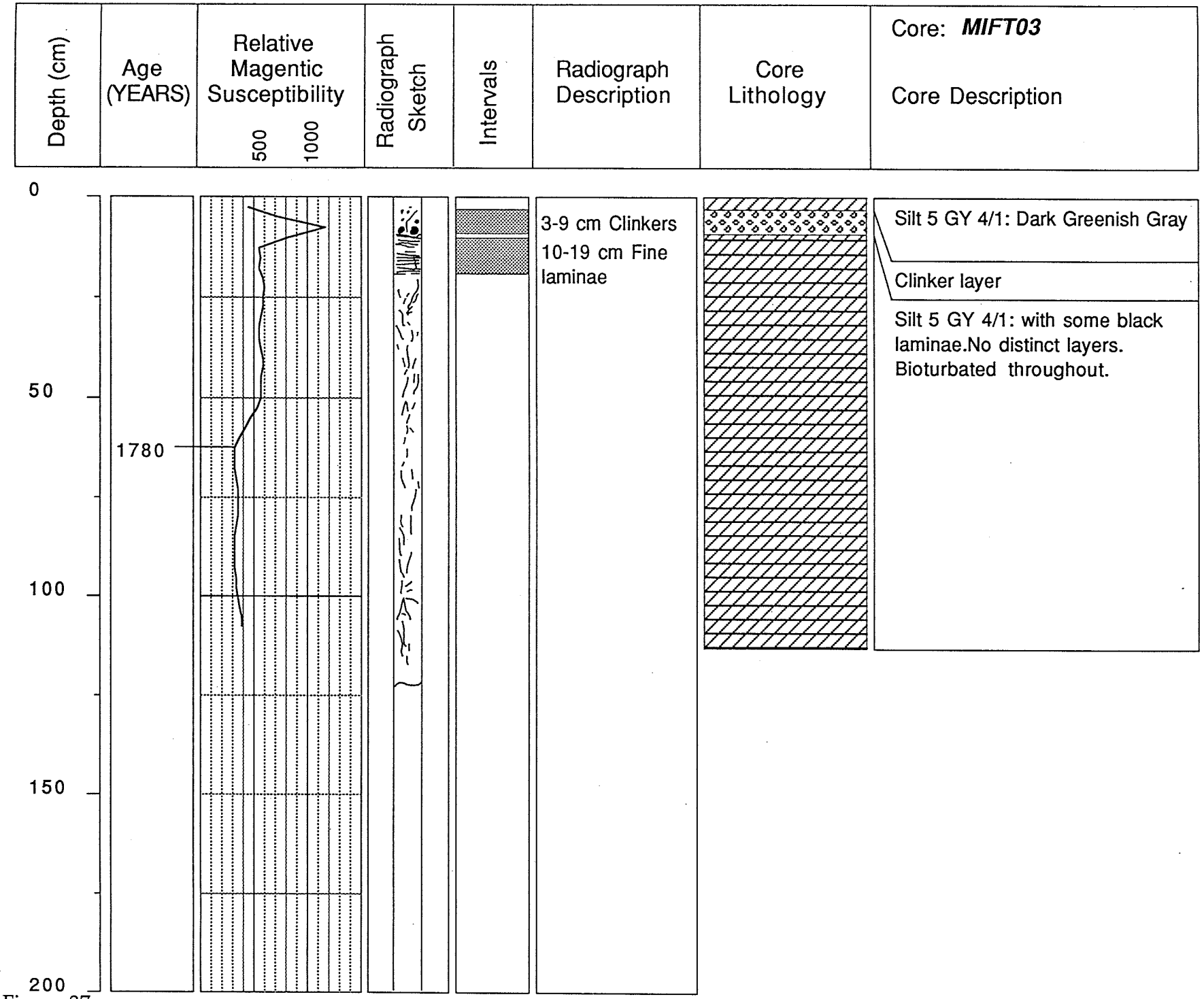
Depth (cm)
Age (YEARS)
Relative Magentic Susceptibility
500
1000
Radiograph Sketch
Intervals
Radiograph Description
Core Lithology
Core: MIFT03
Core Description
0
50
100
150
200
1780
3-9 cm Clinkers
10-19 cm Fine laminae
Silt 5 GY 4/1: Dark Greenish Gray
Clinker layer
Silt 5 GY 4/1: with some black laminae.No distinct layers. Bioturbated throughout.

Figure 37

MIDDLEBURY COLLEGE MARINE SCIENCES
Geological Sample Data Sheet

Vessel & Cruise: Baldwin Leg: B93-01

Station: 1 Date (DY/MO/YR): 16-09-93

General Location: Center channel south of caissons

Bottom Topography: flat Sediment Thickness: N/A (sec)

☑ Core ☐ Ponar# MIFT-04 Len. of corer: 7 ft Chief Scientist: Pat Manley

Personnel: Tom Manley /Art Cohen /Fred Fayette /C. Goodrich /

/ / / / /

	START	ON BTM	END
Time:	1:50	1:57	
Depth :	21.1 ft		
GPS			
Lat.:	43° 50.312'	43° 50.312'	
Long.:	73° 22.889'	73° 22.889'	
LORAN-C			
Lat. :			
Long.:			

Weight on Corer: 40 (kg) Trigger length: 18 (ft)

Free fall length: 37.2 (in) Dist btwn TW /cutter: 102 (in)

Optim. for 7 ft core: 40 kg on corer, 20 kg on trigger, Trig len. 18 feet, Dist btwn TW and cutter 102cm

Brief Description:

Mud on core head fins

No noticable horizons on PDR

Not much water above piston

Addition Station Work at same location:

Remarks:

No sediment in the core catcher

Length of core: 200 cm

Sketch:

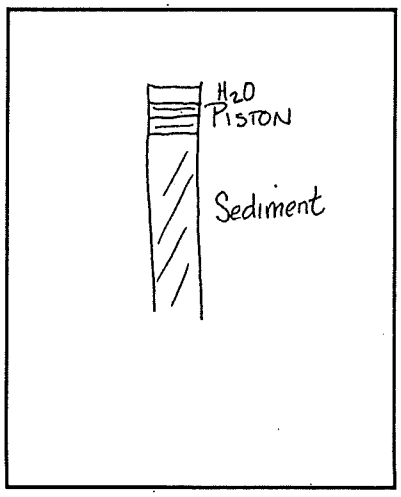

Figure 38

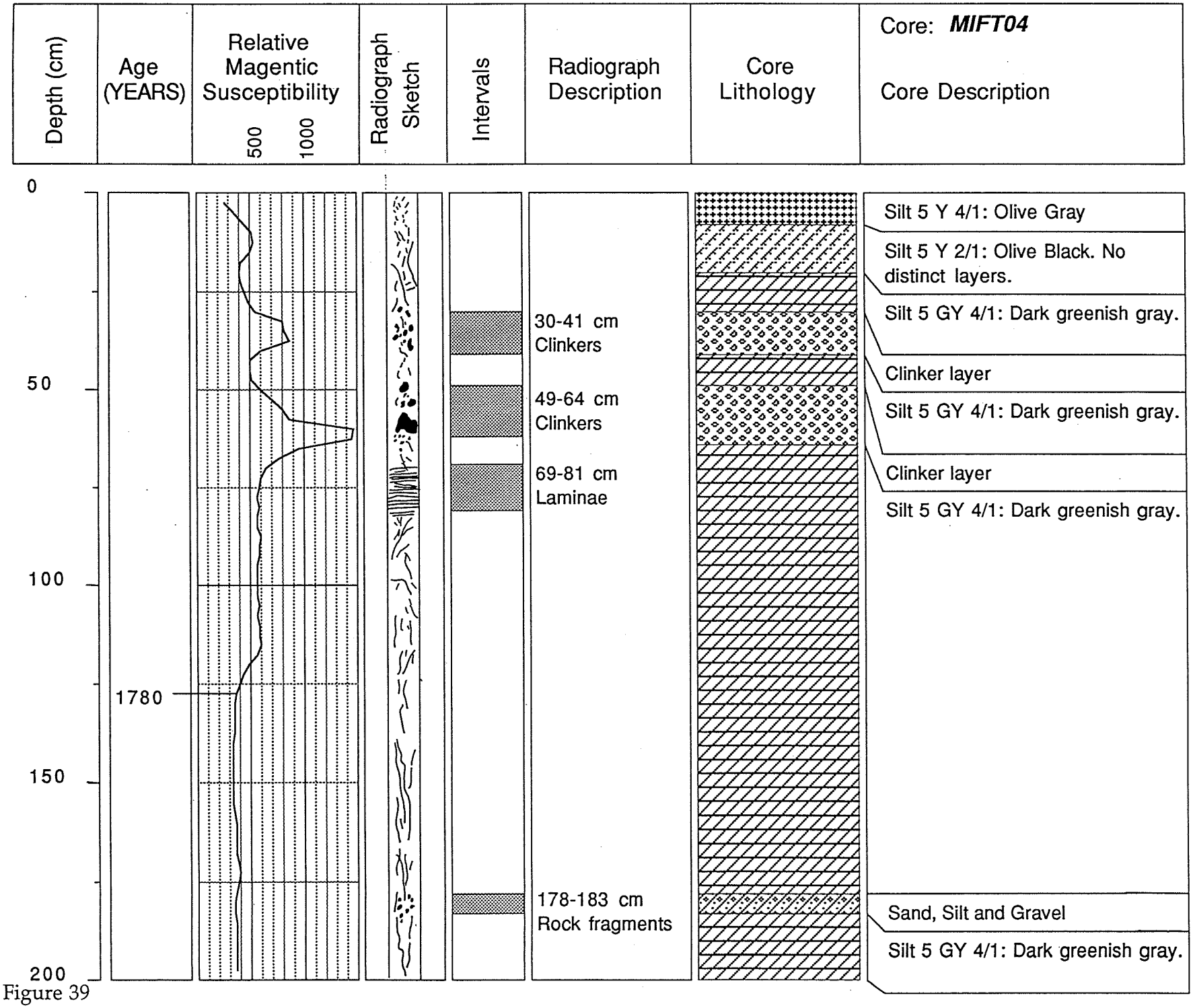
Depth (cm)
Age (YEARS)
Relative Magentic Susceptibility
500
1000
Radiograph Sketch
Intervals
Radiograph Description
Core Lithology
Core: MIFT04
Core Description
0
50
100
150
200
1780
30-41 cm Clinkers
49-64 cm Clinkers
69-81 cm Laminae
178-183 cm Rock fragments
Silt 5 Y 4/1: Olive Gray
Silt 5 Y 2/1: Olive Black. No distinct layers.
Silt 5 GY 4/1: Dark greenish gray.
Clinker layer
Silt 5 GY 4/1: Dark greenish gray.
Clinker layer
Silt 5 GY 4/1: Dark greenish gray.
Sand, Silt and Gravel
Silt 5 GY 4/1: Dark greenish gray.

Figure 39

MIDDLEBURY COLLEGE MARINE SCIENCES
Geological Sample Data Sheet

Vessel & Cruise: Baldwin Leg: B93-01

Station: 1 Date (DY/MO/YR): 16-09-93

General Location: 100 ft off VT shore landing, 100 ft east of caisson #2

Bottom Topography: flat Sediment Thickness: N/A (sec)

☑ Core ☐ Ponar# MIFT-05 Len. of corer: 7 ft Chief Scientist: Pat Manley

Personnel: Tom Manley /Art Cohen /Fred Fayette /C. Goodrich /

/ / / / /

	START	ON BTM	END
Time:	2:58	2:58	
Depth :	16 ft		
GPS			
Lat.:	43° 50.179'	43° 50.179'	
Long.:	73° 22.85'	73° 22.85'	
LORAN-C			
Lat. :			
Long.:			

Weight on Corer: 40 (kg) Trigger length: 18 (ft)

Free fall length: 0 (in) Dist btwn TW /cutter: 102 (in)

Optim. for 7 ft core: 40 kg on corer, 20 kg on trigger, Trig len. 18 feet, Dist btwn TW and cutter 102cm

Brief Description:

Mud on core head fins

No noticable horizons on PDR

Addition Station Work at same location:

Remarks:

Suction pull out

Length of core: 214 cm

Figure 40

Sketch:

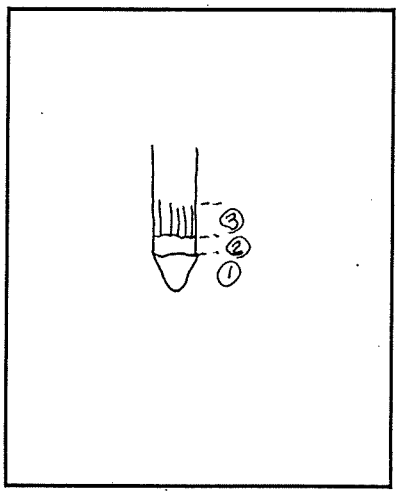

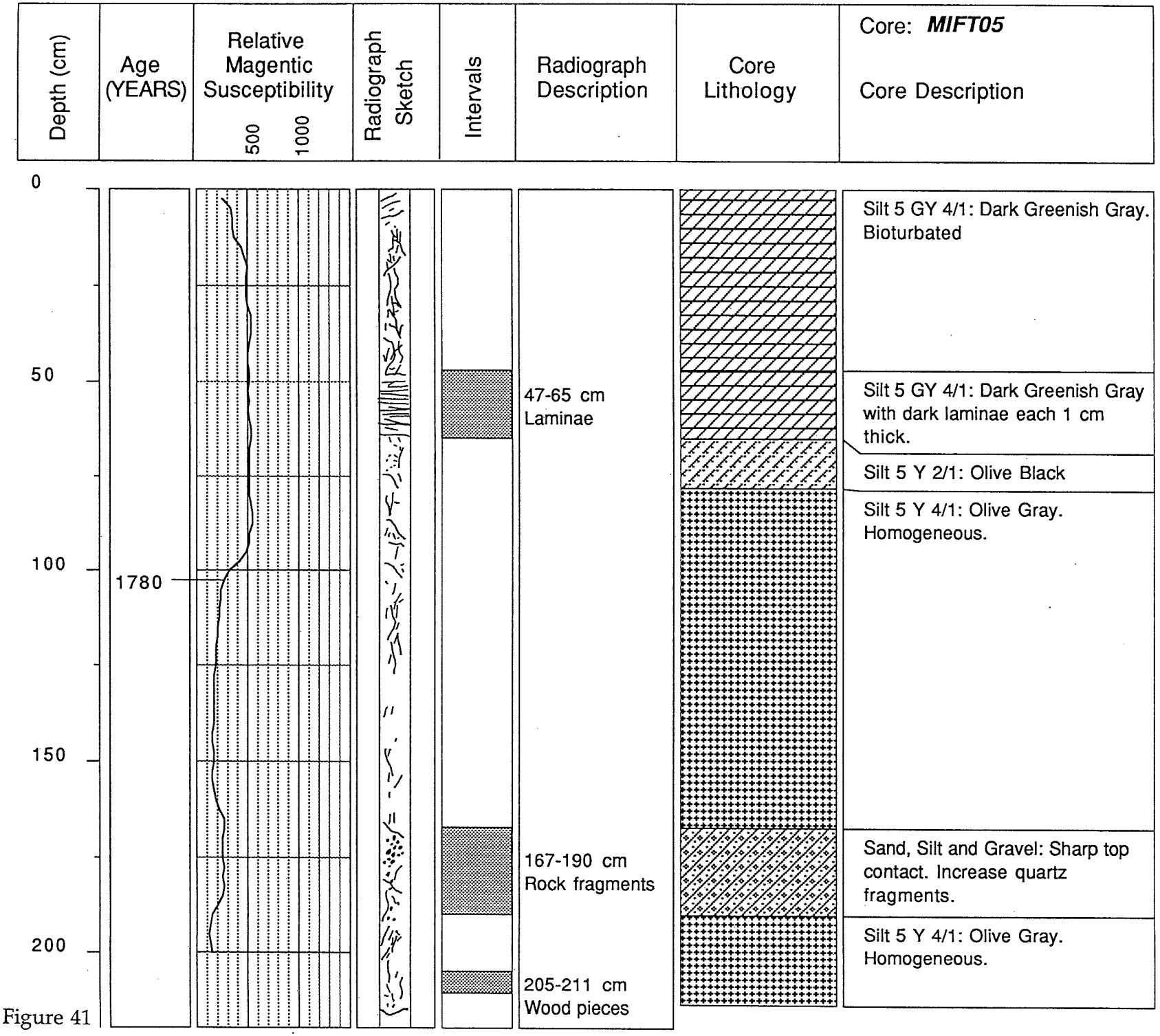
Depth (cm)
Age (YEARS)
Relative Magentic Susceptibility
500
1000
Radiograph Sketch
Intervals
Radiograph Description
Core Lithology
Core: MIFT05
Core Description
0
50
100
150
200
1780
47-65 cm
Laminae
167-190 cm
Rock fragments
205-211 cm
Wood pieces
Silt 5 GY 4/1: Dark Greenish Gray. Bioturbated
Silt 5 GY 4/1: Dark Greenish Gray with dark laminae each 1 cm thick.
Silt 5 Y 2/1: Olive Black
Silt 5 Y 4/1: Olive Gray. Homogeneous.
Sand, Silt and Gravel: Sharp top contact. Increase quartz fragments.
Silt 5 Y 4/1: Olive Gray. Homogeneous.

Figure 41

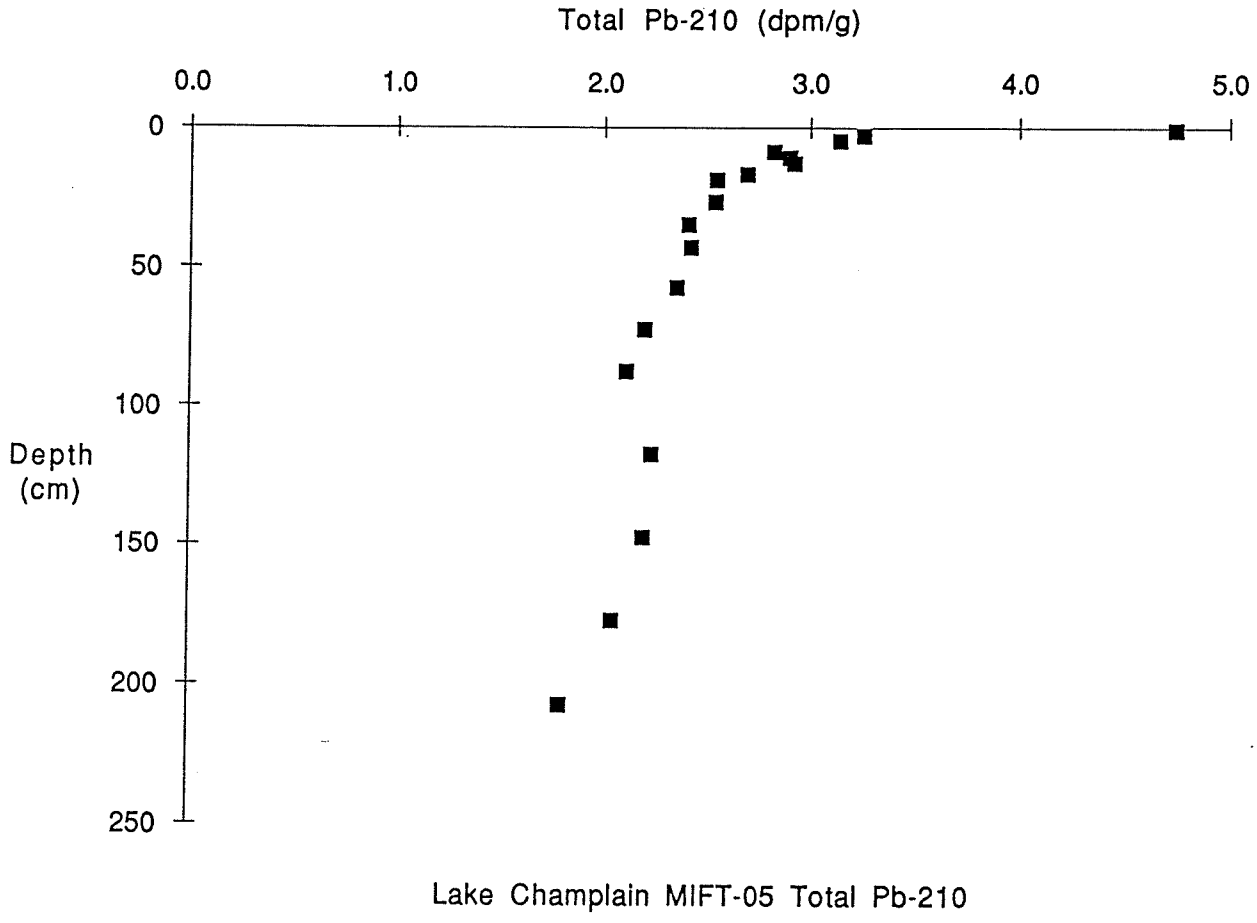
Total Pb-210 (dpm/g)
0.0
1.0
2.0
3.0
4.0
5.0
0
50
100
150
200
250
Depth
(cm)
Lake Champlain MIFT-05 Total Pb-210

Figure 42

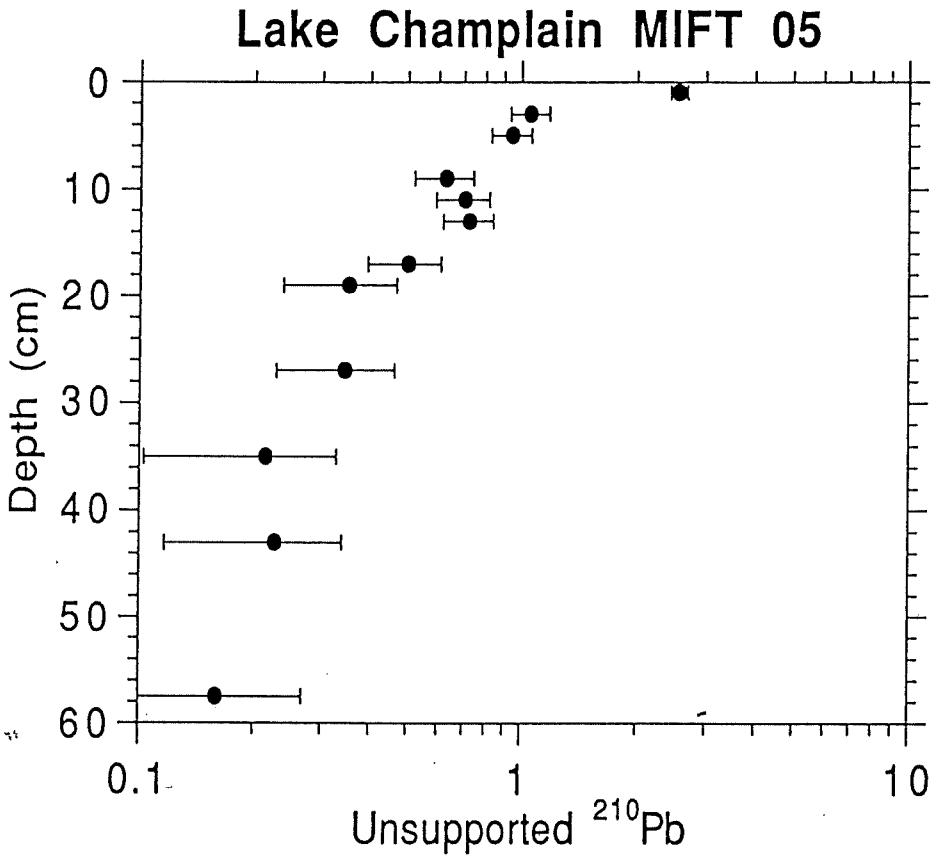
Lake Champlain MIFT 05
Depth (cm)
0
10
20
30
40
50
60
0.1
1
10
Unsupported ^{210}Pb

Figure 43

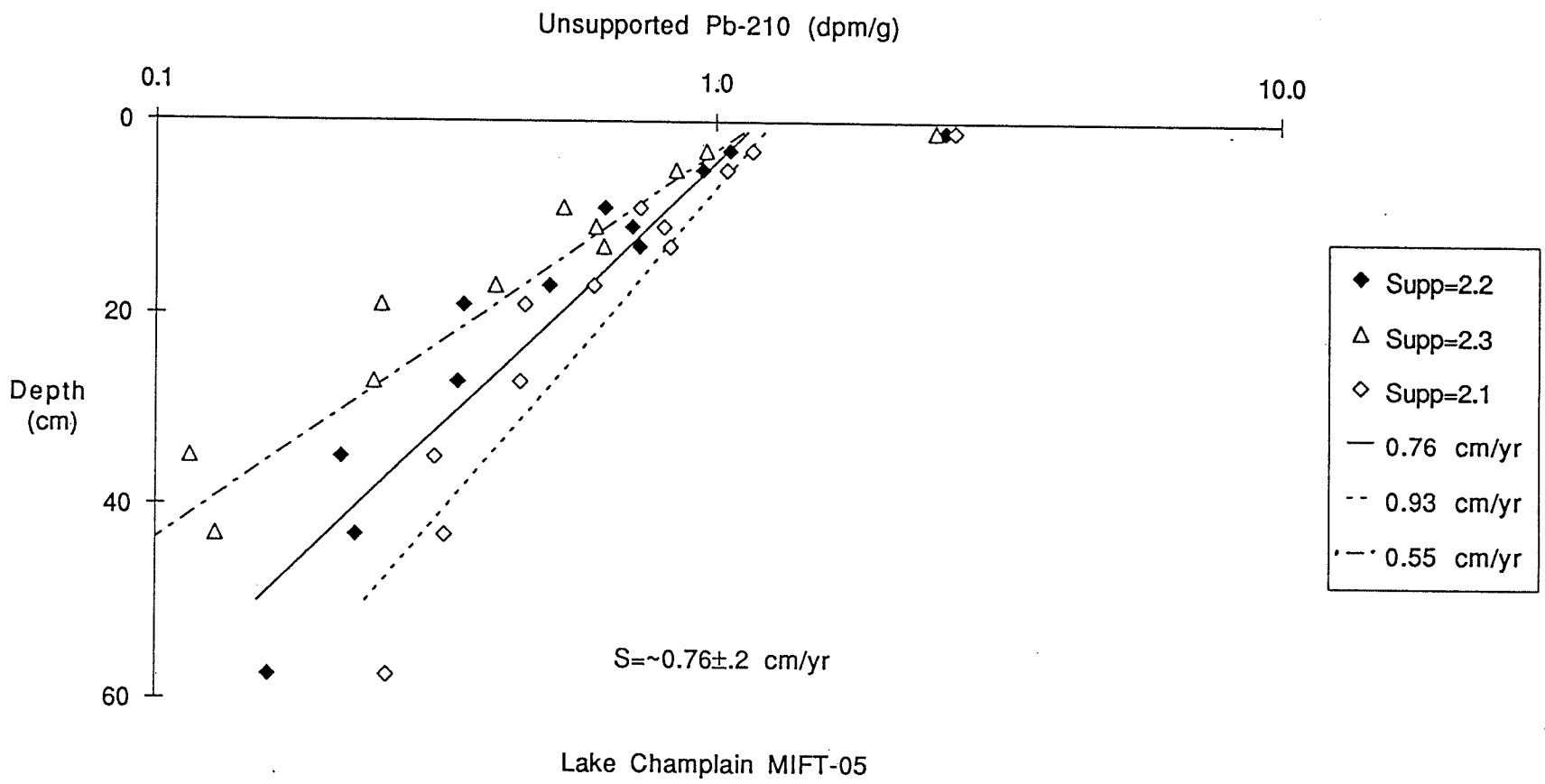
Unsupported Pb-210 (dpm/g)
0.1
1.0
10.0
0
20
40
60
Depth
(cm)
Supp=2.2
Supp=2.3
Supp=2.1
0.76 cm/yr
0.93 cm/yr
0.55 cm/yr
S=~0.76±.2 cm/yr
Lake Champlain MIFT-05

Figure 44

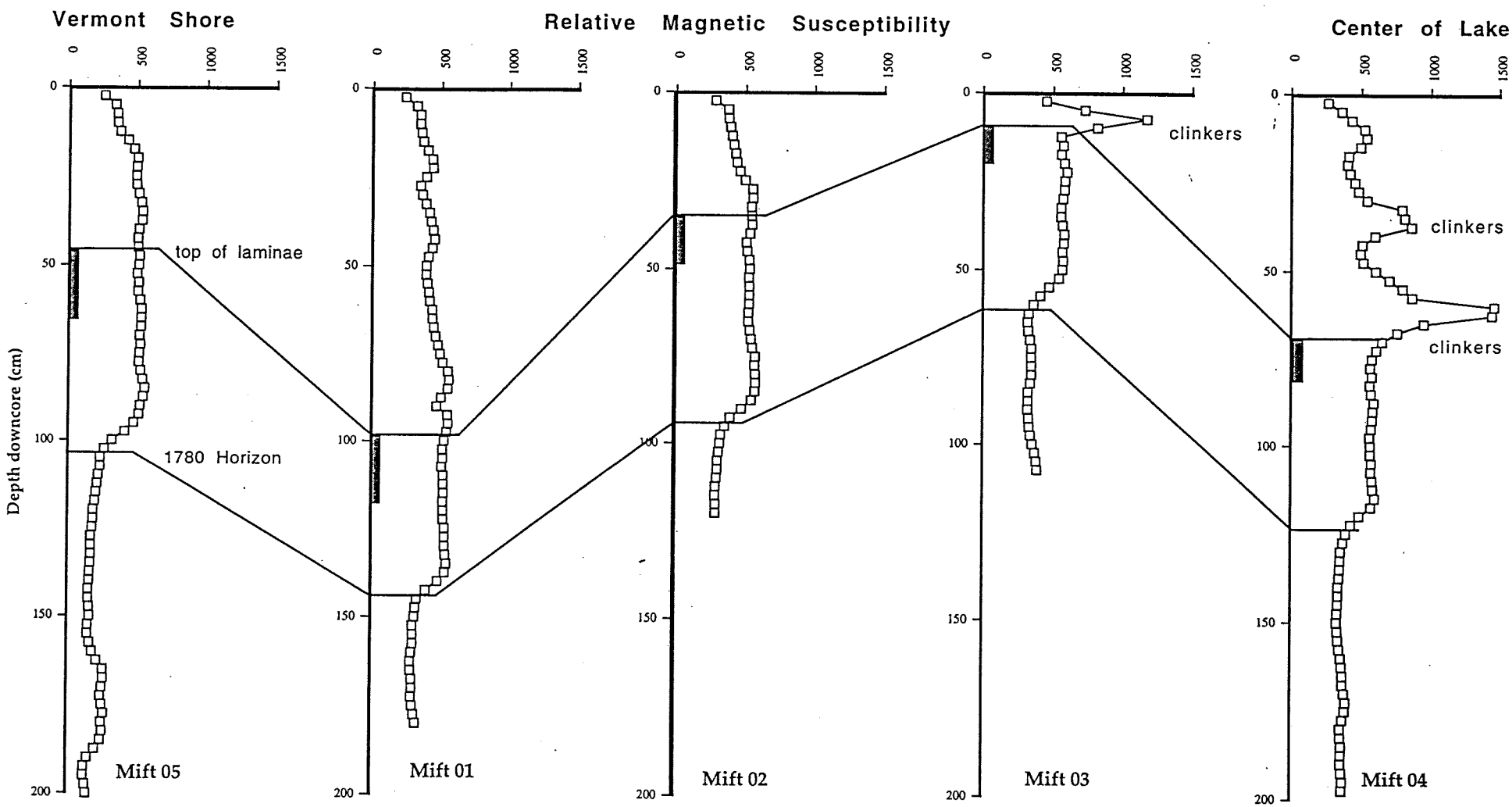
Vermont Shore
Relative Magnetic Susceptibility
Center of Lake
0
500
1000
1500
50
100
150
200
Depth downcore (cm)
top of laminae
1780 Horizon
clinkers
clinkers
clinkers
Mift 05
Mift 01
Mift 02
Mift 03
Mift 04

Figure 45